# STRUCTURED ILLUMINATION MICROSCOPY USING DIGITAL MICROMIRROR DEVICE

by

Rahul Singh

Submitted in partial fulfilment of the requirements
for the degree of Master of Applied Science

at

Dalhousie University
Halifax, Nova Scotia
November 2014

## Table Of Contents

## List Of Tables

## List Of Figures

## ABSTRACT

Structured illumination microscopy (SIM) increases resolution of optical microscopes substantially. However, simulation of this process using mathematical models is still a novel notion. **Purpose:** To design a program to simulate the process of SIM and study its application on biological samples. **Method:** Pre-defined images of microscopic samples were blurred and then reconstructed using a simulation designed in MATLAB. Experimental application of SIM and simulated reconstruction of images obtained using a microscope was then performed. **Results:** Considerably high resolution images were obtained from the simulation, which was also supported by the pixel intensity plots, signal to noise ratio and peak signal to noise ratio analyses. Resolution of images of samples obtained from experimentally performing SIM on a microscope were also similar to their simulated reconstruction. **Conclusion:** SIM is a desirable option for optimally imaging biological microscopic samples, physically as well as through simulation process.

## LIST OF ABBREVIATIONS AND SYMBOLS USED

| | |
|---|---|
| SI | Structured Illumination |
| PSF | Point Spread Function |
| NA | Numerical Aperture |
| OTF | Optical Transfer Function |
| SNR | Signal to Noise Ratio |
| PSNR | Peak Signal to Noise Ratio |
| MSE | Mean Squared Error |
| PALM | Photoactivated Localization Microscopy |
| STORM | Stochastic Optical Reconstruction Microscopy |
| STED | Stimulated Emission Depletion Microscopy |
| 2D | Two Dimensional |
| 3D | Three Dimensional |
| SLM | Spatial Light Modulator |
| LCD | Liquid Color Display |
| LED | Light Emitting Diode |
| SIM | Structured Illumination Microscopy |
| DMD | Digital Micromirror Device |
| DLP | Digital Light Processing |
| MEMS | Micro Electromechanical Systems |
| SRAM | Static Random Access Memory |
| IP | Illumination Pattern |
| CCD | Charged Coupled Device |
| CMOS | Complementary Metal Oxide Semiconductor |
| WXGA | Wide Extended Graphics Array |
| $\lambda$ | Wavelength |
| n | Refractive Index Of A Material |

| | |
|---|---|
| $\Theta$ | Angle Of Convergence of Light on Surface of Medium |
| d | Distance Between Two Points |
| $\otimes$ | Convolution |
| x,y | Coordinates On Cartesian Axes |
| F | Fourier Transform of Variables |
| $P_{signal}$ | Power of Signal |
| $P_{noise}$ | Power of Noise |
| $A_{signal}$ | Amplitude of Signal |
| $A_{noise}$ | Amplitude of Noise |
| $MAX_I$ | Maximum Signal Value of Original Image |
| $\sum$ | Summation |
| $m$ | Rows of Pixels |
| n | Columns of Pixels |
| f(x, y) | Original Image |
| $f_0$ | Frequency of Pattern |
| $\Phi$ | Phase |
| $\delta$ | Delta |
| $I_{excitation}$ | Intensity of Excitation Pattern |
| i | Number of Patterns Used |
| h(x) | Input Signal |
| $h_i(x)$ | Output Signal |
| $H(f)$ | Fourier Transform of Input Signal |
| $H_i(f)$ | Fourier Transform of Output Signal |
| $\sigma_x$ | Sigma x |
| $\sigma_y$ | Sigma y |
| f(x, y) | Input Image |
| h(x, y) | Output Image |
| $F(f_x, f_y)$ | Fourier Transform of Image |

| | |
|---|---|
| $OTF_i$ | OTF Components |
| $OTF_i^*$ | Conjugate of OTF Components |
| $H(f_x,f_y)$ | Fourier Transform of Output Image |

## ACKNOWLEDGEMENTS

I would like to express my gratitude towards my supervisor, Dr. Michael Cada for giving me the opportunity to work as his student on this project. His guidance has been of utmost significance towards my graduate school experience. His experience and expertise in various domains of electrical and computer engineering have always furthered the skills I have acquired through this learning process. The photonics lab and its members have been a constant support towards my experience as a student and an aspiring engineer and I thank them for their support.

I would like to thank Dr. Alan Fine whose proficiency in the field of optics and imaging has been a bolster for the foundations of this project. I would like to thank him for providing me the opportunity to work with him and learn new concepts about microscopes, their functioning and innovations in this field. I would like to express my gratefulness to the members of the Physiology and Biophysics Lab under Dr. Alan Fine, who have been a great team and have been there to help me in case of confusions and conflicts.

I would like to thank Dr. Kamal El-Sankary and Dr. William J. Phillips for agreeing to participate as members of the thesis committee. Their availability for the same is reflective of their support towards the proceedings associated with this project and its completion.

And most of all, I would like to thank my family who have supported my ambitions throughout my life and nurtured me to become what I am today. It is all because of their patience and constant faith in me that I have been able to achieve my goals. I thank them for everything.

# CHAPTER 1

# INTRODUCTION

## 1.1 Super-Resolution Microscopy

The smallest object that a naked human eye can see clearly is only as big as 0.1mm. With technical advancements, it has become possible for us to view even smaller objects with much clarity and detail, using specific visual aids like microscopes. The field of using microscopes for the purpose of viewing small samples and objects that cannot be seen with the unaided eye is called Microscopy. The evidence of use of microscopes for more comprehensible viewing of small objects can be found as early as 1609 when Galileo Galilei had developed an *Occhiolino*, or a compound microscope. However, this equipment could only magnify the size of an object to a certain limit after which the clarity or the resolution of the object being viewed was lost. With the improvement in technology available to magnify objects beyond the physical ability of the finest of magnifying lenses, resolution of optical microscopes has been outshined by other microscopes like electron and scanning probe microscopes. Despite this, optical microscopy still remains a valuable aspect in this domain and hence researchers have been constantly trying to improve the characteristics of optical microscopes.

It is theorized that even the finest of optical microscopes that have been invented since the *Occhiolino* have a limited resolution because of the diffraction limit, a concept that was propounded by Ernst Abbe in 1873 [1]. For instance, using visible green light

of wavelength 500 nanometers and numerical aperture of 1 for viewing an object, the Abbe limit (d) or the diffraction limit will be roughly $d = \lambda/2 = 250$ nm. This is quite large compared to most nanostructures which are approximately 1μm in size or smaller. However, to safely view anything with dimensions smaller than this value using the visible light will be difficult. Thus, the finite spatial resolution associated with optical microscopy, which is limited by diffraction to about 200 nm in the lateral resolution (in the image plane) and about 700 nm in the axial (focus) direction, [2] poses as the main limitation to its use for viewing very small objects. This indicates that the ability to study details of an object using an optical instrument is bound by laws of physics. However, it is possible to bend these laws to reproduce an image to view a given object beyond the diffraction limit. This is done using super-resolution microscopy.

Super-resolution is the process of enhancing the resolution of an optical instrument or any imaging system beyond the limitations of the Abbe limit. Super-resolution can further be studied under two broad categories- "true" super-resolution techniques and "functional" super-resolution techniques. True super-resolution techniques are the ones that enhance resolution by capturing the information contained in evanescent waves. On the other hand, functional super-resolution employs clever mathematical operations to attain super-resolution by means of computation. Additionally, it includes the limitations of the object being imaged for processing [3]. This can be further classified into deterministic and stochastical functional super-resolution techniques. Deterministic techniques make use of the ability of fluorophores to exhibit a non-linear response to excitation while stochastical techniques make use of

the chemical nature of light sources to affect the temporal behavior of fluorophores in the vicinity, hence making them emit light at different times.

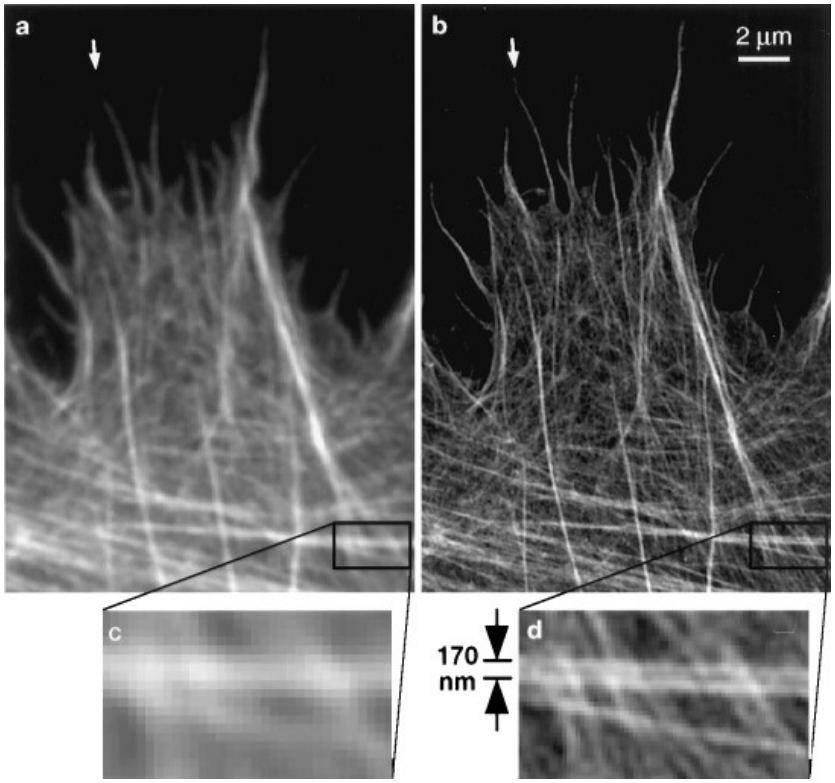

Figure 1.1: Conventional vs. SIM on HeLa cells [4]

One of the fundamental approaches towards breaking the diffraction limit for enhanced resolution is structured-illumination (SI) or patterned illumination, a kind of true super-resolution technique [5][6]. SI relies primarily on specific microscopy protocols and extensive post-exposure analysis of the image using an image processing algorithm. The principle behind use of SI for super-resolution involves the use of patterned light to illuminate an object or sample, often using a single spatial frequency grid. This is done by means of a spatial light modulator. One such device is called a Digital Micro-mirror Device or DMD, which uses LEDs or lasers as illumination source. A DMD basically consists of small mirrors that rotate as they are illuminated. This

results in development of the illumination pattern as a result of interference of light waves. This results in the development of fringes with alternating maximum and minimum intensities. As the contrast is maintained in a focal plane, improved illumination of specimen features that are out of the focal plane is achieved. Measuring the interference fringes, of the illumination pattern and the sample, can thus be used to obtain a higher resolution. This way, the higher frequency features of the sample can be deduced from the fringes and this information can be further computationally restored. [7], [8].

## 1.2 Motivation

Microscopy is an important branch of science, allowing us to study small objects and organisms that cannot otherwise be seen with the naked eye. Besides the option to view enlarged images of these objects, another important principle on which efficient microscopy is founded upon is the resolution. Resolution is the ability of a microscope to discriminate between two closely placed points at distinct from one another.

However, it has been theorized that the resolution of an optical system like a microscope, can only be enhanced to a limit. With the growing need to understand microorganisms for the study of health, disease and role of microorganisms in affecting these processes, it has become important to devise sensitive means to study microscopic objects. As technology has advanced, numerous means have come up to improve the resolution of microscopes. This has often involved use of shorter wavelengths like ultra-violet and X-rays. As much as these radiations have improved resolution, they are known to cause harm to biological specimens. This motivated us towards studying super-resolution and its role in breaking the barrier set up by the theories that define limits to the resolution of optical systems and employ its procedures to attain a safe system for studying biological specimens.

Akin to a multitude of studies looking to devise sensitive and accurate measures of improving resolution, we intended to study the domain of super-resolution specifically Structured Illumination Microscopy or SIM. We intended to study and demonstrate the

applicability of SIM in obtaining highly resolved images of microscopic specimens. However, an important goal of this project was to also look at the utility of simulating the process of SIM. The use of simulation procedures to perform SIM-like manipulations to reconstruct unclear images of microscopic specimens is a novel idea. Due to the lack of evidence in this domain, we intended to further the research in this direction and with our results, encourage the need to study use of simulation processes to achieve the best possible images of microscopic biological samples in a safe environment.

## 1.3 Objectives

1. To design a superresolution algorithm in MATLAB which could be applied to actual 2-D images.
2. To design a simulation of Structured Illumination Microscopy in MATLAB to be used to simulate the complete process of SIM step-wise to reconstruct higher resolution images.
3. To apply and observe the effects of Structured Illumination Microscopy in obtaining images of microscopic specimens observed under a fluorescence microscope.
4. To use a Digital Micromirror Device as the spatial light modulator on a fluorescence microscope to effectively drive the process of Structured Illumination Microscopy.
5. To use the simulated SIM process in MATLAB for reconstructing standard widefield images of specimens and compare the reconstructed images to the ones obtained from the experimental application of Structured Illumination Microscopy.

## 1.4 Organization of thesis

The thesis has been organized into relevant chapters describing different aspects of the project. Chapter 1 entails a brief introduction to the project and outlines our motivation and objectives. Chapter 2 describes the essential theory that outlines major concepts that have been used towards the development of this project. Chapter 3 includes a detailed review of relevant studies that have been conducted towards the purpose of improving resolution in microscopy and their findings. Chapter 4 provides an introduction to procedural implications of structured illumination microscopy and the methodology associated with our project. Chapter 5 gives a detailed description of our results and our interpretation of the same. Chapter 6 goes on to summarize the nature, purpose, methodology and results of this project. Additionally, Chapter 6 also outlines the limitations and any future implication of this study.

# CHAPTER 2

# BACKGROUND THEORY

## 2.1 Resolution and impact of diffraction on resolution

The smallest distance between two point objects that can be distinguished as two distinct entities when being viewed, by an observer or through a camera, within an optical imaging system is known as resolution. Resolution is a property that affects all instruments, digital or analogue, and define the ability to distinguish between two indications, which are essentially objects for an optical instrument [9].

Since visible light is used as an illumination source for the purpose of optical imaging, its properties act as variables that affect the resolution of the imaging system. Of the many properties that light exhibits, one of its wave properties important for optical imaging is called diffraction. Colloquially, diffraction is basically the "bending" of light. This occurs due to the various obstacles that come in the way of light as it moves within a space or from one medium to another. Even with the smallest apertures in the optical system, this dispersion in light can significantly affect the resolution of an image, making it harder to view objects under a microscope with a high order of detail. The restricted resolution of optical systems has been described by various researchers as mathematical expressions that aid in quantifying the maximum attainable resolution.

A few examples of these include the Rayleigh resolution limit, Sparrow

resolution limit and the Abbe diffraction limit [10], [11], [1] (Table 1, Figure 2.1).

Table 1: Various mathematical expressions describing the diffraction limit

| Method | Mathematical expression | Variables |
|---|---|---|
| Rayleigh resolution limit | $\frac{0.61\lambda}{NA}$ | $\lambda$ – Wavelength<br><br>NA – Numerical aperture |
| Sparrow resolution limit | $\frac{0.47\lambda}{NA}$ | $\lambda$ – Wavelength<br><br>NA – Numerical aperture |
| Abbe diffraction limit | $\frac{\lambda}{2n \sin\theta}$ | $\lambda$ – Wavelength<br><br>n – Refractive index of the medium<br><br>$\Theta$ - Angle of convergence of light on the surface of the medium |

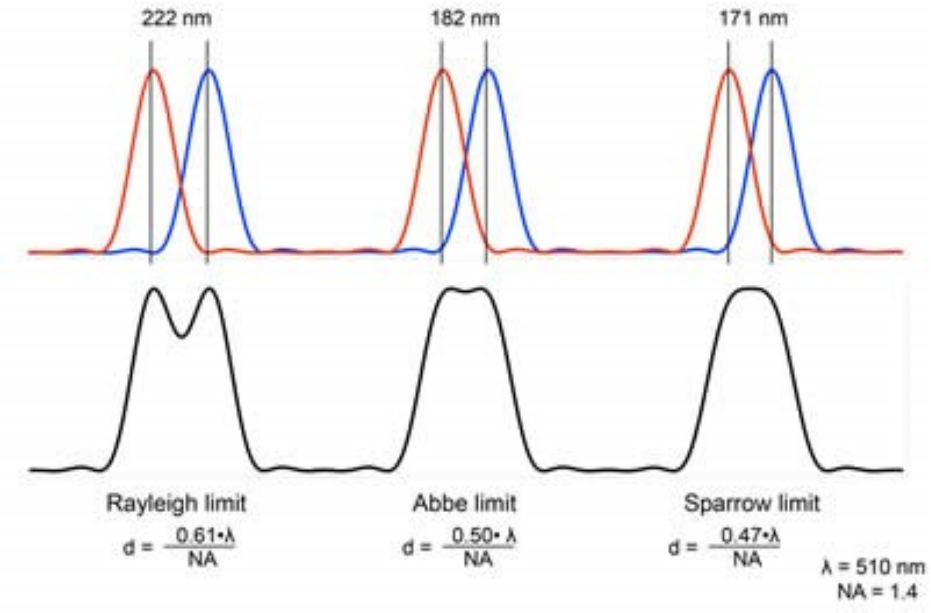


Figure 2.1: Various conventional resolution limits and their definitions [12].

## 2.2 Diffraction limit

Ernst Abbe, a pioneer in the field of modern optics, suggested in 1873 that for all optical systems this finite limitation in resolution due to diffraction can be quantified as the Abbe limit or the diffraction limit [1]. This limit quantifies the maximum point-to-point resolution that can be attained by an optical microscope within the confines of a fundamental physical law.

Ernst Abbe propounded that for light of wavelength $\lambda$, traveling in medium of refractive index $n$ which converges at the surface making an angle of $\theta$ makes a spot with a radius described by the following formula:

$$d = \frac{\lambda}{2n \sin\theta} \qquad [2.1]$$

Here $n \sin\theta$ is the numerical aperture (NA). By recent standards, NA ranges from 1.4 to 1.6 in modern optics. This gives us an approximate value of $\lambda/2.8$ for the Abbe limit ($d$). If we use the green light from the visible spectra, it has a wavelength of approximately 500 nm. Using this value for $\lambda$, the Abbe limit is calculated to be approximately 200 nm. This value is quite large compared to most microscopic objects. However, it is tricky to be able to obtain clear and well-detailed images of objects that are smaller than this size (Figure 2.2).

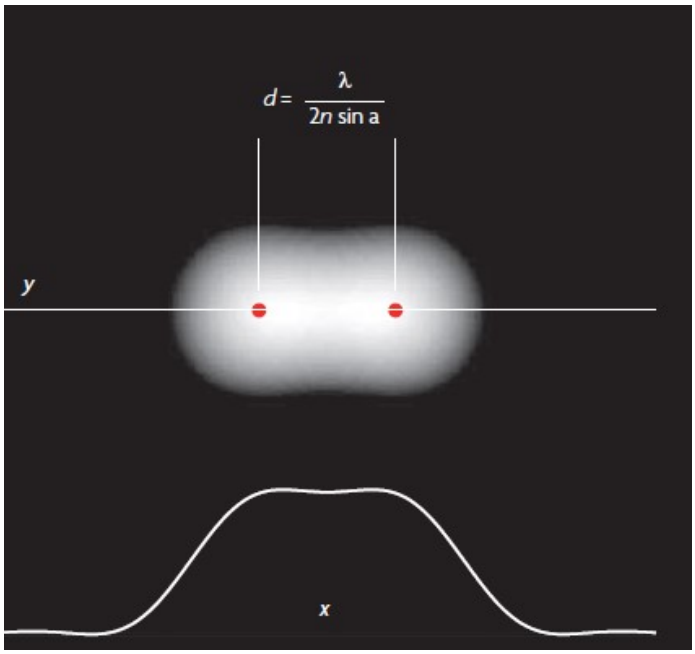

Figure 2.2: Two point objects separated just enough to be resolved. Line graph show intensity along the separation [13].

To work around this limitation associated with the use of visible light for viewing objects under a microscope, other waveforms with shorter wavelengths have been used, for example, ultraviolet and X-rays. A shorter wavelength (λ, one of the variables affecting the value of *d*, as indicated earlier) results in a larger value of the diffraction limit for a constant NA, compared to a longer wavelength. This results in the ability to view even smaller samples and objects and hence results in a better overall resolution. A limitation for these waveforms however, is that they are expensive and lack contrast when being used to obtain images of a sample or an object. These also pose as a potential hazard to most biological samples as well. So, this brings us to think about other ways in which resolution can be improved without damaging the object being viewed. Another technique, which will be described in further sections, is the use of super-resolution measures using visible light to break the confines of diffraction limit on the resolution of optical microscope.

## 2.3 Point spread function

Because of the diffraction limit, the impact of diffraction is the ‘blurring’ of an image. The greater the ‘blur’ associated with an image, the poorer is the quality of that imaging system. Thus, this factor plays a key role in determining how clearly an optical system can obtain an image of an object. This degree of spreading of light that causes the ‘blur’ is often described as the point spread function (PSF).

Before we look at the PSF and its implications on an optical imaging system, it is important to understand the process of interference of waves. Interference is essentially the process of ‘merging' of two or more waves. This interaction results in the formation of a single wave that is a summation of the characteristics of the primary waves. If the frequency of the two waves is same and they oscillate in phase (coherent waves), they tend to add up to give a larger resultant wave. On the other hand, incoherent or out of phase waves often cancel out the amplitude of one or the other waves. This shifts the phase of the resultant wave and makes it quite different from the primary waves. This phenomenon is observed for light as well. In optical systems, when a point source of illumination sends out light waves, diffraction tends to diverge the path of the waves. In this process, one or the other waves interfere among themselves as they hit the surface of the sample or the object being viewed since due to diffraction, many waves do not follow a straight path from the source to the object. PSF describes this retort of an imaging system to a point source.

This concept of PSF is described through Figure 2.3. As point sources of

illumination from an object under the microscope reach the imaging system, they tend to appear as circular spots with the highest intensity of illumination at the center as it spreads outwards to present as a blurry unclear margin. These illuminated centers are called Airy disks while the hazy patterns outside the disks are Airy patterns. These are the result of diffraction that results in incoherent interference among light waves resulting in low intensity of the resultant light waves. The three-dimensional representation of the same near the image plane is what is termed PSF.

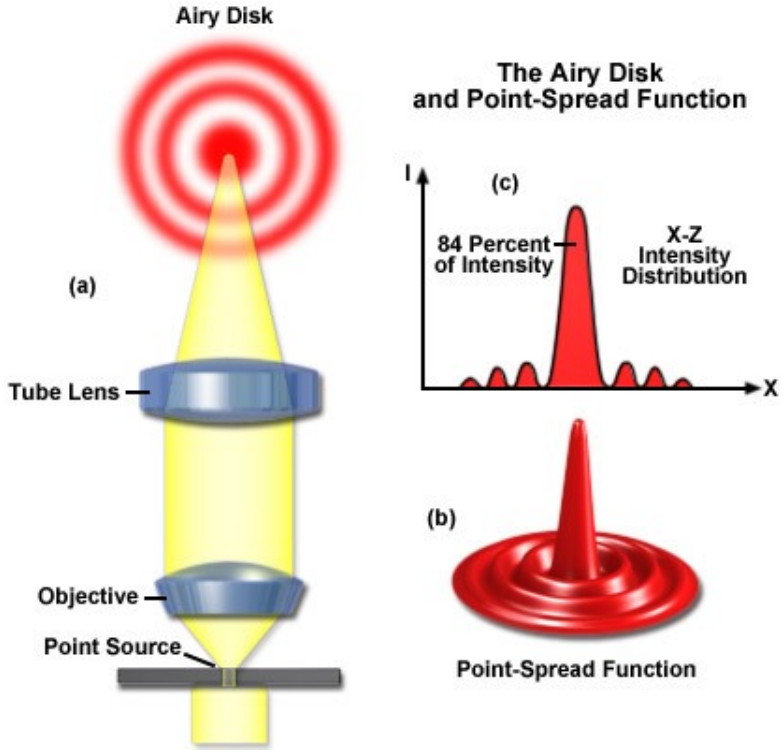


Figure 2.3: (a). Formation of airy disc as a result of diffraction of light, (b). PSF as the three-dimensional representation of the Airy disc, (c). Graph showings that center of the Airy disc represents 84% of the intensity. Obtained from [14].

Functionally, PSF represents the spatial domain of the mathematical function that defines the output of the imaging system. Mathematically, the input delta function for an optical microscope is represented by the point source. The image corresponding to the

interaction of the input and the transfer (output) function of the imaging system is depicted by the PSF [14].

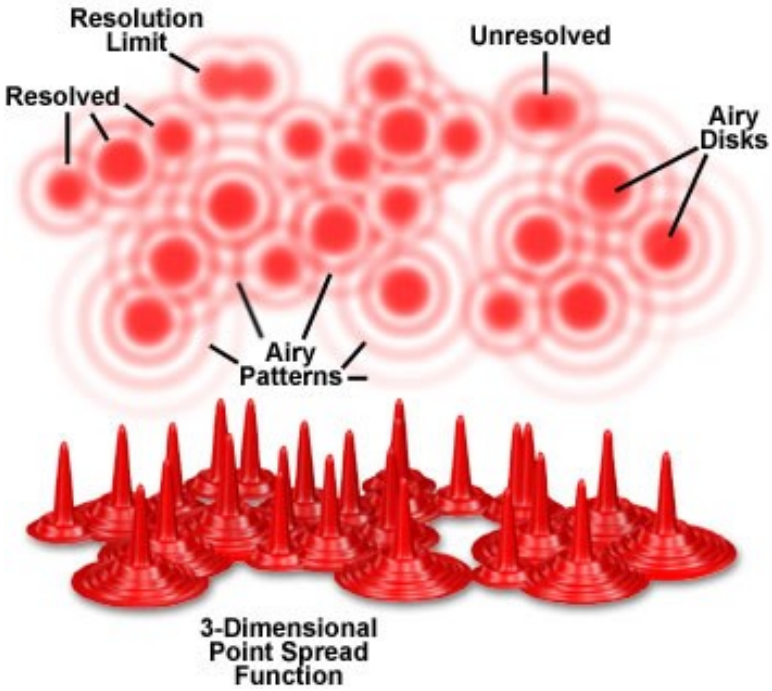


Figure 2.4: Representation of Airy Disks and their PSFs depicting the concept of resolution [12].

As can be observed in the Figure 2.4, when two PSF's (typically described by the diameter of the Airy discs [14], merge together the most illuminated and sharper parts of these two point sources of light get affected by diffraction and interference of their waves. With such interference it becomes harder to tell apart one point source from the other, hence decreasing the resolution of the image. Normally, if the principal diffraction maxima was to coincide with the first minima of the neighboring point source, the resultant image would be well resolved.[1] [2] However, as in this case, since the Airy patterns overlap it reduces the distance between the point sources. As this distance decreases compared to the diffraction limit, the two points cannot be discriminated from

each other as individual points anymore and thus the resolution is affected. We can try and magnify an image indefinitely, but eventually the image will blur and become incomprehensible. Any effort to magnify further will not improve the detailing of the image and its smaller components.

This makes it important to find a way to preserve the resolution of the imaging system as magnification is being done. As pointed earlier, the diffraction limit (Abbe limit) depends upon the wavelength of light and the NA of the objective lens [15]. Since shorter wavelengths (UV and X-rays) have limited implications, it is feasible to try to alter the NA to obtain desired resolution. The radius of the Airy disc is a resultant of the NA of the objective lens and with a higher NA it is possible to improve the resolution. This happens as a result of a narrower PSF.

## 2.4 Optical Transfer Function

An image obtained by an optical system is a convolution of two functions, the object and the PSF. These variables are denoted as a function of their position (r) on the coordinate system (x, y) in a constant time (t) domain. This can be represented as a spatial variant function denoted by the following equation:

$$h(x,y) = f(x,y) \otimes psf \qquad [2.2]$$

Using a Fourier transformation, we can show a frequency and amplitude relationship between the object and the PSF. This helps convert the above function into a spatially constant but frequency variant function. Since convolutions can be conveniently manipulated through their Fourier transform (F), this brings us to the

following equation:

$$H(f_x,f_y) = F(f_x, f_y) \times F\{psf\} \quad (2.3)$$

In the above equation, the multiplication is a representation of the convolution in frequency domain. $F(f_x, f_y)$, $H(f_x,f_y)$ and $F\{psf\}$ represent Fourier transforms of the input image, output image and the PSF respectively as a function of time (t) on the coordinate system (x,y).

The function $F\{psf\}$ is also known as the **Optical Transfer Function** (OTF), which is the transfer or output function of any optical system. It is used by researchers and engineers to describe how the light is projected from an object or sample to a detector. Thus, the PSF impacts resolution in the spatial domain while OTF helps derive the resolution within a frequency domain. Both functions, PSF and OTF, follow the Abbe theory of formation of an image.

## 2.5 Signal to Noise Ratio and Peak Signal-to-Noise Ratio

To mathematically understand a phenomenon, it is important to have a function that describes the features and characteristics of that phenomena. Priemer [16], termed this function as Signal. A signal conveys imperative information about the attributes of a phenomenon. It is essentially digitized information about a phenomenon. In image processing, the pixels of an image describe the attributes of the image and hence act as the signal for this purpose. Every signal is confounded by some irrelevant signals in the surrounding environment. These are termed noise. A power ratio between the signal and

the noise is termed as signal-to-noise ratio or SNR. SNR helps engineers describe the amount of noise that associated with a given signal as measure of 'purity' of that signal. It is the ratio of the power of signal ($P_{signal}$) to the power of noise ($P_{noise}$) and is described by the following function:

$$\text{SNR} = \frac{P_{signal}}{P_{noise}} \tag{2.4}$$

Here 'P' corresponds to average power. A greater SNR corresponds to a larger power of signal suggesting that there is lesser noise associated with the signal. SNR is often also expressed in terms of the logarithmic decibel scale and is 20 times the $\log_{10}$ of the amplitude ratio of signal ($A_{signal}$) and noise ($A_{noise}$). Here 'A' is the root mean square (RMS) amplitude. This function also translates as 10 times the logarithm of the power ratio described in the previous equation:

$$SNR = \left(\frac{P_{signal}}{P_{noise}}\right) = \left(\frac{P_{signal}}{P_{noise}}\right)^2 \tag{2.4}$$

$$SNR_{db} = 10\log_{10}\left[\left(\frac{A_{signal}}{A_{noise}}\right)^2\right] = 20\log_{10}\left(\frac{A_{signal}}{A_{noise}}\right) \tag{2.5}$$

Since the signal for an image is essentially comprised of its pixels and noise is the variability in those pixels, it is safe to say that in image processing, the SNR is the ratio of the mean pixel value to the standard deviation of the pixel values.

Another similar measure of the clarity of an image signal is called the peak signal-to-noise ratio (PSNR). The only mathematical difference between SNR and PSNR is that PSNR is a ratio of maximum power of the signal to the power of the noise. For

instance, if we were to image a sample, the SNR will take an average of all signals coming from the sample and compare it against the average power of the noise associated with that signal. This would mean that the numerator includes an average of the intensity of light coming from all parts of the sample. In PSNR however, the signal component of interest is just the peak component, i.e. the maximum intensity of light coming from the sample or the strongest signal, which is usually at its boundaries due to reflection. PSNR is thus quite useful if we are looking at adjusting the signal contrast in specific regions of interest while SNR gives more of a general picture.

With multiple elements comprising a signal, its dynamic range is quite vast. Hence, like SNR, PSNR is also represented on a logarithmic decibel scale. Much like the SNR, a higher PSNR is generally associated with a higher quality of reconstructed image. The equation for PSNR is as follows:

$$PSNR = 10\,log_{10}\left(\frac{MAX_I^2}{MSE}\right)^2 = 20\,log_{10}\left(\frac{MAX_I^2}{\sqrt{MSE}}\right) \tag{2.6}$$

Here $MAX_I$ represents the maximum signal value from the original image and MSE represents the mean squared error which is the mean of squared error values represented as the difference between the actual image and the reconstructed image. For the purpose of image processing, MSE helps compare the pixels of original image to the degraded image. For a noise-free monochrome image, *MSE* is represented as follows:

$$MSE = \sum_{i=0}^{m-1} \sum_{j=0}^{n-1} [I(x,y) - K(x,y)]^2 \tag{2.7}$$

Here $I$ is the matrix data of the image for $m$ rows of pixels and $n$ columns of pixels. The indices of the rows and columns are $x$ and $y$. $K$ represents the matrix data of the degraded image.

## 2.6 Wiener Deconvolution

The process of reversing the convolution to restore a signal is called deconvolution. It is an inverse filtering technique that finds its use in reconstruction of images in image processing systems. If an image is blurred using a low-pass filter, deconvolution can be employed to attempt to reconstruct the original image by restoring the original signals or the pixels. Every time a signal from an image is altered, either by breaking it down to a blur or by picking up the pixels and restoring the image, some noise is added to the signal. Thus it is important to have an inverse filter that optimizes the tradeoff between deconvolution and reduction of noise. This can be done by means of a unique restoration algorithm for each type of degradation causing the noise and eventually combining them all together.

The Wiener filter is capable of removing the noise while it also inverses the blurring [19]. It works by minimizing the overall MSE in the process. Wiener filter employs Wiener deconvolution for inverse filtering. Wiener deconvolution, a mathematical expression named after Norbert Wiener, is a functional representation in the frequency domain that reduces the influence of deconvolved noise at frequencies with incidences of a poor SNR. Since, estimating the frequency spectrum of most images

is fairly convenient, Wiener deconvolution finds popularity in deconvolution of images among engineers and researchers [7], [20].For a system, convolution of an input signal (x) with an impulse response (p) summated with additive noise (n) that is independent of (*x*) results in the observed signal (h) within the time constant (t) in a time-invariant system. This convolution can be expressed as follows as a function of time (t):

$$h(t) = p(t) \otimes x(t) + n(t) \tag{2.9}$$

However to restore the signal *x* by means of deconvolution to obtain a signal $\hat{x}(t)$, which is an estimate of the input signal in a time constant situation that minimizes the MSE, we need to determine a signal variable $g(t)$ whose relationship with the observed signal in a time constant system with time (t) can be expressed as follows:

$$\hat{x}(t) = g(t) * h(t) \tag{2.10}$$

The Wiener filter can help achieve this reconstruction of signal by means of employing Wiener deconvolution which helps obtain the value for the function $g$ in the same time constant situation. This is done by obtaining the Fourier transform of $g$ i.e. G(f) which is described by the following equation as a function of frequency *f* in the frequency invariant condition:

$$G(f) = \frac{P^*(f)S(f)}{|H(f)|^2 S(f)+N(f)} \tag{2.11}$$

Here $H(f)$ is the Fourier transform of $h$, $S(f)$ is the mean power spectral density of the input signal and $N(f)$ is the mean power spectral density of the noise. $H^*$

is a complex conjugation. Thus the equation described earlier for the reconstructed signal in the time domain, can be filtered in the frequency domain using the following Fourier transform of the equation:

$$\hat{X}(f) = G(f)H(f) \tag{2.12}$$

An inverse Fourier transform of $\hat{X}(f)$ will provide us the value of $\hat{x}(t)$

# CHAPTER 3

# REVIEW OF LITERATURE

## 3.1 Microscopy

The field of studying and observing small objects, invisible to the naked eye, is called microscopy. The word is derived from Greek μικρός (mikrós) meaning "small" and σκοπεῖν (skopeîn) meaning "to look". Microscopy has had a long and ever-changing history with the advancements seen in technology since the first microscope was invented. We started with simple magnifying lenses to building up the simple compound microscope. What is more astounding is that it was two spectacle-makers, Hans Janssen and his son Zacharias Janssen, or Hans Lippershey, who were the pioneers of this invention. [21]. As the curiosity to learn more about microorganisms augmented, the need to develop more sophisticated microscopes seemed pragmatic. Thus, the first compound microscope came into being in early 1600's.

Following the invention of the first one, other designs of microscopes followed. Galileo Galilei modified the design of his telescope to view miniscule objects in 1610, but it was not until 1624 till he first created an improvisation to the traditional microscope designs. Giovanni Faber was the one to identify Galilei's instrument as a compound microscope and coined this term in 1625 [22]. As more and more sophisticated microscopes developed, the scope of microscopy expanded. From the

simple intent to view small objects, microscopes began gaining popularity among biologists. For instance, Antonie Van Leeuwenhoek discovered blood cells and sperm cells using one of the finer designs of the compound microscope. By 1676, he had already reported the existence of microorganisms [23].

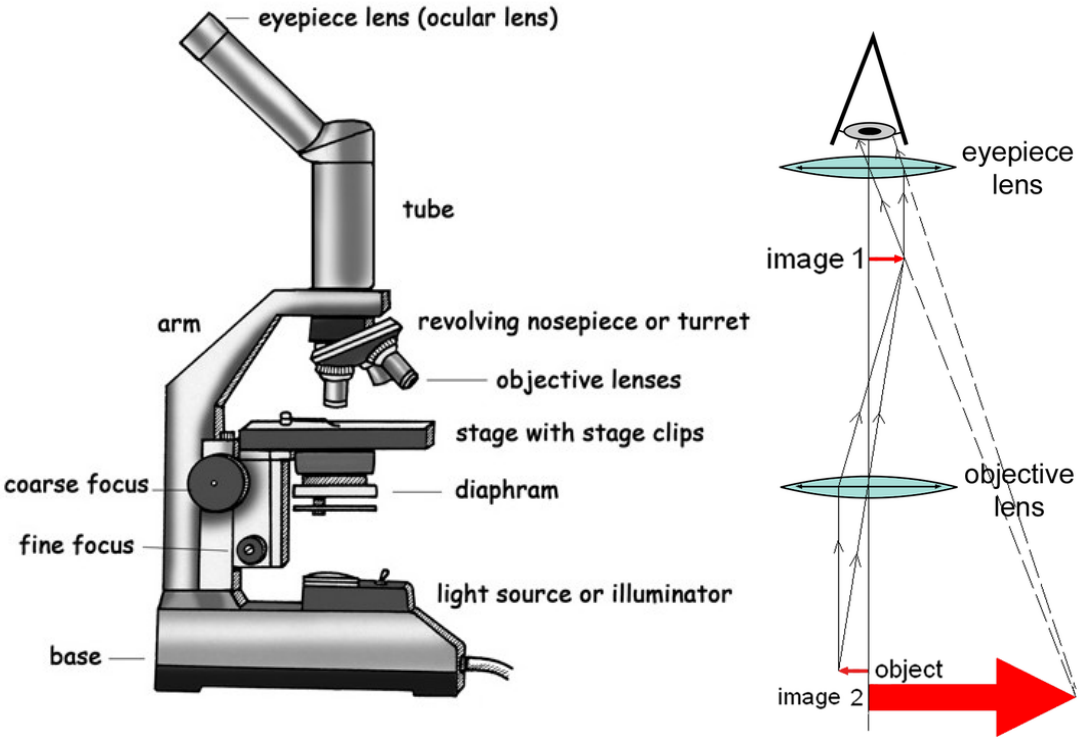


Figure 3.1: Parts of a modern compound microscope and ray diagram of the compound microscope: An inverted magnified image of the sample is produced by the objective lens and the eyepiece projects a further magnified virtual image into our eye. [25]

The major part of advancements in the mechanics and mechanism of microscopes was during the 18$^{th}$ century, mostly in Italy. For the most part, major changes were being made to devices that help attain good focus or hold specimens in place. As solutions to different errors in the use and applicability of microscopes were found, better microscopes were developed. With Chester Moor Hall's discovery of the combination lenses to reduce chromatic aberrations, finer and more accurate microscopes were

designed. The first one with these adjustments was developed in 1774 by Benjamin Martin [24].

In 1964, Humes and Gooding [26] used a conventional compound microscope as a dissecting microscope for the study of copepods. They used a wooden slide to mount their specimen in an attempt to study the organism. In their study, they also suggested the use of Harding's [27] design, where an individual could operate the microscope with knee movements, rendering the hands free for use in dissection. A basic conventional light microscope, like the one used by Humes and Gooding, consists of two convex lenses, one for the eyepiece and the other known as the objective. Although, the instrumentation has become more sophisticated over the years, the basic principles and mechanisms of the working of microscopes are still the same (Figure 3.1).

There are two basic principles of microscopy: magnification and resolution [28]. The ability to enlarge an object or an area under the field of a microscope is called magnification. Magnification can be a result of use of a set of magnifying lenses or other physical principles that vary depending on the type of microscope in use. However, as much as it is important to increase the size of the image of an object, it is also important that we are able to view it as a set of well-defined comprehensible images and not just a blur. This ability to view two or more closely spaced objects as distinct is known as resolution. The higher the resolution of a microscope, the greater its ability to provide clear magnified images of the object of interest.

Researchers have worked for long to come up with radical options for improving upon these principles on which microscopes are based. For instance, in his book in 1901, Bausch describes the basic features, types and uses of the microscopes and the possibilities of manipulating the instrument to enhance its properties [29]. Bausch described manipulations like addition of magnifiers, use of magnifiers of different magnifying powers, etc. to increase the magnification. He further acceded to the limitation of a microscopes resolution as is defined by the Abbe's diffraction limit (described in earlier sections). As Bausch addresses this issue in his text, he furthers a manipulation to the microscopes by means of using sub-stage illuminator or condenser known as the Abbe condenser. This set up has two designs. A three lens system with a NA of 1.42 and a two lens system with NA of 1.20. These manipulations were known to improve the resolution of a microscope by means of altering the volume and angle of illumination.

However, despite such manipulations, it has been difficult to break the physical barrier of the diffraction limit. Use of shorter wavelengths has been helpful to some extent. For instance, a much recent study on study of hydrophilic structures of the cells made use of X-rays to image the sample [30]. They were able to obtain very clear and high resolution images, unlike the optical microscope that was being used for comparison. Despite the perks of a better resolution, the researchers identified the use of X-rays as a major limitation to study cellular and sub-cellular iron distribution in a cell due to poor detection limits. Additionally, other researchers have identified the use of such short wavelengths in being harmful for a live biological specimen [31]. Thus, this

brings us to believe that optical or light microscopy, being a safer procedure, can be manipulated to improve resolution and further avenues in this direction need to be explored.

## 3.2 Super-resolution Microscopy

In an attempt to improve the resolution of optical microscopes by breaking through the barrier of the diffraction limit, Superresolution microscopy came into being. Super-resolution techniques essentially allow us to attain a resolution greater than the diffraction limit.

There are three basic methods of achieving Superresolution in the field of microbiology [30], (Figure 3.2):

1. **Single molecule localization based techniques:**

   These include photoactivated localization microscopy (PALM) that works by activating individual molecules using low-level activation light, usually the violet spectrum of visible light. This helps in localizing every single molecule of interest, and this helps in identifying their location. Once all molecules are localized, stochastic optical reconstruction techniques (STORM) are used to superimpose the location of these molecules. This technique makes use of Gaussian function to do so. Once the locations (by the order of nanometric precision) are superimposed upon one another, a super-resolved image can be obtained.

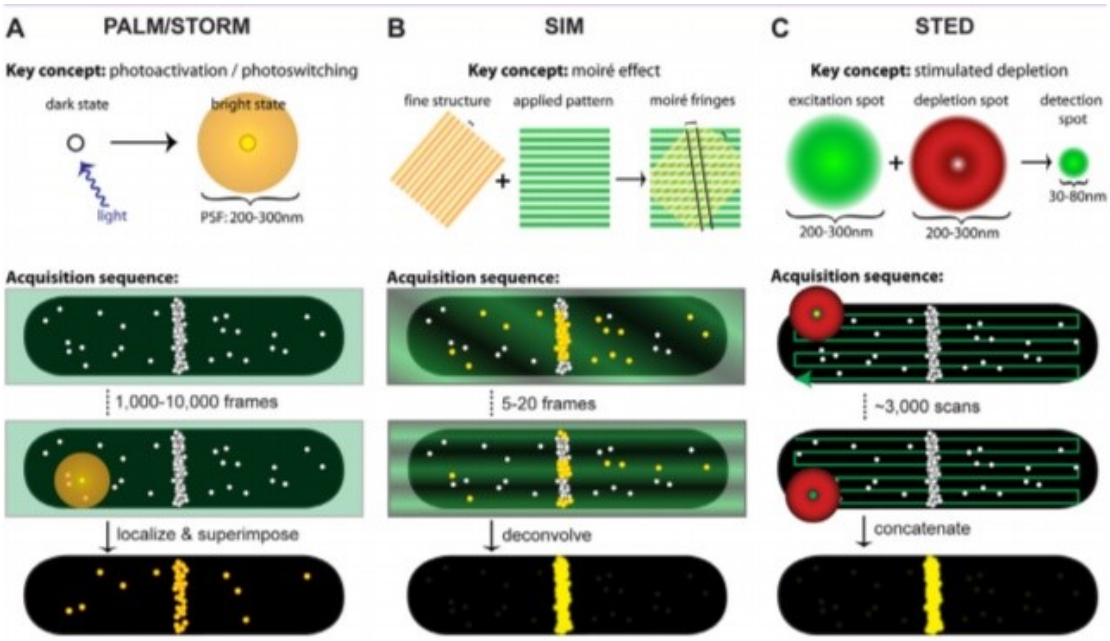


Figure 3.2: Superresolution techniques: A. PALM/STORM techniques used for attaining super-resolution by means of photolocalization of stimulated particles. Positions of activated fluorophores is acquired in the acquisition sequence. As they are localized, the images are superimposed to attain super-resolution. B. SIM technique is used to attain super-resolution by means of the moiré effect. Fringed illumination pattern is projected upon the sample as interference of the patterned light and structures of the sample results in super-resolution. Deconvolution methods and Fourier transformation is done to functionally resolve the image. C. STED is another method of obtaining super-resolution by projecting a series of excitation and depletion beams to the sample. As a series of fluorophores are excited, and molecules become visible before they fluoresce, images are taken and concatenated to obtain a super-resolved image. (Obtained from Coltharpe and Xiaou, [30])

PALM was first used by Betzig et al, 2006 [31] in an attempt to devise a method to image intracellular proteins at nanometer spatial resolution. They activated sets of photoactivable protein molecules which were further localized from 2-25 nm. After bleaching the sample, the cumulative positions of the sets of protein molecules were obtained and used for superresolution imaging. The researchers were successful at imaging small protein particles like vinculin, acting and retroviral protein Gag using this method.

Simultaneous to the development of the PALM technique, Rust et al, [32] developed another photolocalization technique to attain superresolution. The researchers made use of photoswitchable fluorophores where the activated fluorophores went through a series of imaging cycles for the process of localizing their positions. Only a fraction of fluorophores were activated in one imaging cycle and another fraction over the consecutive cycles. As all the positions were obtained, they were aggregated to obtain superresolution. The resolution these researchers obtained was to the order of 20 nm.

These two techniques work hand in hand, and have helped researchers attain superresolution for imaging live cells with much precision [33]. These methods eventually became quite well-known for obtaining sub-diffraction resolution.

2. **Point Scanning Method:**

The second method of obtaining superresolution is a point scanning method. The most common technique that has been used for this purpose is called stimulated emission-depletion or STED. This technique makes use of concentric excitation and depletion beams that are projected at the sample. The fluorophores get excited in the diffraction-limited zone by the emission beam. The depletion beam on the other hand brings the molecules, neighboring the 30-80 nm central zone, to the ground state before they completely fluoresce. This leads to the formation of a super-resolution point spread function. These beams systematically

get projected onto the entire sample in an attempt to obtain all the super-resolved images.

Hell et al, [34] devised this technique and employed it as early as 1994. They obtained a resolution of 35 nm in wide field microscopy. They also propounded the use of this technique to obtain three-dimensional images of translucent samples. Similar technique was then used by other researchers as they obtained sub-diffraction limit resolution and were successful in obtaining not just high resolution images, but essentially three-dimensional images of the structures of interest [35], [36], [37].

3. **Structured Illumination Microscopy:**

The third technique, and the highlight of this project, for attaining superresolution images is called structured illumination microscopy or SIM. This technique was being developed by Neil, Juskaitis and Wilson [38] and then perfected by Gustaffson [7] around the time when STED had started gaining popularity. This technique works in principle with the moiré effect that is primarily just a visual perception that results from combination of two or more superimposed patterns with lines or dots. SIM makes use of excitation light to develop an illumination pattern that can be superimposed upon the structures to be imaged. Interference from this illumination pattern and the illumination from different structures can then undergo Fourier transformation to obtain

superresolution images. Further, details of the same are discussed in the following section.

Thus, it is safe to say that superresolution has exceptional application in the domain of microscopy, especially for imaging microbiological structures and organisms using visible light. The various methods have proved useful in their respective applications. However, there are still gaps in the evidence of use of functional methods of superresolution, like SIM, in providing unprecedented results within the scope of resolution of microscopes. This area needs greater exploration to strengthen the available evidence to drive the use of this technique in practical and commercial scenarios.

## 3.3 Structured Illumination Microscopy

Structured illumination microscopy or SIM is one of the techniques that helps attain resolution beyond the diffraction limit, as explained by Ernst Abbe. It was first introduced by Neil et al [38] after a study that was examining the use of optical sectioning procedure to eliminate the background noise that is observed in wide field microscopy. They imaged a lily pollen grain using their set up, and they found that their images, obtained from wide field optical microscope, were at par with confocal microscopes. Additionally, all the background noise that was basically out-of-focus could be eliminated using SIM. This helped attain high resolution images with greater focus.

Following this, Gustaffson et al, made use of the same principle to improve the lateral resolution in a linear [7] and a non-linear form [39]. In the first experiment, the researchers illuminated the sample with a series of excitation light patterns. These patterns were then processed linearly to reconstruct the image. The resolution of the reconstructed image was twice the original image (Figure 3.3). In the second experiment, the researchers primarily demonstrated SIM making use of the non-linearity that occurs due to saturation of excitation. By this method of image processing, they were able to attain a resolution of <50 nm.

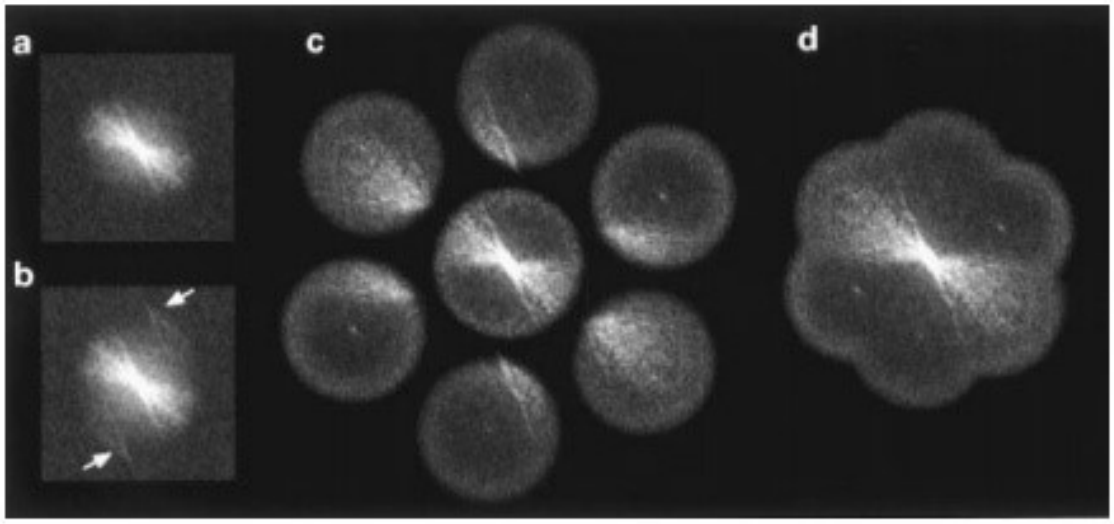


Figure 3.3: Application of SIM and linear image processing. All pictures represent Fourier transformed images: A. Original image of the sample with normal illumination, B. Image of sample with SI; notice arrows represents displaced information from other regions superimposed on the normal information, C. Recombination of images, D. Reconstructed image using information from other patterns; notice that in the final reconstructed image gain details by an order of 2 beyond the original image [7].

SIM is a simple procedure and has gained vast popularity among the scientists and researchers. It can be performed to obtain 2D or 3D images [40] and works well on

transparent specimens in unification with fluorescence microscopy [41] by excluding emission from fluorophores have a potential to add noise to the actual image signal.

These experiments reinforced the importance and application of SIM. However, it is important to understand how the SIM actually works. The illumination pattern, which is the unique feature of SIM, can be produced in different ways. The interference pattern that is obtained during SIM is often described as fringes that are known to be sinusoidal in nature. Often researchers have made use of a mechanically moving diffraction grating at low speed to produce these sinusoidal fringes [7]. However, the low speed of the motion of these gratings was also the cause of low precision of the phase shifts that resulted due to the interference of the illumination pattern and the sample upon superimposing the two.

Thus, techniques were developed to increase the precision of movement and speed of this motion. One such way to overcome the limitations of physical grating use in SIM can be achieved by the use of spatial light modulators or SLM. An experiment conducted by Chang et al. [40] made use of the SLM to obtain desired images. The researchers intended to generate interference illumination patterns are four positions: $0^{o}$, $45^{o}$, $90^{o}$ and $135^{o}$. They used a LCD SLM to for altering the patterns and noticed that this process was quite rapid and very precise. Additionally, they obtained the four interference patterns at a high contrast and equivalent periods. This allowed them to attain high and accurate lateral resolution. This study was done on biological specimen

and proved useful for the same. An SLM is essentially a mask placed between the light source and object that helps selectively illuminate the sample. The most widely used light source in these spatial modulators for the purpose of illumination is the light emitting diode or LED. It is known to be cost-effective and with the narrow emission bandwidths, LED's have a low spatial coherence which results in reducing any speckle noise. One such SLM that can uses LED as a light source is called the Digital MicroMirror Device or DMD.

## 3.4 Digital Micromirror Device

A Digital Micromirror Device (DMD) is an optical semiconductor micro electromechanical (MEMs) device used for DLP projection technology (Figure 3.4). It was invented by Dr. Larry Hornbeck and Dr. William E. "Ed" Nelson of Texas Instruments in 1987.

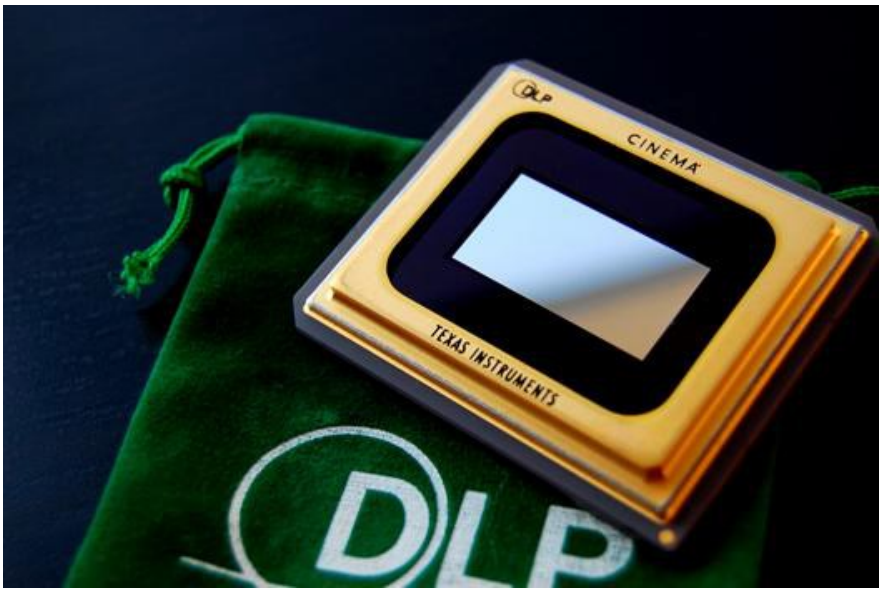


Figure 3.4. A Digital MicroMirror Device chip [42].

The DMD is a type of SLM, often called a pixelated spatial light modulators. A pixelated spatial light modulator contains a montage of distinct elements and can operate by transmission or reflection [43]. A DMD on the other hand makes use of multiple small mirrors with discrete pixel elements that are only a few micrometers in size. Hence, it is operated by means of reflection. Besides being an SLM, a DMD is also considered to be a microelectronic mechanical system or MEMS. It consists of millions of micromirrors that are controlled by underlying CMOS electronics. Because DMD uses reflection for its operation, it becomes an optical MEMS device. DMD has greater speed, precision and broadband capability that puts it above its other counterparts for the purpose of spatial light modulation. [44]

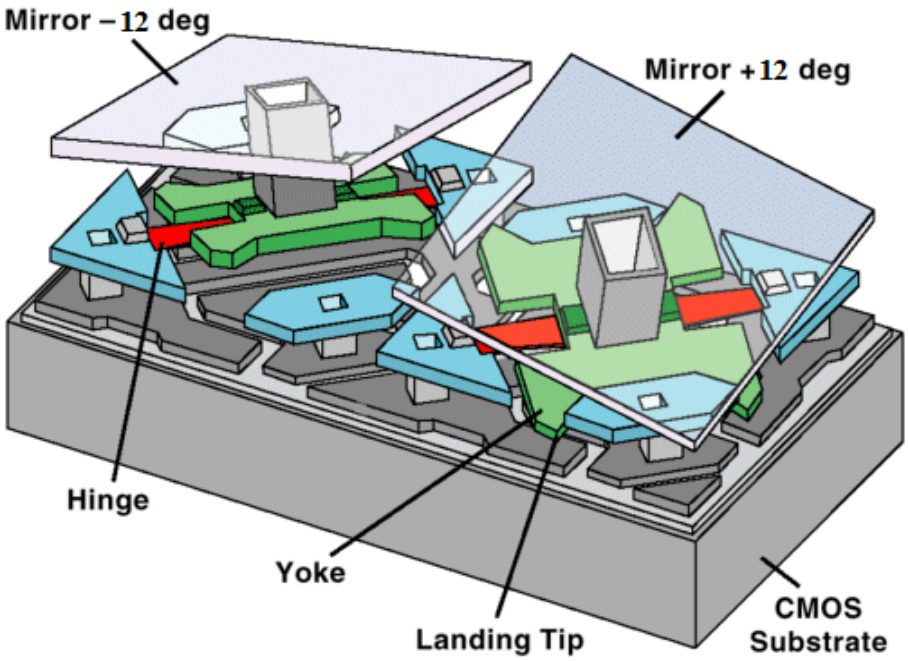


Figure 3.5. Two DMD pixels. The figure shows the position in which the mirrors are mounted that help attain the on and off stages of the DMD [45].

A DMD consists of a multitude of these micromirrors. These are specifically tilting in nature that provide for its ability to generate interference illumination patterns. The tilting is caused by torsion-hinges that connect the micromirrors to their mount. The hinges permit tilting to either a +12 degree or –12 degree state or the on and off stages. In the on state, light from the projector bulb is reflected into the lens making the pixel appear bright on the screen. In the off state, the light is directed elsewhere (usually onto a heatsink), making the pixel appear dark (Figure 3.5)[45].

Each mirror is mounted atop a static random access memory (SRAM) cell. This allows application of voltage to either one of the address electrodes, creating an electro-static attraction. This generates quick rotations in the mirror until the landing tips make contact with the electrode layer. At this point the mirror is electro-mechanically "latched" in its desired position [46].

DMD finds wide applications in the field of microscopy for its high speed, efficiency and easy availability. Many researchers have employed it to obtain high resolution images. Dan et al [47], used a DMD with low coherence LED as an illumination device to obtain superresolution in optical sectioning microscopy. They used the DMD for fringe projection and were successful at obtaining lateral resolution of 90 nm and an optical sectioning depth of 120 μm. Their result indicated the efficacy of use of DMD to obtain superresolution in 2D microscopy and good optical sectioning depth in

3D microscopy. Additionally, the DMD was found to be cost effective, speckle noise free and permitted an ease of access to multi-switchable wavelengths.

Thus, this project is aimed at designing a functional model of reconstructing blurred images with high resolution above the diffraction limit. Additionally, we intend to make use of the DMD to obtain high resolution two-dimensional images of specimens as seen through a fluorescence microscope. The following sections further describe our methods and results.

# CHAPTER 4

# STRUCTURED ILLUMINATION MICROSCOPY

## 4.1 Introduction

### 4.1.1 Principle of SIM

Structured illumination microscopy uses sinusoidal illumination to heterodyne the high frequencies of the image into the passband of the imaging system.

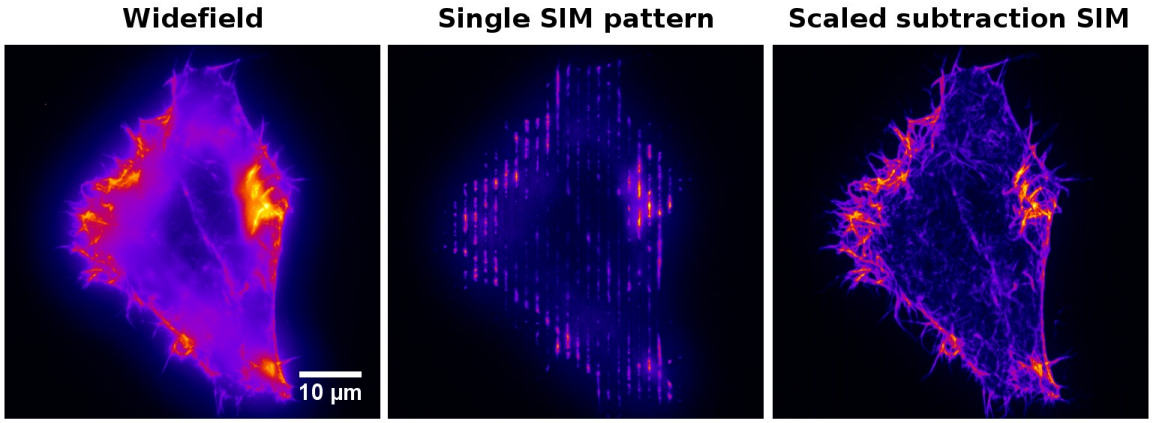


Figure 4.1: Imaging Process Structured Illumination Microscopy done on a biological sample. The central image shows the excitation pattern superimposed [48].

As described earlier, SIM makes use of the moiré effect. Moiré effect is basically a visual perception that is a result of interference of a pattern of lines or dots. The changing orientations result in shifting of high frequency components that make up the moiré pattern. These components are shifted so that it lied within the bandwidth of the microscope. This is a result of a frequency mixing process. Usually, a grid lying in the aperture of an illuminating device helps create the moiré effect. The moiré effect thus,

helps attain finer spatial frequencies from the sample. These can then be functionally processed through Fourier transformation. The information in the interference pattern that is otherwise hidden, can be extracted now. To create the interference pattern or the fringes, SIM makes use of the grating as a mask or SLMs such as DMDs (Figure 4.2).

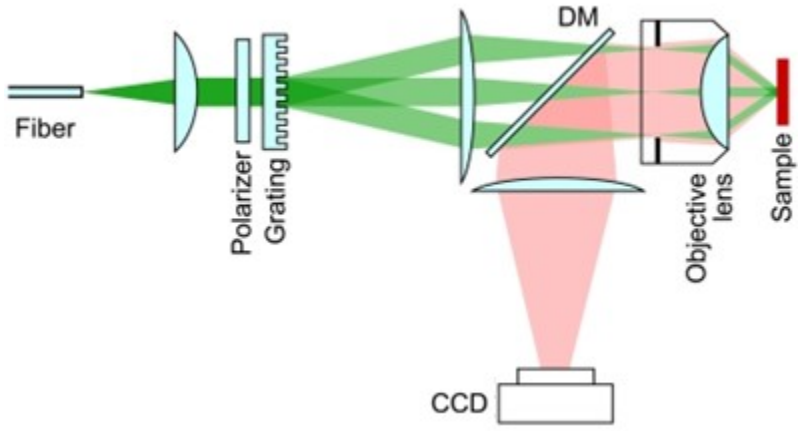


Figure 4.2: A set-up of a structured illumination microscopy using a grating [48].

The grating results in development of an excitation field that is sinusoidal in nature. The grid can be shifted by means of rotating the micromirrors that make up the DMD. This shift rotates the illumination pattern. As multiple low resolution images are obtained, they can be appropriately collated to make one high resolution image.

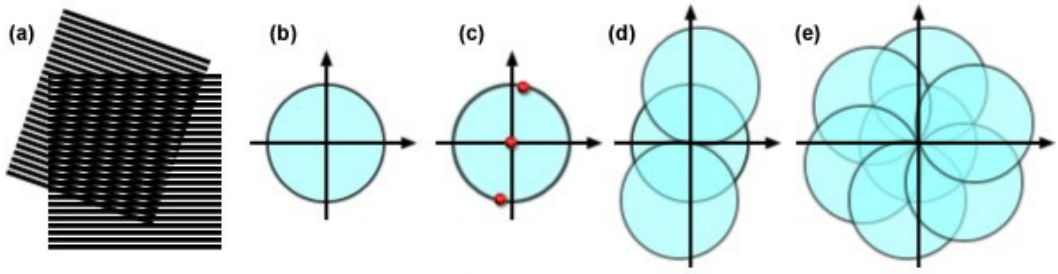


Figure 4.3: The concept of SIM: The moiré effect resulting in interference patterns is shown in figure (a). (b) Represents the low resolution information (the circular observable region) (c) depicts the sinusoidal interference in frequency domain while (d) is representative of offset regions caused by the interference. (e) Represents the collation of multiple low resolution images from different orientations and phases. [7]

As the high resolution elements are extracted, they are then aggregated together to form the final high resolution reconstructed image. Other irrelevant information, mostly the blur associated with out-of-focus elements can be rejected. As an end result, a higher lateral and axial resolution output can be attained. (Figure 4.3) The optical sectioning strength for the 3D SIM and the spatial resolution for 2D SIM increases as the spatial frequency of the fringes increases. In the upcoming section the complete understanding of structured illumination microscopy is developed.

### 4.1.2 Illumination Pattern and Reconstruction Components

Structured light is vital for structured illumination microscopy. The sample is to be illuminated by structured light heterodyne the high frequencies of the image into the passband of the imaging system. For this project, the illumination mask is in the form of a one dimensional grid that presents as a sinusoidal pattern that can be mathematically expressed as follows [7]:

$$I_{excitation} = 1 + \cos(2\pi f_o x + \varphi) \tag{4.1}$$

Here φ is the phase and $f_0$ is the frequency of the pattern. In Matlab, this equation can be implemented in discrete Fourier transforms which, in frequency domain, can be described as follows:

$$I_{excitation} = \delta(f) + \frac{1}{2}\delta(f+f_0)e^{-i\varphi} + \frac{1}{2}\delta(f-f_0)e^{i\varphi} \tag{4.2}$$

If an illumination pattern is applied on an input signal h(x), it can be presented as:

$$h_i(x) = h(x) \cdot (1 + cos(2\pi f_o x + \varphi)) \tag{4.3}$$

The Fourier transform of this equation can then be represented as:

$$H_i(f) = H(f) + \frac{1}{2}H(f + f_0)e^{-i\varphi} + \frac{1}{2}H(f - f_0)e^{i\varphi}. \quad (4.4)$$

The three components formed in Equation 4.4 have high frequency information contained in them which as separate components can be showing by Figure 4.4 [40].

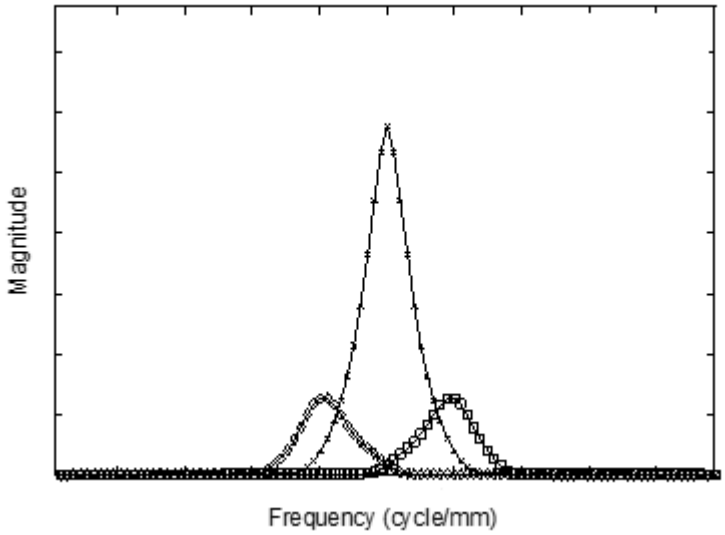


Figure 4.4: The observed $H_i(f)$ is a sum of three contributions required for superresolution.

The components characterized by $f + f_0$ and $f - f_0$ are the higher order frequencies that contain information outside the passband of the optical system which are used to create the higher resolution image. In order for these to be represented within the passband, the frequency $f_0$ must be less than the cut-off frequency of the OTF of the optical system [38].

Thus the resultant signal $H_i(f)$ along with the illumination pattern aliases some higher frequency components down into the passband. [7], [49], [50] Thus, the passband

allowed by the OTF, now has various overlapped components of higher and lower frequencies [51].

The observed $H_i(f)$ is a sum of three contributions, and it is not possible to separate them using a single$G_i$. In order to get the three components in Equation 4.4, the three different illumination pattern should be applied with at least three phase values. In the case of two-dimensional images at least three phases and different orientations are required [52].

### 4.1.3 Blurring Process

By definition, the point spread function (PSF) describes the response of an imaging system to a point source or point object. Consider that we are viewing an original image, *f(x)*, through an Linear Translation Invariant (LTI) imaging system, the information that can be observed through it, (x), is the information allowed by the PSF of that system, [7] , [40] , [49], [51].

$$h(x) = PSF * f(x) + n(x) \tag{4.5}$$

Where * is convolution and *n(x)* is noise present in the system. This principle can be better understood in the frequency domain:

$$H(f) = OTF \cdot F(f) + N(f) \tag{4.6}$$

Where H(f), F(f), and N(f) are the Fourier transforms of h(x), f(x), and n(x), respectively, and the Optical Transfer Function (OTF) is the Fourier transform of the PSF. [52].

As we can see that the output signal, h(x), has a different peak value and has lost some of the details that existed in the input, f(x).This means that the PSF has widened and blurred some of the details of f(x) [51], [52].The following figures (Figure 4.7) represents the above in the frequency domain:

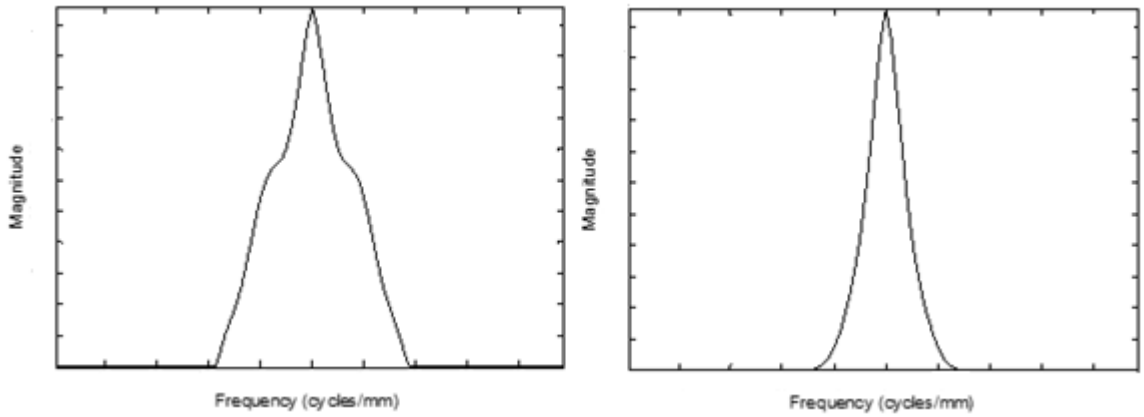


Figure 4.5: Effect of PSF on a signal in frequency domain. Left: Input signal Fourier transform, F(f), Right: Output signal Fourier transform, G(f).

Here the OTF caused the output, H(f), to lose frequency components beyond the cutoff frequency of the OTF that existed in the input, F(f) [51], [52]. Representing a microscope system mathematically by equations (4.5) and (4.6) allowed researchers to develop Superresolution techniques [49], [51], [52].

Abbe's theory [1] showed that diffraction limits define a finite range of spatial frequencies that can be transmitted through a microscope. Consecutively, we can design a PSF with a shape that would represent the effect of viewing an image through the lens of a microscope. The same phenomena can be applied to simulate the process of structured illumination microscopy mathematically, which would further allow us to simulate the effects of an imaging system on an image in Matlab.

$$OTF = e^{-2((\sigma_x \pi (f_x - 255))^2 + (\sigma_y \pi (f_y - 255))^2)} \quad (4.7)$$

To simulate the effects of blurring which is introduced by a typical optical microscope, we will have to select an OTF that would replicate this effect mathematically. In this simulation, only the effects of blurring has been taken into account. Other type of noise errors have been neglected. The OTF of an optical microscope can be represented by [49], [51].

### 4.1.4 Applying Structure Illumination

After the generation of illumination patterns and blurring of the image, the process of structured illumination is to be performed. Since we are implementing structured illumination microscopy with three phase shifted images, we would need three illumination patterns with phases, φ=0, $\frac{2\pi}{3}$, and $\frac{4\pi}{3}$. Appling these phase to equation 2.3, structured illumination pattern takes the form:

$$i = 1 + \cos(2\pi\ (f_0 x + f_0 y) + \varphi) \quad (4.8)$$

The components are selected so that the excitation pattern is located within the passband determined by the OTF so that higher frequency components can be viewed and extracted [49], [51]. These illumination patterns, seen as a pattern of parallel stripes on h*(x, y),* are coded in Matlab.

For 2D images, let us assume an image to be represented as f(x,y). The illumination patterns are imposed on the image, $F(f_x, f_y)$, which the Fourier transform of the image. In Fourier domain, H(f) is the transform of the output image h(f). The imposition of these three illumination patterns and the effect of viewing these images through an optical microscope can represented as:

$$\begin{aligned} H1(f) &= F(f_x, f_y)(Pattern1(\varphi = 0)) \cdot OTF \\ H2(f) &= F(f_x, f_y)\left(Pattern2(\varphi = \tfrac{2\pi}{3})\right) \cdot OTF \\ H3(f) &= F(f_x, f_y)\left(Pattern(\varphi = \frac{4\pi}{3})\right) \cdot OTF \end{aligned} \tag{4.9}$$

Where IP stands for illumination pattern. In simple terms we now have three equations to solve for three components. All these equations are solved in Matlab in Fourier space, which can be represented as:

$$\begin{bmatrix} \mathrm{H1(f)} \\ H2(f) \\ \mathrm{H3(f)} \end{bmatrix} = \begin{bmatrix} e^{j0} & e^{j0}e^{-j0} \\ e^{j0} & e^{j\frac{2\pi}{3}}e^{-j\frac{2\pi}{3}} \\ e^{j0} & e^{j\frac{4\pi}{3}}e^{-j\frac{4\pi}{3}} \end{bmatrix} \times \begin{bmatrix} \mathrm{D_1} \\ \mathrm{D1_1} \\ \mathrm{D2_1} \end{bmatrix} \tag{4.10}$$

Where $D_1$ represents the central unshifted band, $D1_1$ represents shifted sideband on one side and $D2_1$ represents the other shifted sideband for the first image when i=3. Each component has different frequency information used to create a higher resolution image. Rearranging to solve for the one unshifted and two shifted components Equation (4.2) can be rearranged as

$$\begin{bmatrix} \mathrm{D_1} \\ \mathrm{D1_1} \\ \mathrm{D2_1} \end{bmatrix} = \begin{bmatrix} e^{j0} & e^{j0}e^{-j0} \\ e^{j0} & e^{j\frac{2\pi}{3}}e^{-j\frac{2\pi}{3}} \\ e^{j0} & e^{j\frac{4\pi}{3}}e^{-j\frac{4\pi}{3}} \end{bmatrix}^{-1} \times \begin{bmatrix} \mathrm{H1(f)} \\ H2(f) \\ \mathrm{H3(f)} \end{bmatrix} \tag{4.11}$$

When we solve for the three independent linear components in Matlab, one component is unshifted and other two of the components are shifted [52]. These shifted components carry the frequencies that were not accessible by the passband of the OTF. The unshifted component is retained as it is and the shifted components are to be moved in Fourier space to shift the spatial frequencies of these components from being centered at f - $f_o$ and $f + f_o$ to being centered at 0 [49], [51], [52]. After the shifting of these components towards 0, all of these components can be combined appropriately to obtain a superresolved image.

### 4.1.5 Reconstruction Process

Wiener deconvolution can be used to increase image resolution by a factor of 2 [7] and [49]. In this thesis we used Wiener deconvolution for image reconstruction for super-resolution while neglecting external errors introduced because of noise.

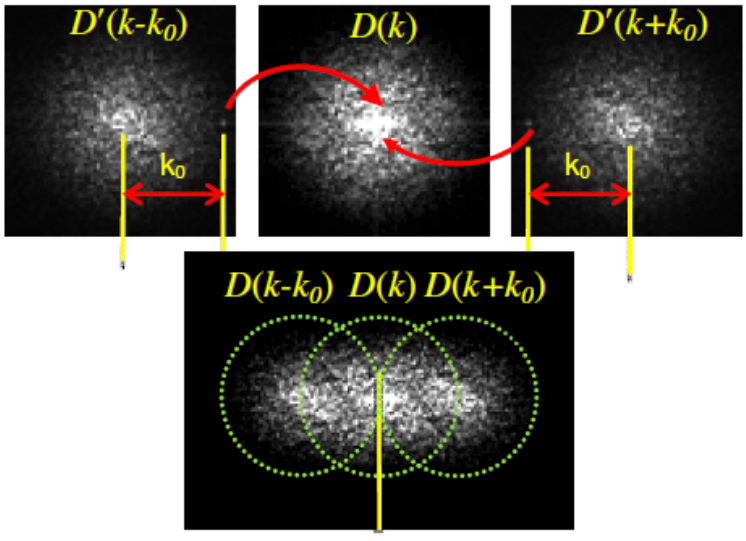


Figure 4.6: Two shifted components and one original unshifted component acquired with 0° illumination pattern at three phases, reconstructed to form a higher resolution image in Fourier space. [40].

For calculation of these three components, required for super-resolution, each component is considered to be a separate low resolution image. Each lower resolution image would need a separate and different OTF. Centralbands of these components are left as it is but the sidebands of these components are to be shifted back to the central frequency. The components can now be represented as

$$\mathrm{D_1}: (\mathrm{fx}, \mathrm{fy}) = \mathrm{OTF} \times \mathrm{F}(\mathrm{fx}, \mathrm{fy})$$

$$\mathrm{D1_i}: (\mathrm{fx}, \mathrm{fy}) = \mathrm{OTF} \times \mathrm{F}(\mathrm{fx} - \mathrm{fxi}, \mathrm{fy} + \mathrm{fyi}) \tag{4.12}$$

$$\mathrm{D2_i}: (\mathrm{fx}, \mathrm{fy}) = \mathrm{OTF} \times \mathrm{F}(\mathrm{fx} + \mathrm{fxi}, \mathrm{fy} - \mathrm{fyi})$$

These components are for one single image illuminated by one of the phases of the three phases. The low resolution component bands showed in Equation 4.13 can be used to define the shifted versions of the OTF corresponding to the components. These are required for the deconvolution in Matlab. For the central unshifted band: $\mathrm{OTF1} = \mathrm{OTF}\ (\mathrm{fx} + 0, \mathrm{fy} + 0)$; for the shifter band 1: $\mathrm{OTF2} = \mathrm{OTF}\ (\mathrm{fx} + \mathrm{fox1}, \mathrm{fy} - \mathrm{foy1})$ and for shifted band 2: $\mathrm{OTF3} = \mathrm{OTF}\ (\mathrm{fx} - \mathrm{fox1}, \mathrm{fy} + \mathrm{foy1})$.

Since these patterns in Fourier space represent different perspective of the same object, we have to figure out to how to use these components for resolution enhancement so that each low resolution image can contribute to increase in image quality. Wiener deconvolution for such purpose was introduced in [7], [53] to deconvolve different images acquired from various other sensors. Here it would be used with various shifted OTFs. So the shifted version of the components as represented in Figure 4.8 can be defined as

$$D1 = Centralband1\,(fx + 0, fy + 0)$$

$$D2 = Sideband11\,(fx - fx1, fy + fy1) \tag{4.14}$$

$$D3 = Sideband21\,(fx + fx1, fy - fy1)$$

Components represented in Equation 4.14 and 4.15 are used to reconstruct the image using Wiener deconvolution as proposed in [7] [49] [52]:

$$F(f_x, f_y) = \frac{\sum_{i=1}^{3} OTF_i^* \cdot D_i}{\varepsilon + \sum_{i=1}^{3} |OTF_i|^2} \tag{4.16}$$

Where $OTF_i$ represents the components defined in 4.14, $*$ represents the conjugate of $OTF_i$, $D_i$ represents $i$ = 1 to 3 representing three images and $\varepsilon$ is noise to signal ratio. $F(f_x, f_y)$ is inverse Fourier transformed to given us the superresolved image f(x,y).The next section explains the complete simulated process of structured illumination microscopy.

## 4.2 Simulation

### 4.2.1 Simulation Design

The simulation process was designed on Matlab 2013a. The computer used was an Acer 5740G, 2.27-GHz Intel Core i5-430M processor and 4GB of DDR3 RAM.

The Matlab code was written step by step in accordance with the simulation design which is shown in Figure 4.7:

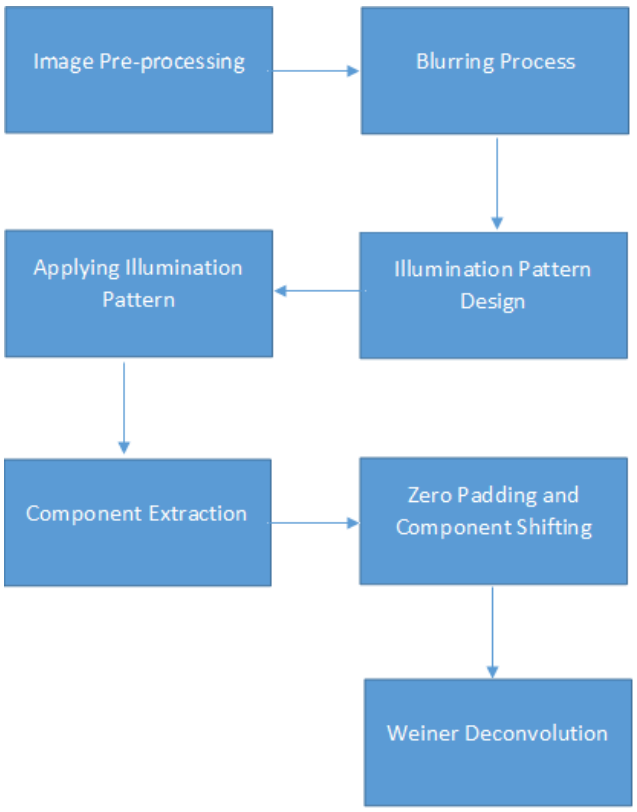


Figure 4.7: Simulation Process

### 4.2.2 Image acquisition and pre-processing

The first step for the simulation deals with reading an image for the complete process. To assess effectiveness of the simulation a total of four images were used. All of the images used were high resolution images with sharp edges, high level of detail, smooth areas, and contrast, which made them ideal for testing reconstruction methods and to generalize the study in a broader context.

So let us assume an image f(x, y) as represented in the Figure:

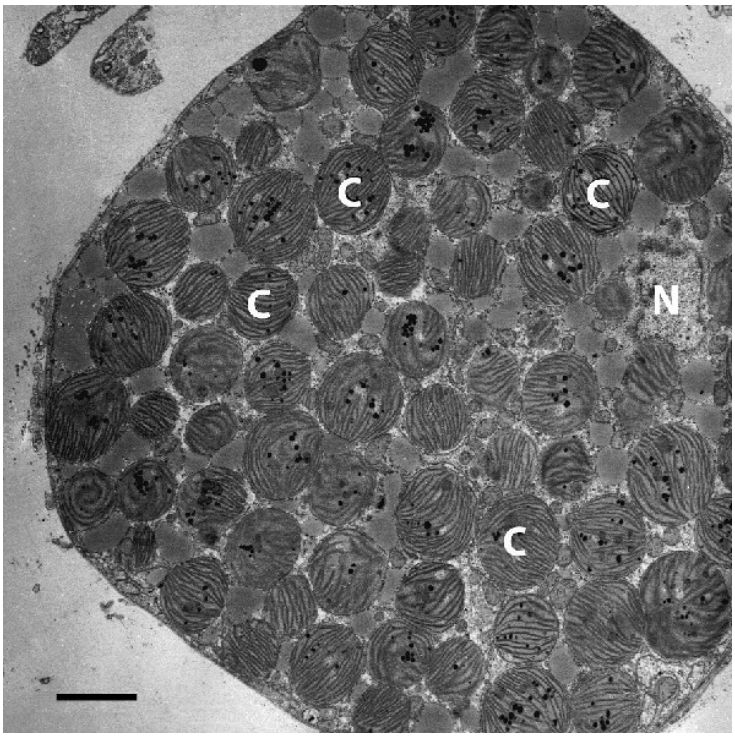


Figure 4.8: An electron microscope image of digestive tubule cell of Elysia clarki, densely packed with sequestered chloroplasts, where C = chloroplast and N = cell nucleus. Scale: 3 μm. Image resolution: 2000 × 2000 px [54].

The image was read in Matlab and then greyscaled. The maximum intensity of the image was limited to 1000. After this, 2-D fast Fourier transform was applied to the image to convert the image for Fourier calculation for the next steps. Discrete Fourier transform results in the image as $F(f_x, f_y)$ in frequency domain. For simulating the SIM process and analyzing the theoretical results, we used a total of 4 microscopic images. One has been already shown in Figure 4.8 the other three are shown in Figures 4.9, 4.10, 4.11:

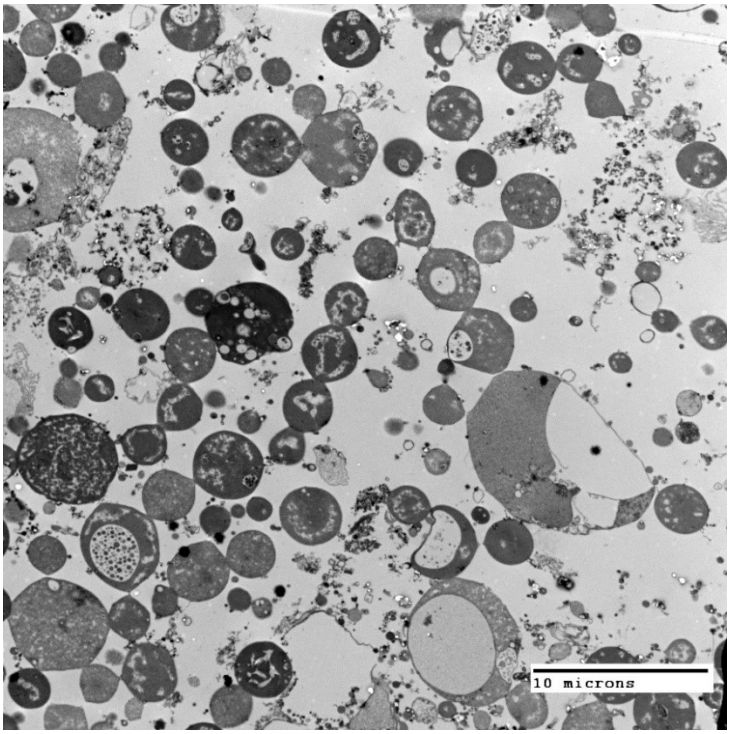


Figure 4.9: An electron microscope image of L-form Bacillus subtilis, showing a range of sizes. Scale: 10 μm. Image resolution: 1824 × 1824 px [55].

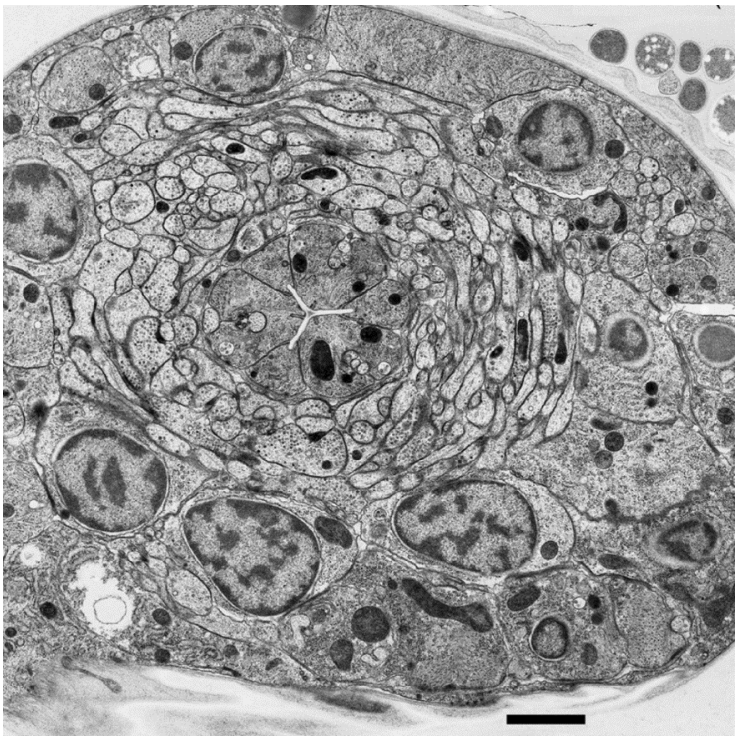

Figure 4.10: 3-FOLD EMBRYO( Nerve Ring) of frozen C. elegans. Scale: 1 μm. Image resolution: 1020 × 1020 px [56].

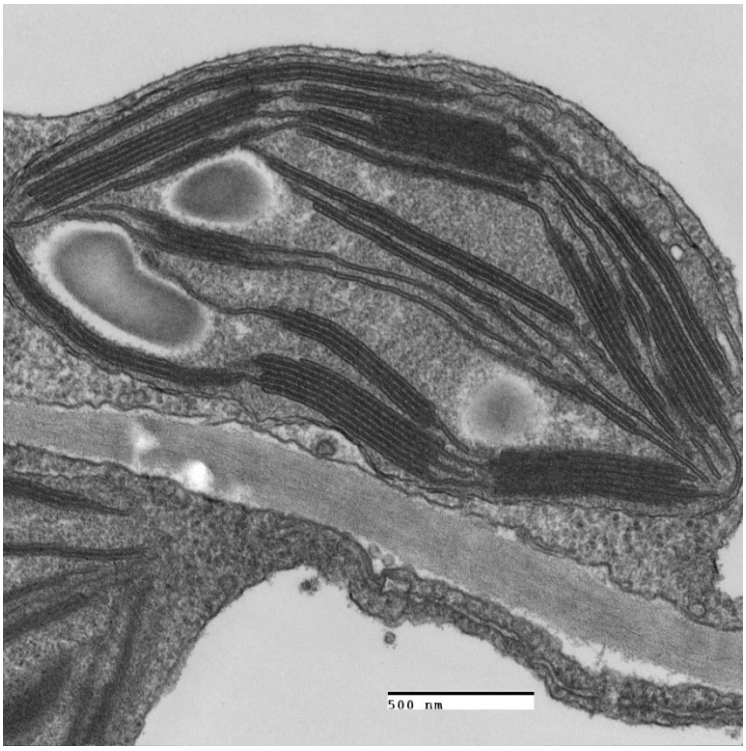


Figure 4.11: Transmission electron microscope image of a chloroplast of Coleus blumei. Scale: 500 nm. Image resolution: 2048 × 2048 px [57].

### 4.2.3 Blurring Process

For the purpose of simulating an image to seem as one obtained from a low resolution microscope, a blurring process was conducted using the software.

The OTF described in Equation: was realized in Fourier space in Matlab. Then the function $F(f_x, f_y)$ was multiplied with the OTF which resulted in

$$H(f_x,f_y) = F(f_x,f_y) \cdot \text{OTF} \tag{4.17}$$

Since $F(f_x, f_y)$ is matrix in space hence (.) represents element-wise multiplication. Applying inverse Fourier transforms to $H(f_x,f_y)$ resulted in it being converted back to the

spatial domain resulting in the blurry image, h(x, y) which can be seen in the resultant image in the Figure 4.12.It can be clearly seen that the image has lost it sharpness and small features are blurred to such an extent that the fine structures present in the image are no more resolvable, i.e., the blurred image has lost its resolution to some extent.

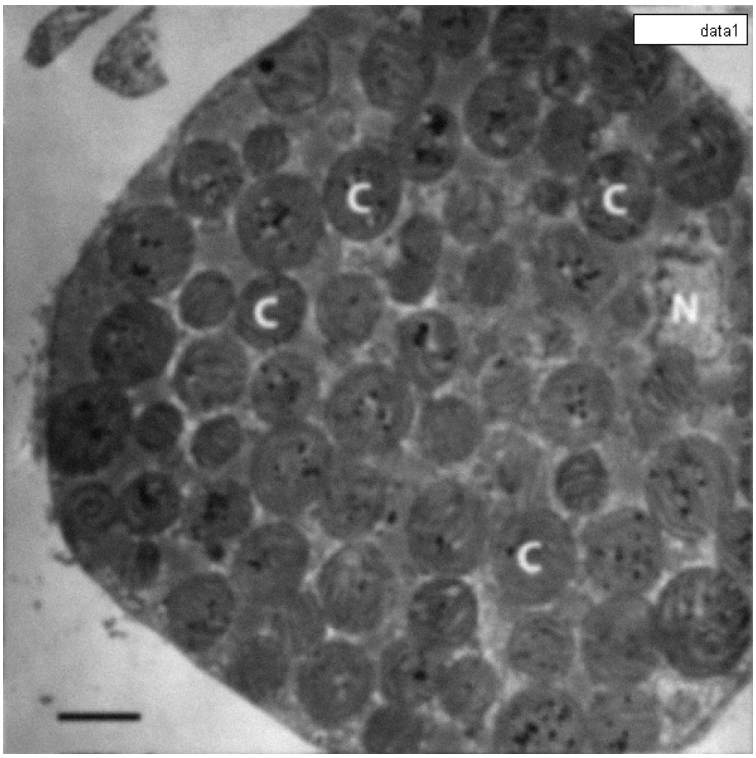


Figure 4.12: Blurred image of Figure 4.10

Thus, because of the OTF, the higher frequency components were blurred and hence became hard to recognize.

### 4.2.4 Illumination Pattern

For this project, we decided to perform the structured illumination microscopy process using three illumination patterns. The illumination patterns were coded as a two

dimensional matrix in Matlab. The dimensions of the matrix were kept equal to the dimensions of the input image f(x, y).

The illumination patterns were created using Equation 3.2 with phase shifts of $\varphi=0$, $\frac{2\pi}{3}$, and $\frac{4\pi}{3}$. The illumination pattern can be seen in the following Figure 4.13:

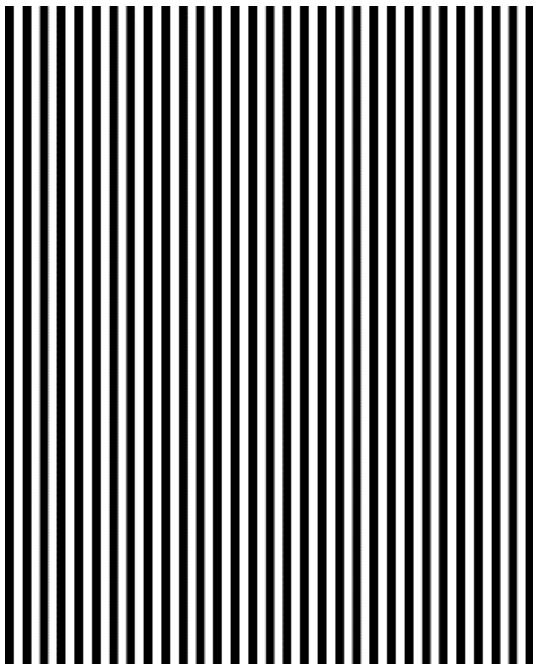

Figure 4.13: Illumination Pattern with phases, $\varphi=0$

These illumination patterns were applied to the image $H(f_x, f_y)$ resulted in a pattern of parallel stripes to be imposed on the image. For this process, both the image and the pattern first underwent 2-D fast Fourier transform and then element wise multiplication was done between the image and the illumination pattern in Matlab. 2-D inverse fast Fourier transform was applied to the result after the pattern application process.

### 4.2.5 Image Reconstruction Process

**Component Extraction:** In the reconstruction process, the first step was to extract the SI components in accordance to the Equation 4.3. The inverse matrix in the equation was entered in Matlab, which was multiplied altogether with the three image files procured after pattern application in matrix form.

**Shifting of Components towards 0:** We ended up with three independent linear components in Matlab of which one component was not shifted and other two of the components were shifted [5]. The unshifted component was retained as it was and the shifted components were to be moved in Fourier space to shift the spatial frequencies of these components from being centered at $f - f_o$ and $f + f_o$ to being centered at 0 [2], [4], [5]. For this process we used a function in Matlab, FourierShift2D.m, which is quite famous in the Matlab community. This function shifted the components cyclically. The function used the Fourier shift theorem. It utilized the principal that real inputs should give real outputs which stands true for images.

**Wiener Deconvolution:** The three low resolution images were then reconstructed using Wiener deconvolution process according to the Equation 4. The equation was realized in Matlab and the components of the two shifted images, which had now been shifted towards 0 of the unshifted image, were deconvoluted. The reconstructed images were expected to result in higher resolution or super-resolved images.

The results from the image reconstruction process and their mathematical analysis will be discussed in Chapter 5.

## 4.3 Experiment

After the theoretical model was developed and the complete process of structured illumination microscopy process simulated in Matlab, we wanted to test our model with actual experimental data. We decided to experimentally perform structured illumination microscopy in the lab. The experiment used an optical microscope modified for fluorescence and a Digital MicroMirror Device to provide structured illumination for the process.

### 4.3.1 Experimental Set-up

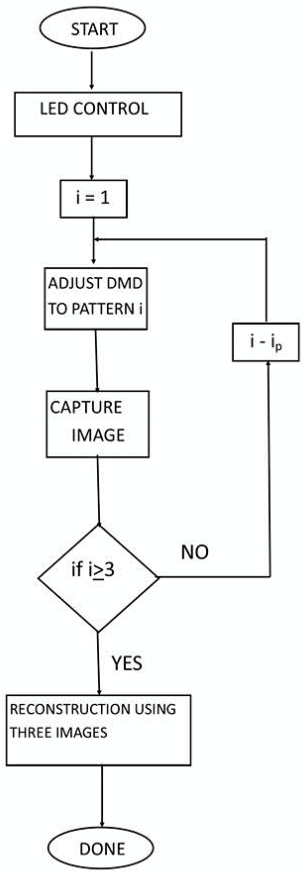


Figure 4.14: Flowchart representation of the experimental setup

The complete experimental setup can be understood by the flowchart in Figure 4.14. The main components of the experiment will be explained in the following sections.

### 4.3.2 Apparatus

#### 4.3.2a Fluorescence Microscope

The microscope used for this experiment was a Nikon Eclipse E600 which had been modified for fluorescence microscopy.

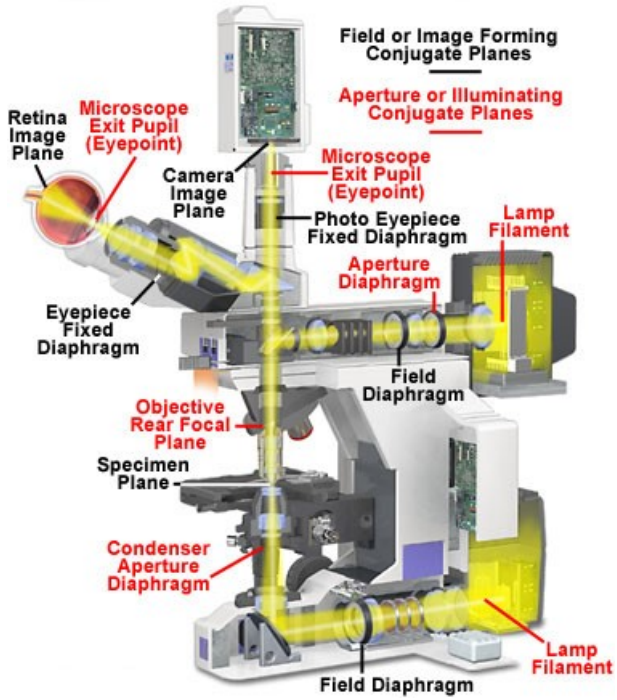


Figure 4.15: Nikon Eclipse E600; Notice the Epi-Illuminator or the Mercury Lamp illumination source which would be replaced with a DMD for this study. [58]

It was fitted with a Nikon 10X objective with 0.45 aperture. For this experiment, a Nikon Blue Excitation Filter Block B-1A was fitted in the microscope. It worked by passing excitation blue light of wavelength ~ 470-490 nm through itself. The original illumination source in our microscope was a Nikon HMX-4 Mercury Lamphouse. This

light source was removed from the microscope and the DMD was integrated through the Aperture Diaphragm.

### 4.3.2b. Digital Micromirror Device

A Digital Micromirror Device, manufactured by Texas Instruments, was used as a spatial light modulator in structure illumination microscopy. The DMD used for the purpose of this project was LightCrafter 4500 by Texas Instruments. It houses its own set of RGB LEDs as it illumination source.

Figure 4.16: LightCrafter 4500

The Lightcrafter 4500 comes with its own set of integrated optics. The LightCrafter 4500 featured a 0.45 WXGA chipset with its own light engine. Features:

- Two configurable input/output triggers
- RGB LED light engine with 150L light output
- Onboard LED Driver with 0-5A LED Driver
- Native DLP4500 resolution (912x1140)
- Image or video display up to WXGA resolution (1280x800)

### 4.3.2c. Charge-coupled Device Camera

A CCD camera from AmScope model MU300 was used to capture images for the experiment. The camera had a 3.1 Megapixel 1/2" color CMOS sensor which supports a maximum resolution of 2048 x 1536 pixels.

## 4.3.3 Procedure

The first step was to integrate the DMD with the microscope so that the illumination pattern produced by the DMD can be viewed in the sample plane of the microscope. The original illumination source of the microscope was removed to make way for the DMD. When the DMD was being integrated to fit as the Light Source of the Fluorescence Microscope, a problem was discovered with the Light Crafter 4500. The DMD chip was not in the same axis as its lens system. The focusing lens was found to be a bit off axis in respect to the DMD chip. So the integrated lens system had to be removed

Figure 4.17: LightCrafter 4500 with its integrated optics removed.

The DMD was then placed in front of the aperture at a distance equal to the focal length

of the DMD chip. For DMD to successfully project without loss in intensity and contrast in the focal plane of the microscope, the incoming light from the DMD had to be in a straight axis with the Aperture Diaphragm of the microscope. The image from the DMD was finally resolved on the sample plane of the microscope but there was a huge loss in intensity. The intensity pattern produced was faint when views on a sample object.

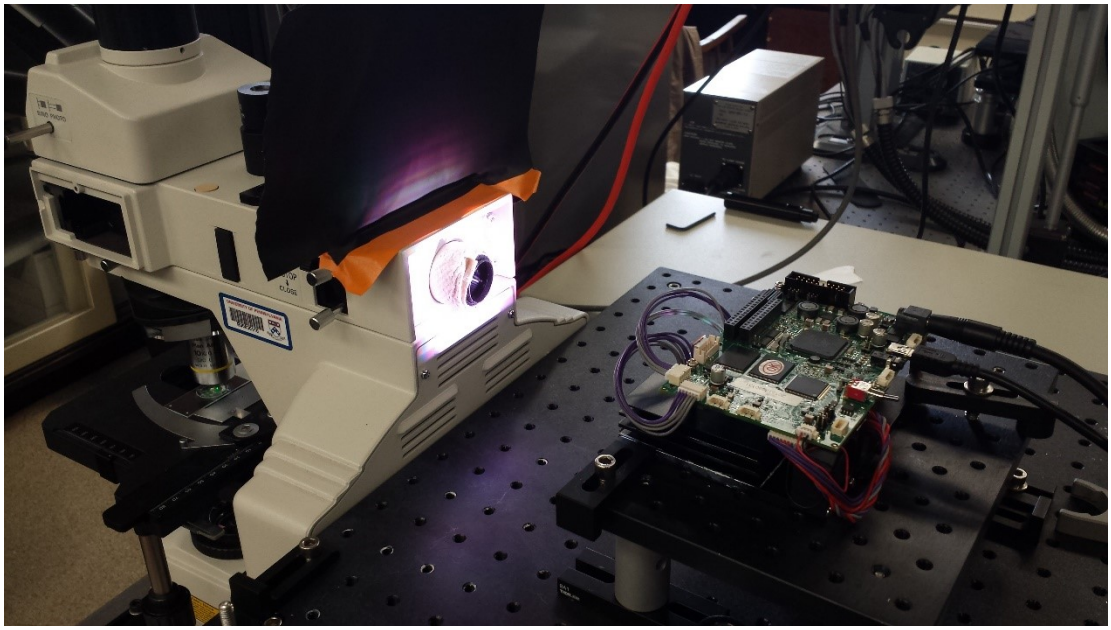

Figure 4.18: DMD placed on the axis of the Aperture Diaphragm of the microscope.

For the experiment, a fixed cover slip containing fluorescence fibers was used. Fluorescent materials have characteristic light absorption and emission spectra. Upon absorption of photons of the excitation wavelength, fluorochromes become excited into a higher, unstable energy state. This instability is then relieved by the subsequent production of photons of a lower energy emission wavelength. Here, the fluorescence fibers absorbed the blue light and emitted green light.

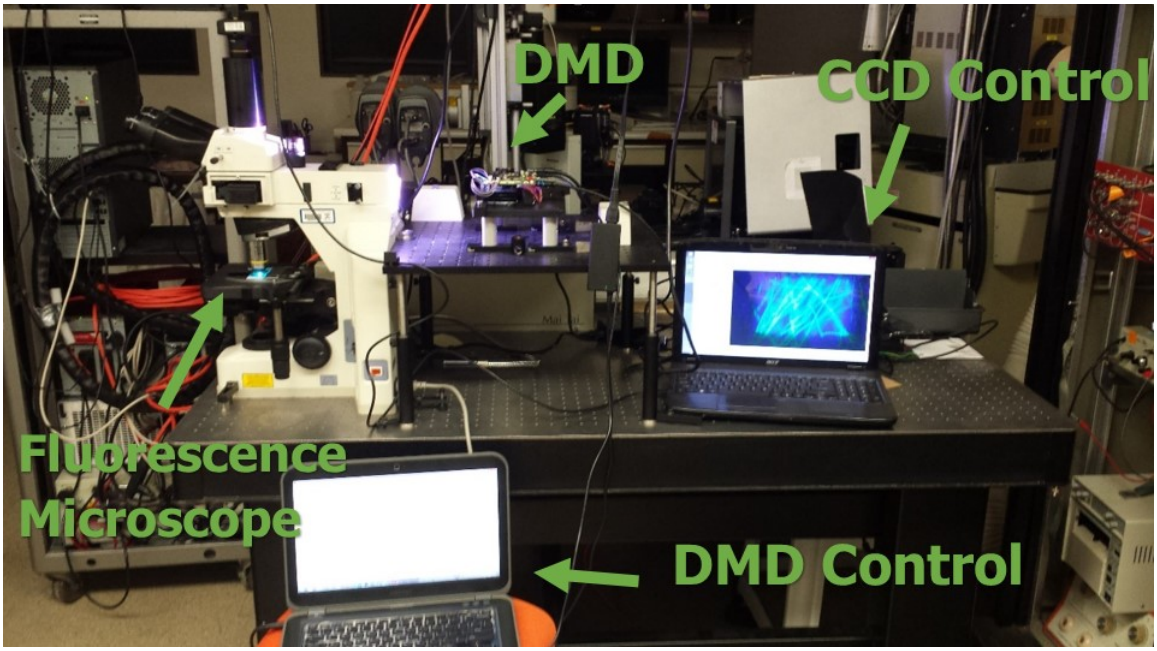

Figure 4.19: The complete experimental setup

.

For implementing structured light illumination, high accuracy fringe patterns of 912 x 1140 pixels with phases, $\varphi = 0$, $\frac{2\pi}{3}$, and $\frac{4\pi}{3}$ patterns were created in Matlab in Bitmap image format.

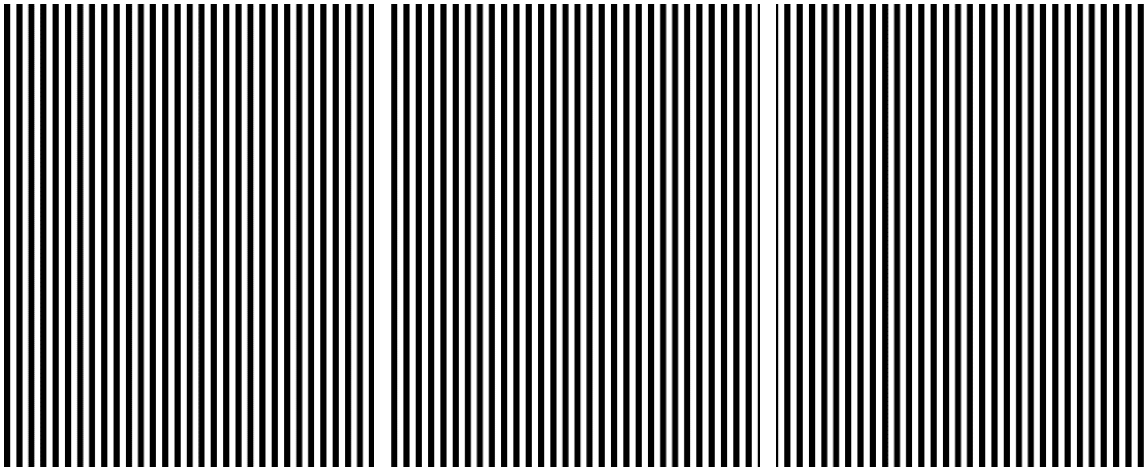
Figure 4.20: Phase shifted illumination Pattern with phases, φ=0, $\frac{2\pi}{3}$, and $\frac{4\pi}{3}$, respectively

All of the images were pixel matched to the pixel elements of the DMD to increase the effectiveness of the pattern. The uniformity tested with Matlab can be seen as shown in Figure 4.21:

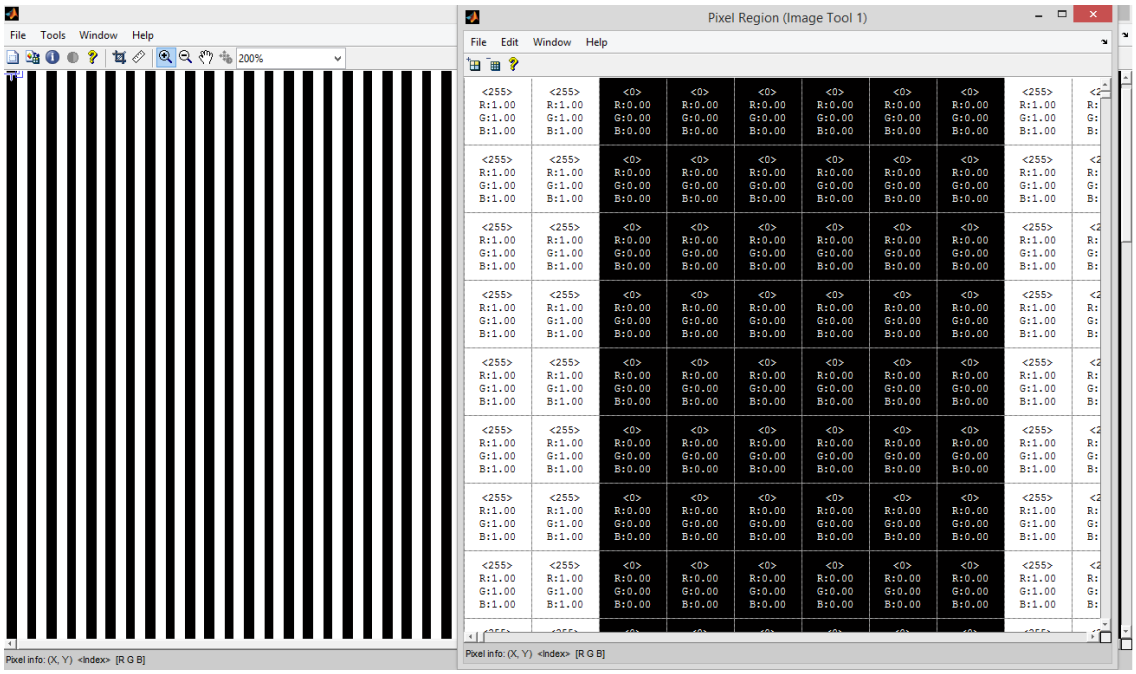


Figure 4.21: Pixel matching and inspection in Matlab

All of the patterns with different phase shifts and periodicity were stacked on an .IMG image file and a custom firmware was created to be loaded on the DMD SRAM. The Texas Instruments original firmware present on the DMD was deleted from the DMD's memory and the custom firmware was loaded by connecting the DMD with a computer through a microUSB cable. The patterns were then controlled by the LightCrafter 4500 GUI for projection in Pattern Sequence mode as shown in Figure 4.22. For each pattern, Pattern Exposure was done for 5 seconds, Image Load Time was set to 200 milliseconds and an internal trigger of 5 second was applied.

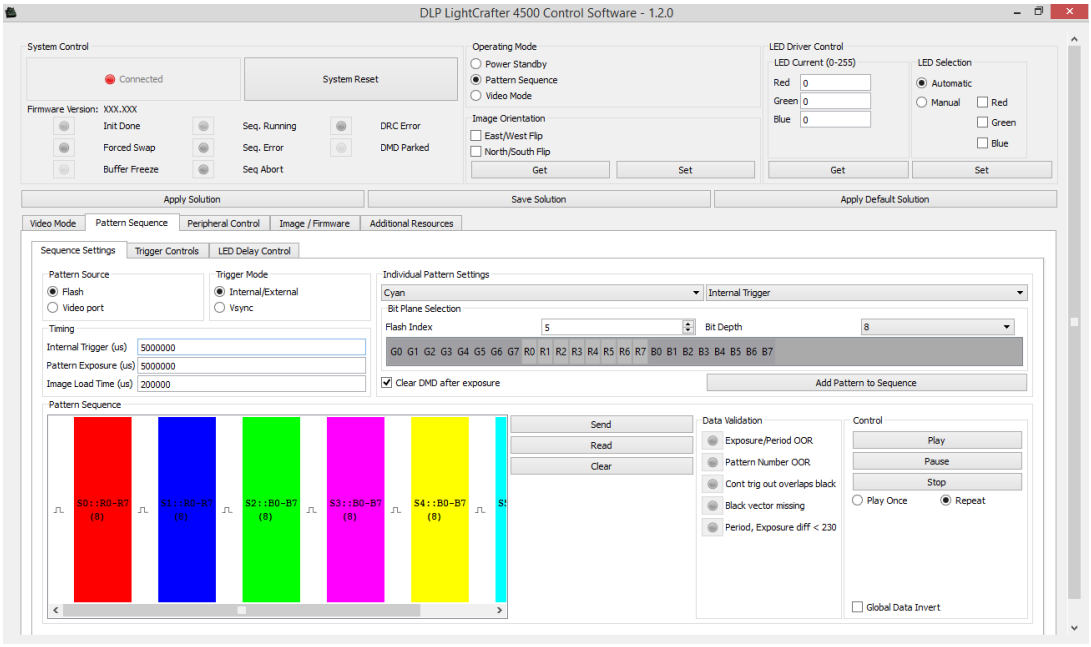


Figure 4.22: DMD Control setting in Pattern Sequence mode on LightCrafter 4500

Image acquisition was performed with the CCD camera with Exposure Time set to 0.601ms and Gain set to 3. After the application of structured illuminated light, the sample appears to be as shown in the following Figure 4.23.

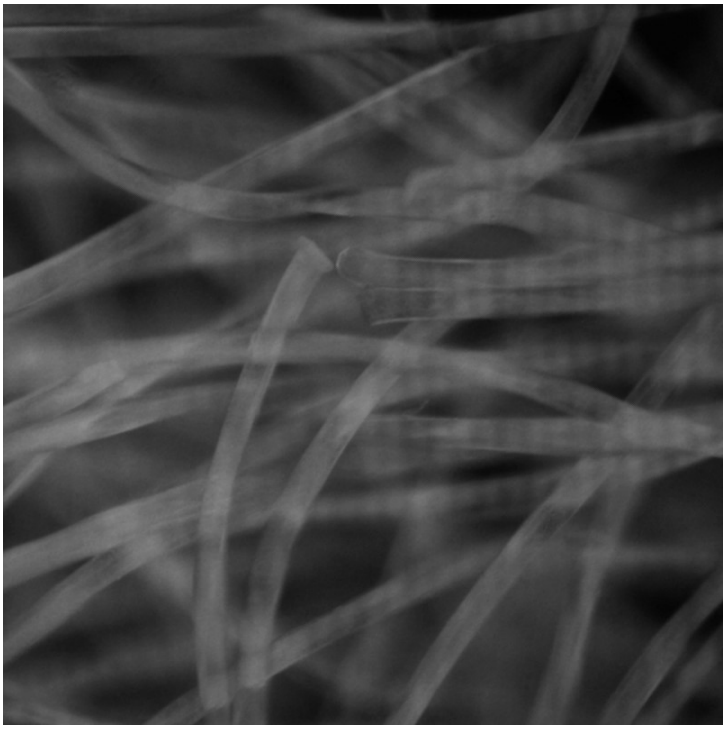

Figure 4.23: Structurally Illuminated view of the Fluorescence Fibers as seen by the CCD

Two computers were used for the experiment, one was used for DMD Control for patterns display and the other one was used for Image Acquisition. The captured images were reconstructed by the same algorithm as discussed in section 4.3 but with the OTF blurring process removed. The results of the reconstruction process would be discussed in the following Chapter 5.

# CHAPTER 5

# RESULTS AND DISCUSSION

The objective of this thesis was to develop the process of Structured Illumination Microscopy mathematically and then extended it to actual experimental setup. During this research the process of structured illumination microscopy was successfully developed mathematically and then the complete process was realized in Matlab as a simulation. Then our understanding of the concept was extended to an experiment which featured a fluorescence microscope and a Digital MicroMirror Device which was used to create structured illumination.

We noticed that our algorithm successfully super-resolved blurred images during reconstruction in the simulated tests. A considerable order of magnitude of resolution was gained in each of the 4 test images used in this research. In case of the experiment, we noticed that we obtained higher resolution images compared to the standard wide field image obtained through the same setup.

The results of reconstruction process from the simulation testing of the algorithm and the experimental setup with their interpretations are described further in this chapter.

## 5.1 Reconstruction and Qualitative Analysis of Images

We used a total of four images to test our simulation algorithm. All of these images haven been shown in Section 4.3 as Figures 4.10, 4.11, 4.12 and 4.13. All of these images had been taken through electron microscopes. The reason for using these images to test the algorithm was that these images have very high resolution and high image detail. Such images are ideal to compare reconstruction algorithms because it becomes easier to differentiate high contrast sharp edges and structures.

One of the important methods of comparing blurred images from superresolved images after reconstruction is visual inspection of images. Since reconstruction process introduces scaling and some noise in the images, some researchers believe visual inspection to be the most important criteria of comparing reconstructed images. For instance Schaefer et al [59] developed an algorithm using a parameter optimization approach for the purpose of artefact analysis and reduction. Although this was a secondary hypothesis, they concluded that the data they obtained using their algorithm was actually quite comparable to their interpretation by visual inspection of the images. For the purpose of our results, all of the reconstructed images are compared with their blurry images in the following figures (Figure 5.1, 5.2, 5.3, 5.4).

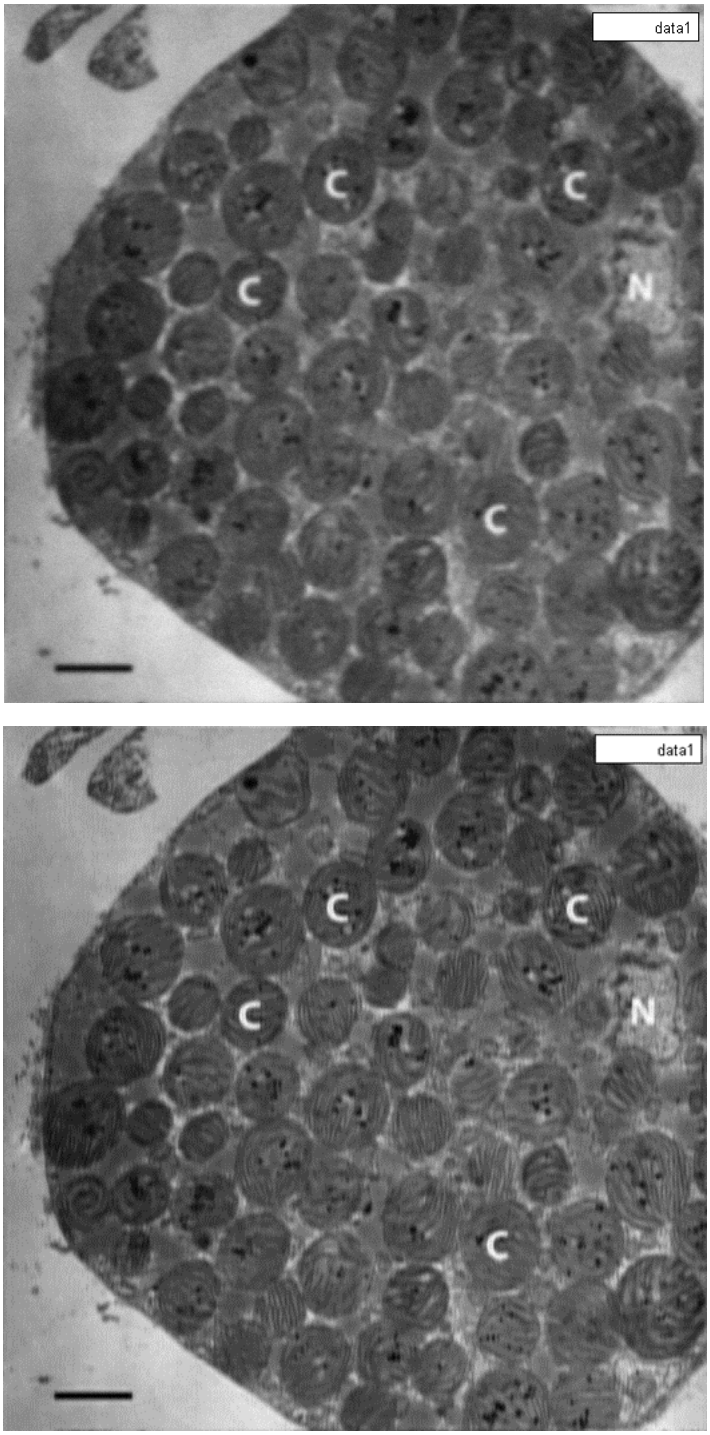


Figure 5.1: Top: Blurred image of digestive tubule cell of Elysia clarki; Bottom: The reconstructed image. Scale: 3 µm. There is a clear increase in the resolution and sharpness of the image. The blur has been reduced to a lot of extant, we can clearly see the shapes of structures in chloroplasts that we couldn't see in the blurred image. Scale: 3 µm [54]

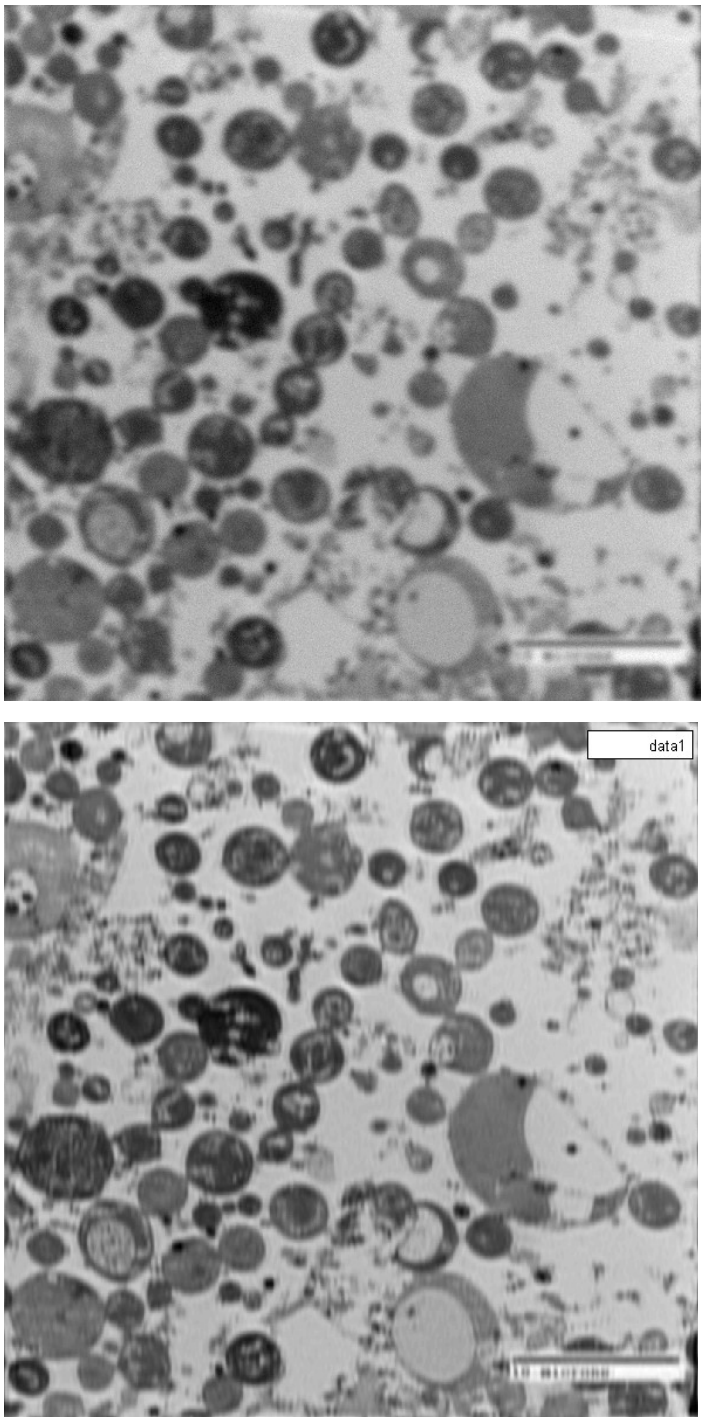


Figure 5.2: Top: Blurred image of L-form Bacillus subtilis; Bottom: The reconstructed image. The blur reduced to a lot of extant. There is a clear increase in the sharpness of the image. The fine structures at the top right side of the image are much more clear, well defined and sharp to see. Thus there is a clear increase in resolution. Scale: 10 μm [55].

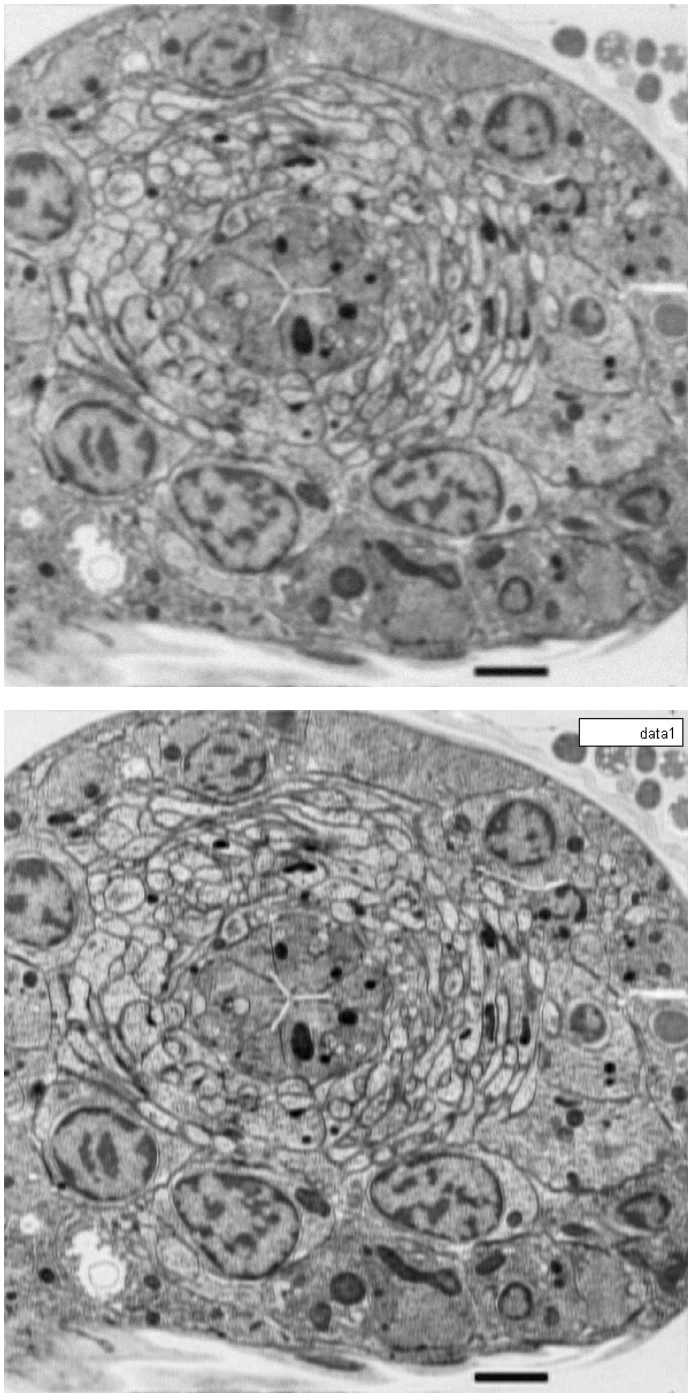


.Figure 5.3: Top: Blurred image of FOLD EMBRYO (Nerve Ring) of frozen C. elegans. Bottom: The reconstructed image. The image has become sharper and more resolved. The structures inside the nerve ring section has sharper edges. The matter scattered inside is much more defined and recognizable rather than a blur. Scale: 1 μm [56].

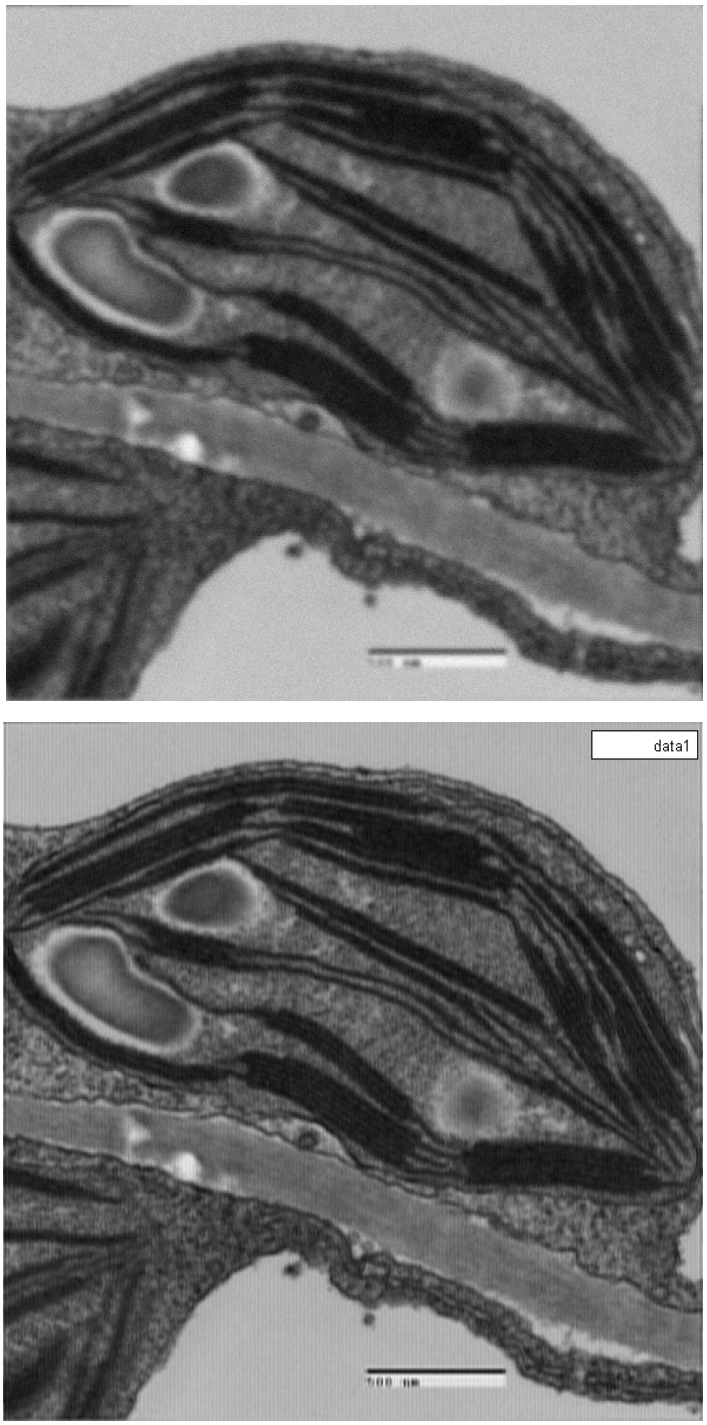


Figure 5.4: Top: Blurred image of a chloroplast of Coleus blumei; Bottom: The reconstructed image. There is an increase in the detail which is more visible in the tubule structures in the middle of the image. The lines are clearly separated and it is evident that the resolution has increased. The blur in the image is considerably less than and sharpness and contrast of structures has clearly improved. Scale: 500 nm [57].

## 5.2 Quantative analysis of the reconstructed images

The quantative analysis of the reconstructed images can be done by two ways. The first method for the analysis is known as Intensity profile. Intensity Profile plots pixel intensity of a selected area against the scaled distance of that selected area on the image. This process gives us information on the level of sharpness between two images. Intensity Profile can be measured between two images on ImageJ. The use of Intensity Profile has already been implemented by various researchers because of its effectivness in differentiating a normal image from a super-resolved image [47], [60], [61], [62].

A second way to do quantative analysis of reconstructed images is by examining the values of Peak Signal-to-Noise Ratio(PSNR) of an image with that of the others. The PSNR of the reconstructed image should be higher as compared to the PSNR of the original image to show that the image has gained more detail during the process [17], [18]. The effects of scaling and other effects introduced during reconstruction are not taken into account by both, the SNR and PSNR . But even then both the parameters remain important to science because of their merits among researchers.

**Analysis of reconstructed image 1:** The following Figure (5.5) shows the Intensity Profile of the blurred image and the reconstructed image from the Figure 5.1:

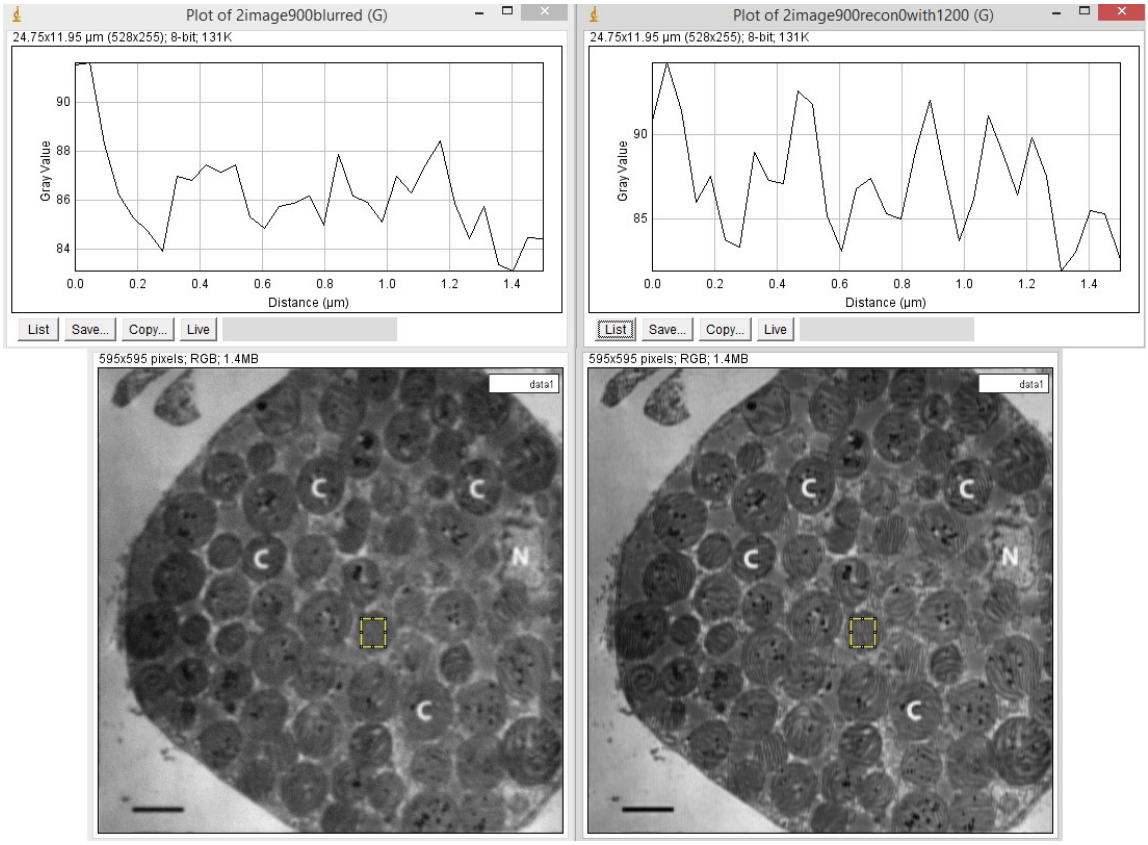


Figure 5.5 Intensity Profile of Image 1; Left: Intensity Profile of the blurred image; Right: Intensity Profile of the reconstructed image.

From the intensity profile of the blurred image it can be seen that due to blurring, the intensity peaks have lost their sharpness and have lost their edgy peaks which clearly represents loss of detail. Whereas intensity profile of the reconstructed image contain sharp and prominent peaks which represents that the more details with sharp features are present in the reconstructed image. This that the image has been super-resolved.

Table 2: Comparison of SNR (log value) and PSNR (log value) for Figure 5.5

| Metric | Blurred Image | Reconstructed Image |
|---|---|---|
| SNR | 0.2077 | 5.4684 |
| PSNR | 38.9243 | 46.4060 |

A higher signal to noise ratio of an image is representative of greater amount of signal being processed compared to the background noise. For peak signal to noise ratio, a higher ratio is representative of greater peak signal being processed compared to background noise. Thus they are well representative of an image's quality and resolution [64]. What we have here are the log values for these variables. Lower log values for the reconstructed image mean that the actual values are higher suggesting that the reconstructed image has higher resolution and better quality compared to the blurred image.

**Analysis of reconstructed image 2:** The following Figure (5.6) shows the Intensity Profile of the blurred image and the reconstructed image from the Figure 5.2:

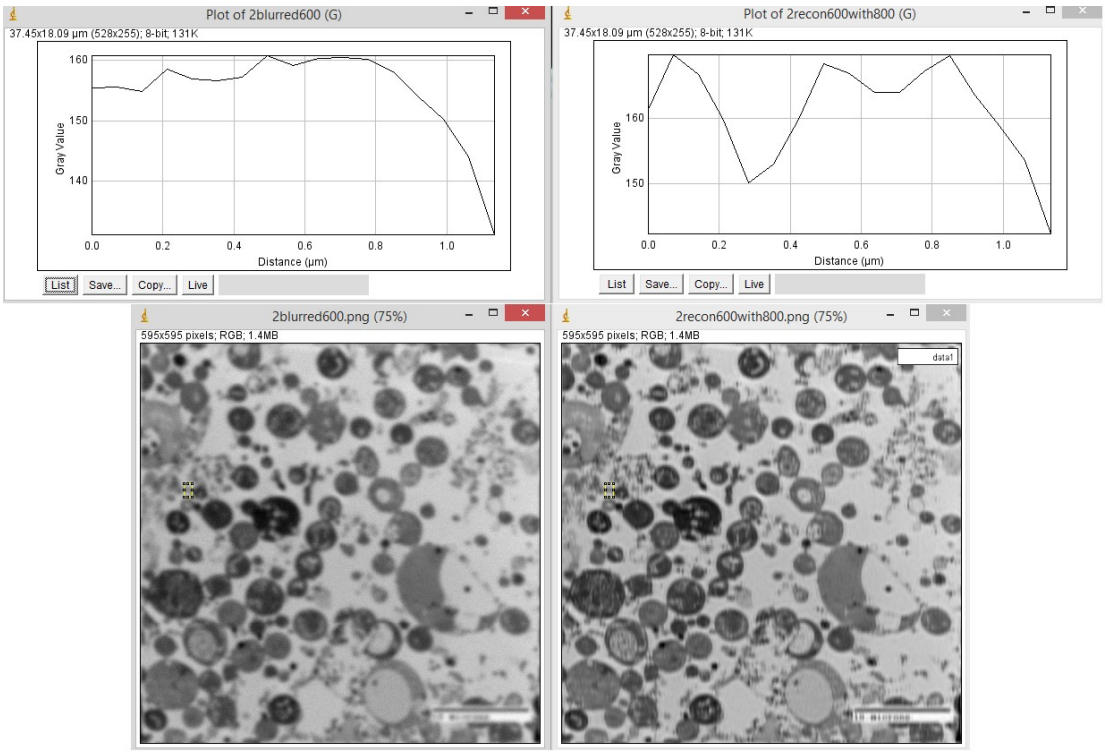


Figure 5.6 Intensity Profile of Image 2; Left: Intensity Profile of the blurred image; Right: Intensity Profile of the reconstructed image.

In the case of Image 2, the intensity profile provided similar results as Image 1. The number of intensity peaks on the intensity plot for reconstructed image showed sharper peaks . There were also more number peaks that were identifiable distinctly for the reconstructed image compared to the blurred image. What was peculiar for this image was that unlike the original image, areas with lower gray values on the reconstructed image exhibited sharp peaks suggesting that those were regions that were primarily blurred but could be successfully reassembled with the simulation process.

Table 3: Comparison of SNR (log value) and PSNR (log value) for Figure 5.6

| Metric | Blurred Image | Reconstructed Image |
|---|---|---|
| SNR | 0.2221 | 5.7135 |
| PSNR | 41.4438 | 49.8993 |

Values of SNR and PSNR are larger for the reconstructed image as compared to the original blurred image indicating that there has been improvement in terms of quality and resolution. A higher value of PSNR usually indicates that the reconstruction has produced a higher quality image.

**Analysis of reconstructed image 3:** The following Figure (5.7) shows the Intensity Profile of the blurred image and the reconstructed image from the Figure 5.3:

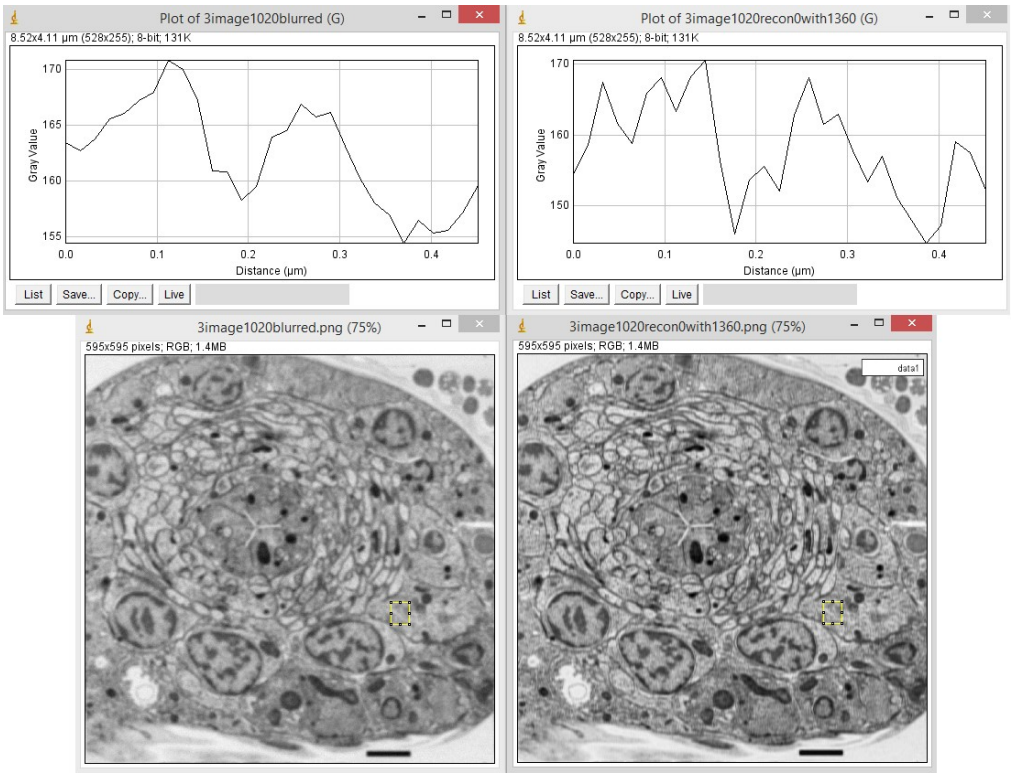


Figure 5.7 Intensity Profile of Image 3; Left: Intensity Profile of the blurred image; Right: Intensity Profile of the reconstructed image.

Much like the previous two images, in this example as well, the intensity plots of reconstructed image exhibited sharper and greater number of intensity peaks compared to the blurred image. Here the higher gray value areas were better identifiable for the reconstructed image compared to the blurred image. But all in all the reconstructed image exhibited better clarity and sharpness compared to the blurred image.

Table 4: Comparison of SNR (log value) and PSNR (log value) for Figure 5.7

| Metric | Blurred Image | Reconstructed Image |
|---|---|---|
| SNR | 0.2317 | 5.4378 |
| PSNR | 41.6898 | 49.0634 |

The SNR and PSNR log values were lower for reconstructed image, suggesting higher actual values for these variables. Thus the reconstructed image had higher resolution compared to the blurred image.

**Analysis of reconstructed image 4:** The following Figure (5.8) shows the Intensity Profile of the blurred image and the reconstructed image from the Figure 5.4:

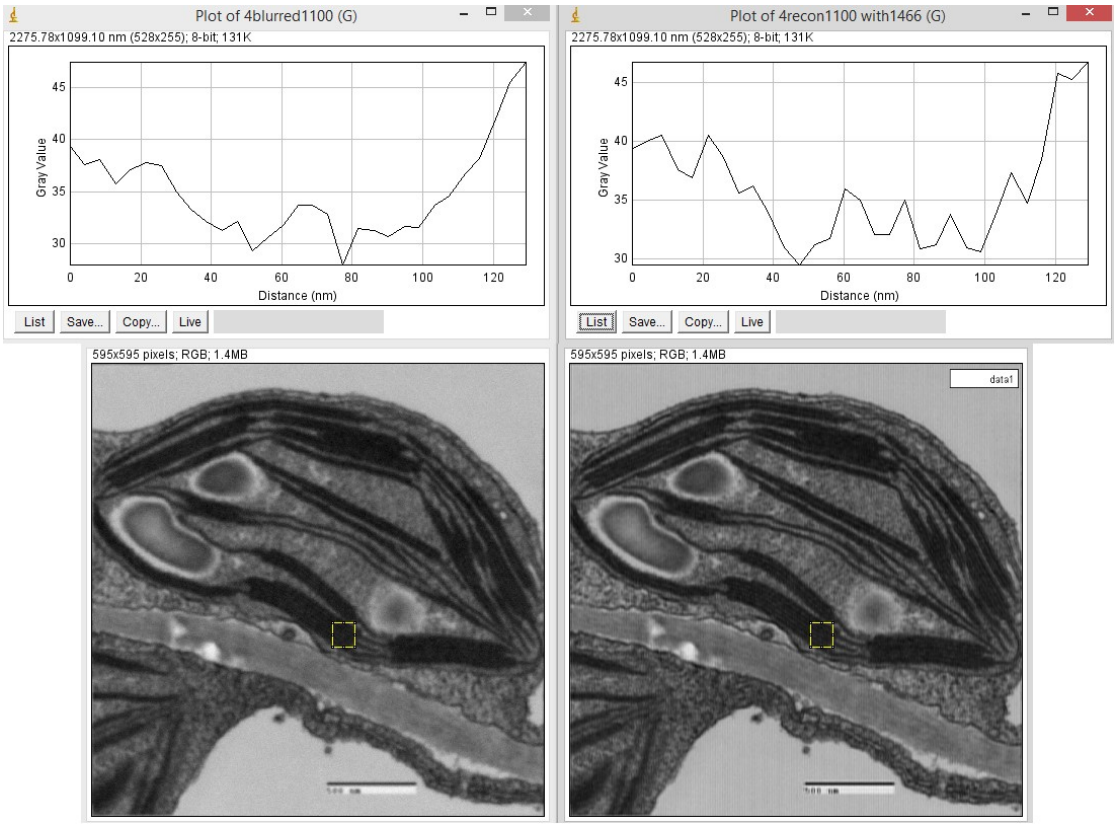


Figure 5.8 Intensity Profile of Image 4; Left: Intensity Profile of the blurred image; Right: Intensity Profile of the reconstructed image.

The intensity plots for the reconstructed image showed highly distinct peaks for the gray value. It is quite noticeable between the distances of 60-80 nm where in the intensity plot of the blurred image we could obtain a single peak which is represented by

two peaks in the intensity plot of the reconstructed image. This clearly shows that regions that were not identifiable in blurred image were successfully reconstructed by the simulation.

Table 5: Comparison of SNR and PSNR for Figure 5.8

| Metric | Blurred Image | Reconstructed Image |
|---|---|---|
| SNR | 0.0916 | 6.0428 |
| PSNR | 36.7134 | 48.7484 |

The SNR and PSNR values for Image 4 were also all higher for the reconstructed image compared to the blurred image suggesting a better resolution and quality for the reconstructed image.

## 5.3 Analysis of Experiment Data

The process of image acquisition was tested with various fringe widths. Because of the weak illumination pattern due to losses discussed in section 4.3.3, the best illumination pattern was found to be the one with a fringe periodicity of 9 pixel/ period.

For the analysis of the each experimental data set, we first analyzed the images obtained after reconstruction of the three SI patterns with the original widefield image. After that we did another comparison between the reconstructed image (through the SI patterns) with a standard widefield image (superresolved mathematically with the simulation algorithm wherein the blurring process removed).

A total of three samples were used for the analysis.

**Sample 1: Microscopic Fluorescence Fibers**

The sample consists a bunch on microscopic fluorescent fibers stacked on a glass slide. The three SI images of the sample captured through the CCD are represented below:

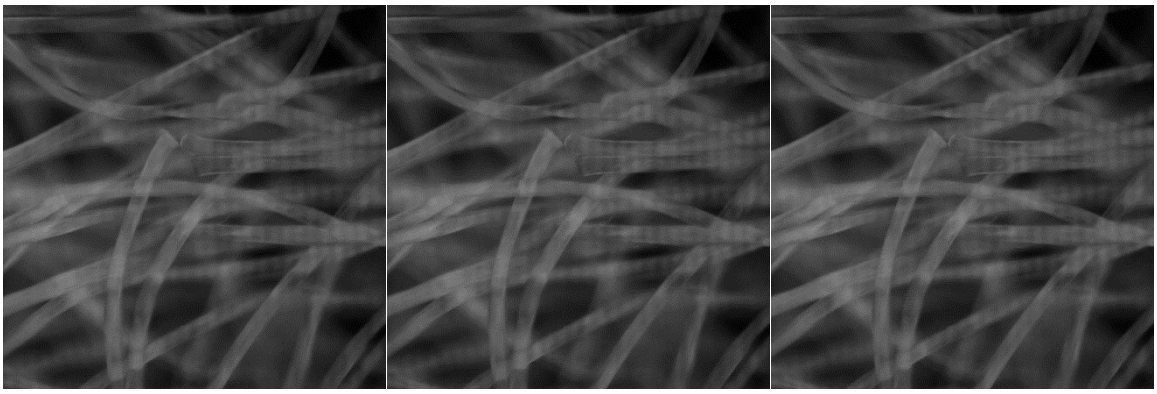

Figure 5.9: Structurally illuminated patterns captured by CCD camera with phases, $\varphi=0$, $\frac{2\pi}{3}$, and $\frac{4\pi}{3}$, respectively

The standard widefield image of the sample can be viewed in the Figure 5.10. The reconstructed image from the SI patterns given in Figure 5.11.

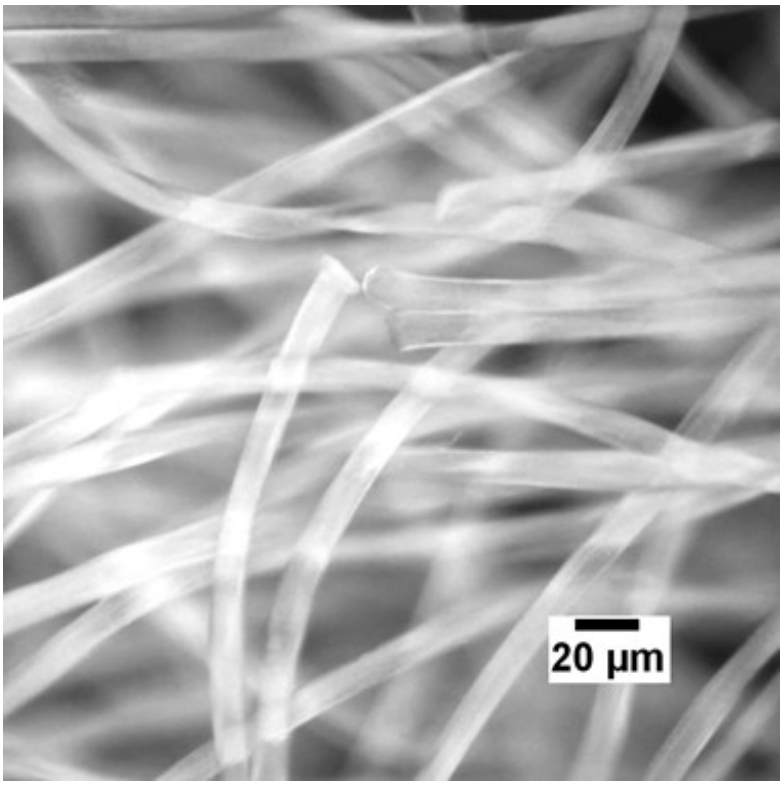


Figure 5.10: Widefield image of the fluorescence fiber sample.

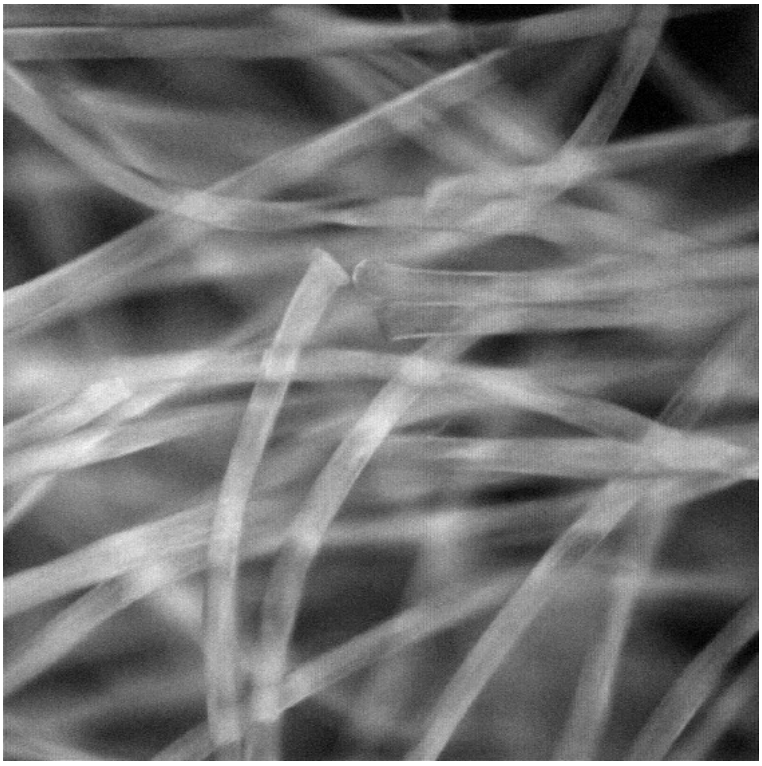

Figure 5.11: SI reconstructed image of the fluorescence fiber sample.

There is definite decrease in the optical blur and resolution is gained in the process. The intensity profile observed in Figure 5.12 showed finer details of separation in the fiber material which was observed better in the reconstructed image than the original image because of the optical blur. The intensity profiles showed higher peaks in SI reconstructed images. A random region was selected to carry of the intensity profile test. The high peak points were indicative of the separation between two structures which was not seen in the original widefield image conforming that resolution was gained.

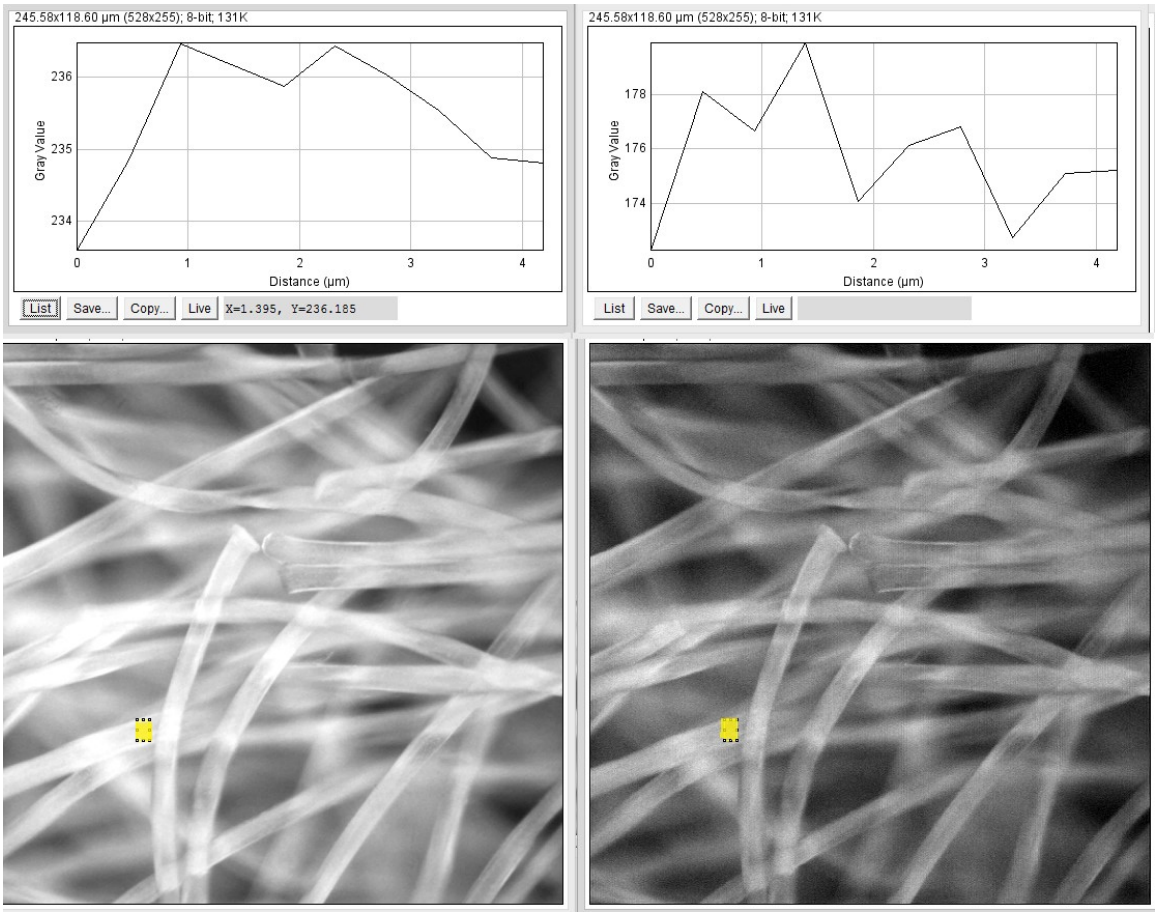


Figure 5.12: Intensity Profile; Left: Intensity Profile of the original widefield image; Right: Intensity Profile of the SI reconstructed image.

These intensity profile plots clearly showed high peaks representing visibly resolved structures which confirmed that we had gained resolution in the image and finer structures were made visible. The SNR and PSNR values of the reconstructed image with original widefield image as reference was calculated as 0.0409 and 19.0130 respectively.

Now the comparison between the experimental SI reconstructed image and the standard widefield image reconstructed through improvised simulation algorithm was conducted. The standard widefield image as shown in the Figure 5.10 was processed through our simulated reconstruction algorithm. This new reconstructed image is shown in the Figure 5.13.

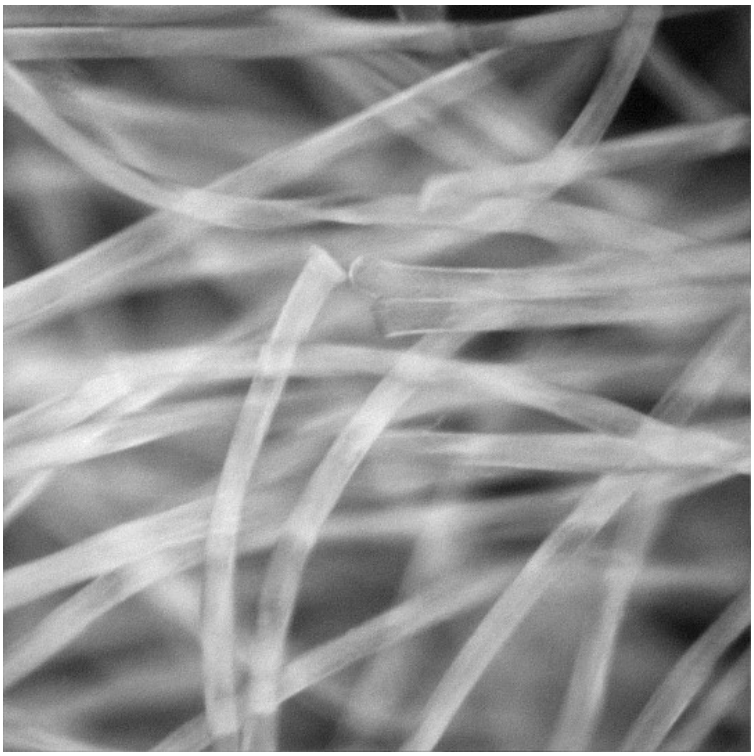

Figure 5.13: Reconstructed image of widefield image of fluorescence fiber sample reconstructed through the simulated reconstruction algorithm.

The second comparison was made between the SI reconstructed image given in Figure 5.12 and simulated reconstruction algorithm's reconstructed image given in Figure 5.13. The same region that was compared during the comparison between standard widefield image and SI reconstructed image were analyzed to help us confirm that actual Structured Illumination Microscopy experiment resolved information in a sample the most. This analysis has been shown in figures 5.14.

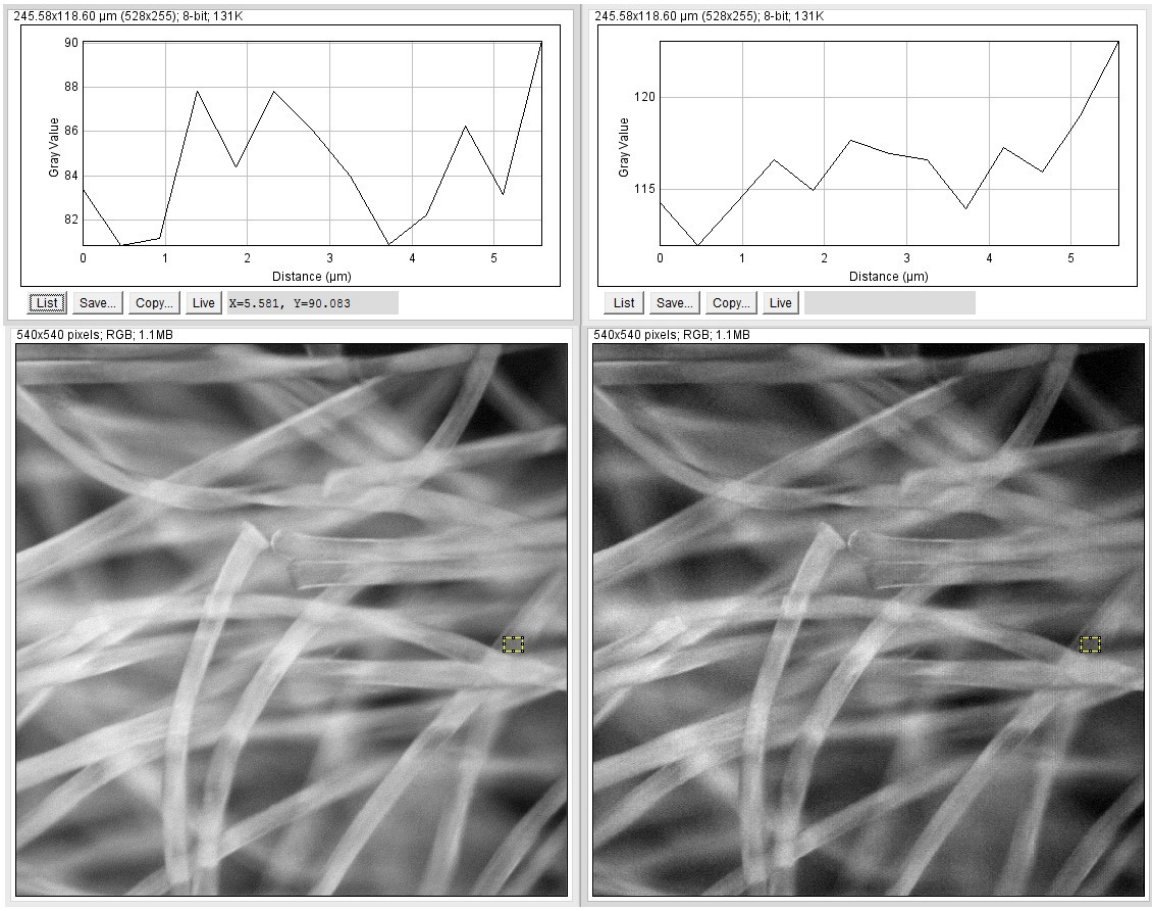


Figure 5.14: Intensity Profile of first region; Left: Intensity Profile of the SI reconstructed image; Right: Intensity Profile of the simulated reconstruction algorithm's reconstructed image.

The simulated reconstructed image, as expected did not reveal any new details as in the case of SIM reconstructed image. The image looked identical to the original

widefield image and the SNR and PSNR values of this image were noted to be 0.0033 and 32.1906 respectively. The intensity profiles of the SI reconstructed image had higher peaks and thus much more resolved information than simulated reconstruction algorithm's reconstructed image.

**Sample 2: Fluorescence Beads**

Fluorescence beads scattered on a glass slide forms this sample.

The three SI images of the sample captured through the CCD are represented below:

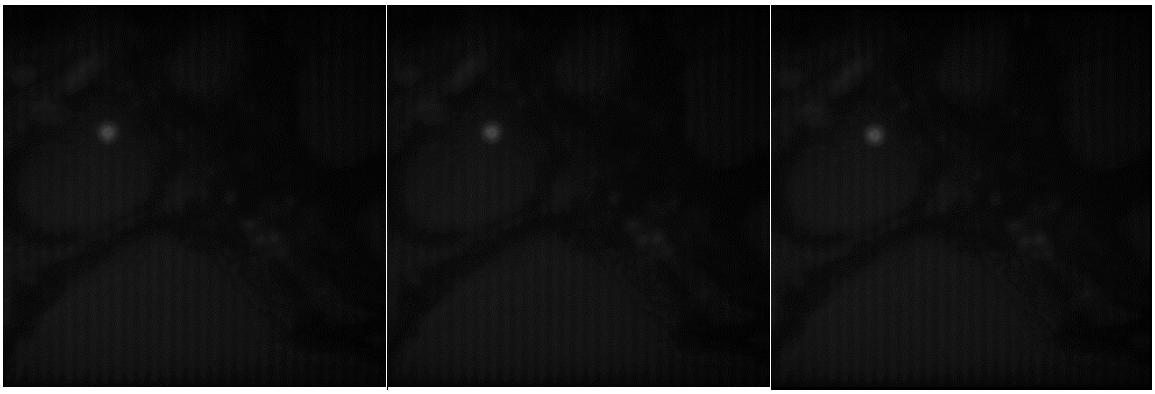

Figure 5.15: Structurally illuminated patterns captured by CCD camera with phases, $\varphi=0$, $\frac{2\pi}{3}$, and $\frac{4\pi}{3}$, respectively

The standard widefield image of the sample can be viewed in the Figure 5.16. The reconstructed image from the SI patterns given in Figure 5.17.

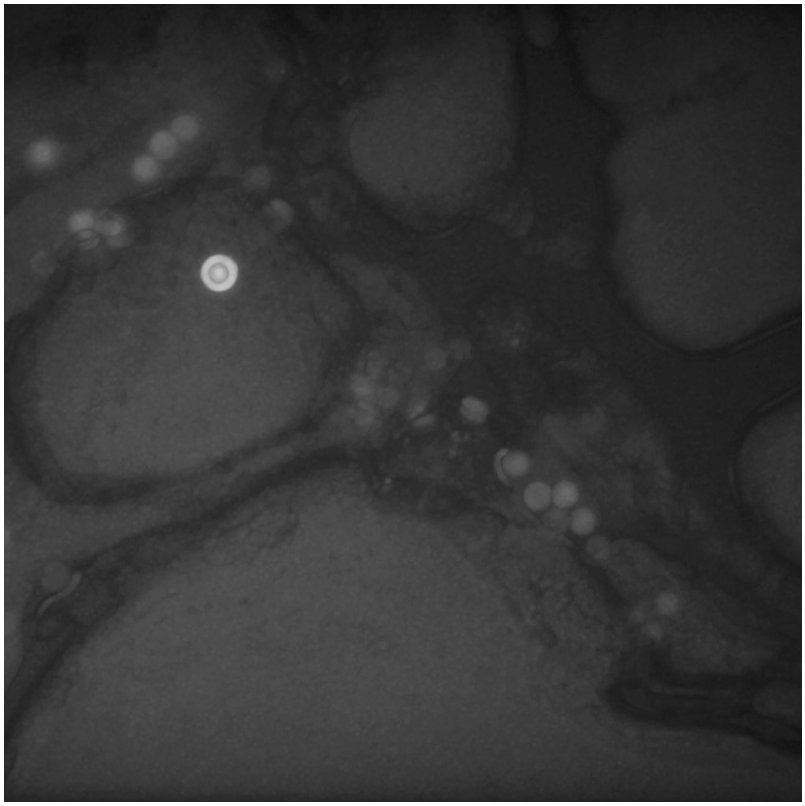

Figure 5.16: Widefield image of the sample.

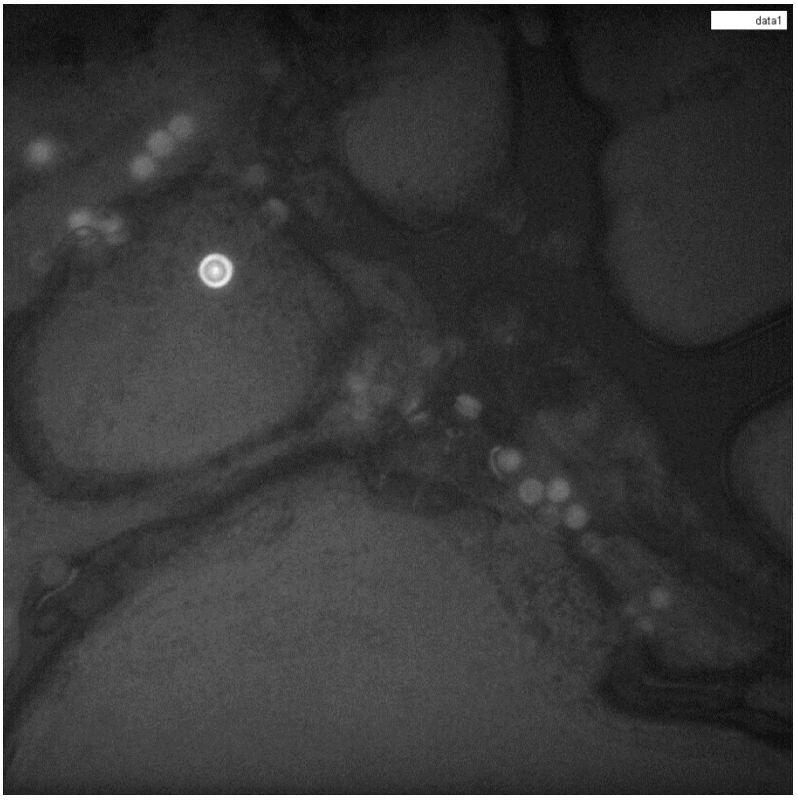


Figure 5.17: SI reconstructed image of the sample.

There is a decrease in the optical blur and resolution is gained in the process. The SI reconstructed image showed finer structures in the dark material of the sample. Also the brightest point in the image, i.e., the bright ring is sharper and more defined and resoluted in the SI reconstructed image. The intensity profiles of areas of the reconstructed image were obtained and we observed higher peaks in SI reconstructed images. The high peak points were indicative of the separation between two structures which was not seen in the original widefield image conforming that resolution was gained.

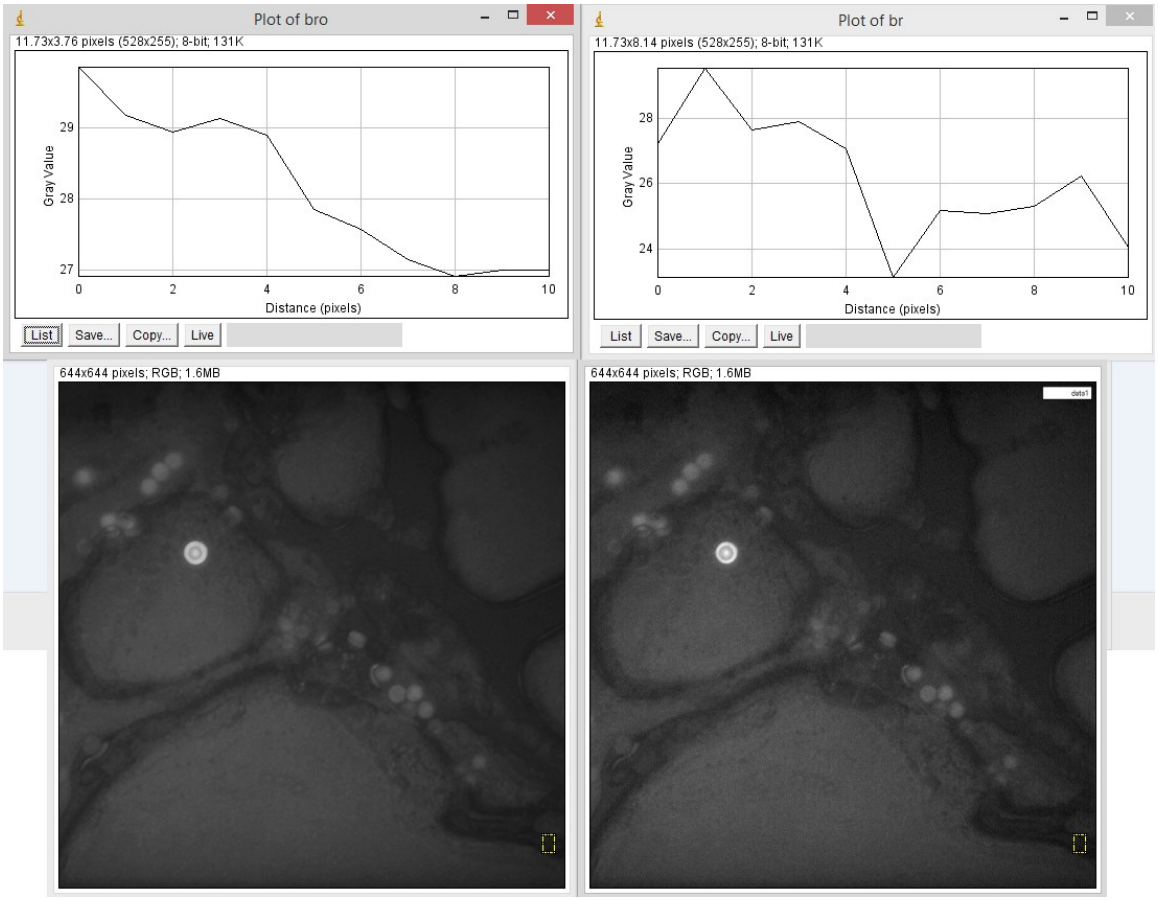


Figure 5.18: Intensity Profile; Left: Intensity Profile of the original widefield image; Right: Intensity Profile of the SI reconstructed image.

These intensity profile plots clearly showed high peaks representing visibly resolved structures which confirmed that we had gained resolution in the image and finer structures were made visible. The SNR and PSNR values of the reconstructed image with original widefield image as reference was calculated as 0.0073 and 23.5550 respectively.

Now the comparison between the experimental SI reconstructed image and the standard widefield image reconstructed through improvised simulation algorithm was conducted. The standard widefield image as shown in the Figure 5.16 was processed through our simulated reconstruction algorithm. This new reconstructed image is shown in the Figure 5.19.

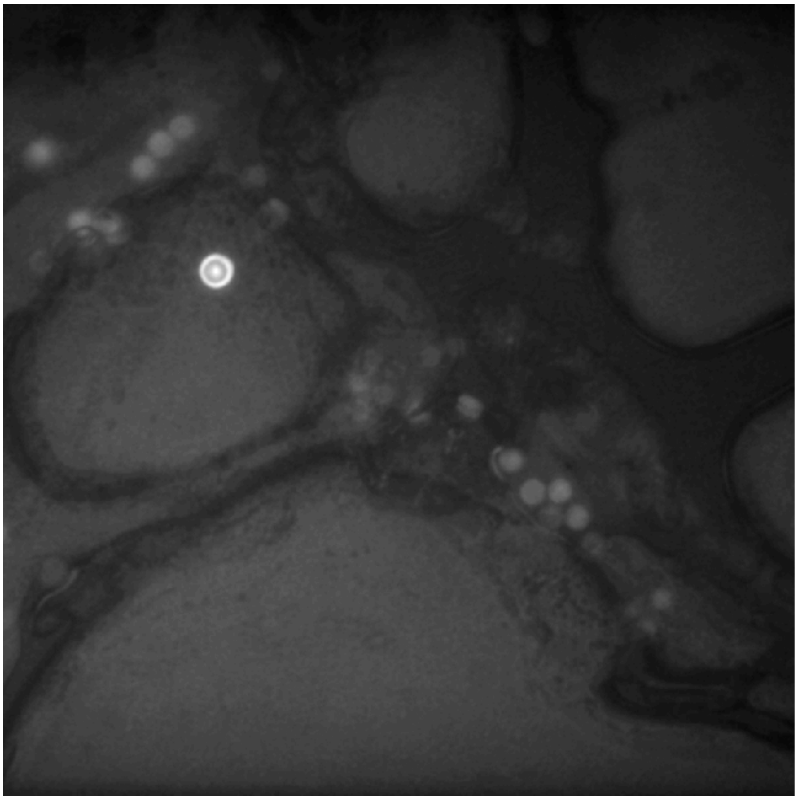

Figure 5.19: Reconstructed image of widefield image of fluorescence fiber sample reconstructed through the simulated reconstruction algorithm.

The second comparison was made between the SI reconstructed image given in Figure 5.16 and simulated reconstruction algorithm's reconstructed image given in Figure 5.19. The same regions was compared during the comparison between standard widefield image and SI reconstructed image were analyzed again to help us confirm that actual Structured Illumination Microscopy experiment resolved information in a sample the most. This analysis has been shown in Figure 5.20.

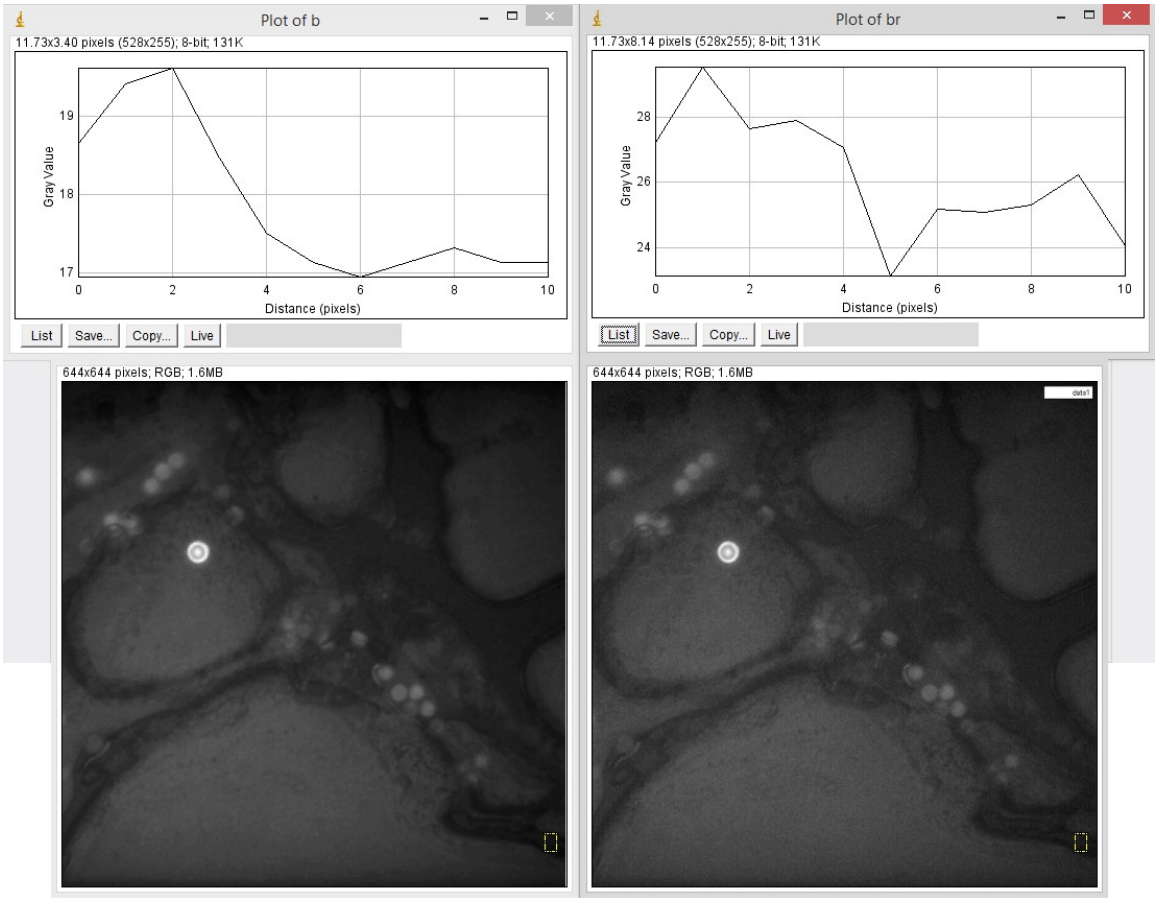


Figure 5.20: Intensity Profile; Left: Intensity Profile of the simulated reconstruction algorithm's reconstructed image; Right: Intensity Profile of the SI reconstructed image.

The simulated reconstructed image, as expected did not reveal any new details as in the case of SIM reconstructed image. The image looked identical to the original

widefield image and the SNR and PSNR values of this image were noted to be 0.0527 and 27.8027 respectively. The intensity profiles of the regions of the SI reconstructed image had higher peaks and thus much more resolved information than simulated reconstruction algorithm's reconstructed image.

**Sample 3: Gold on Glass**

The sample consists of a thin layer of gold (Thickness: 100nm) deposited in geometrical shapes on a circular thin slide of glass. The same analysis as performed for the last two samples was carried out here as well.

The three SI images of the sample captured through the CCD are represented below:

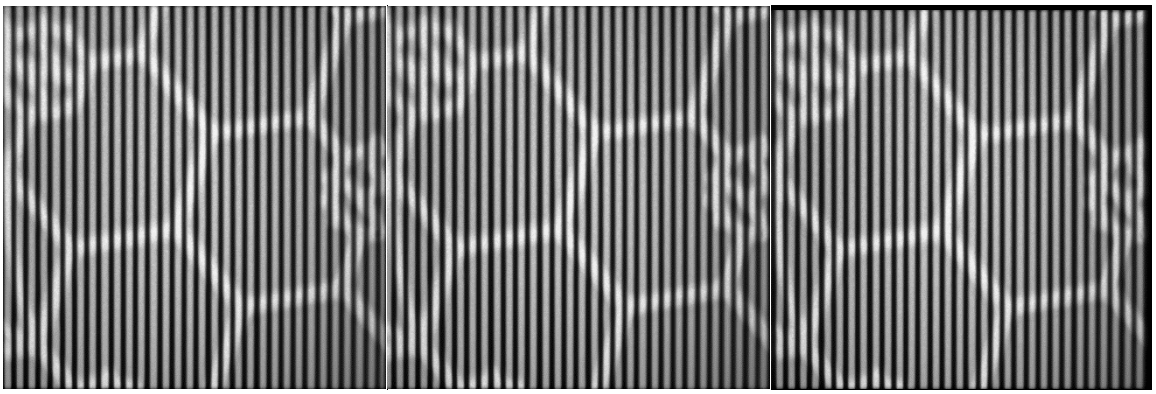

Figure 5.21: Structurally illuminated patterns captured by CCD camera with phases, $\varphi=0$, $\frac{2\pi}{3}$, and $\frac{4\pi}{3}$, respectively

The standard widefield image of the sample can be viewed in the Figure 5.22. The reconstructed image from the SI patterns given in Figure 5.23:

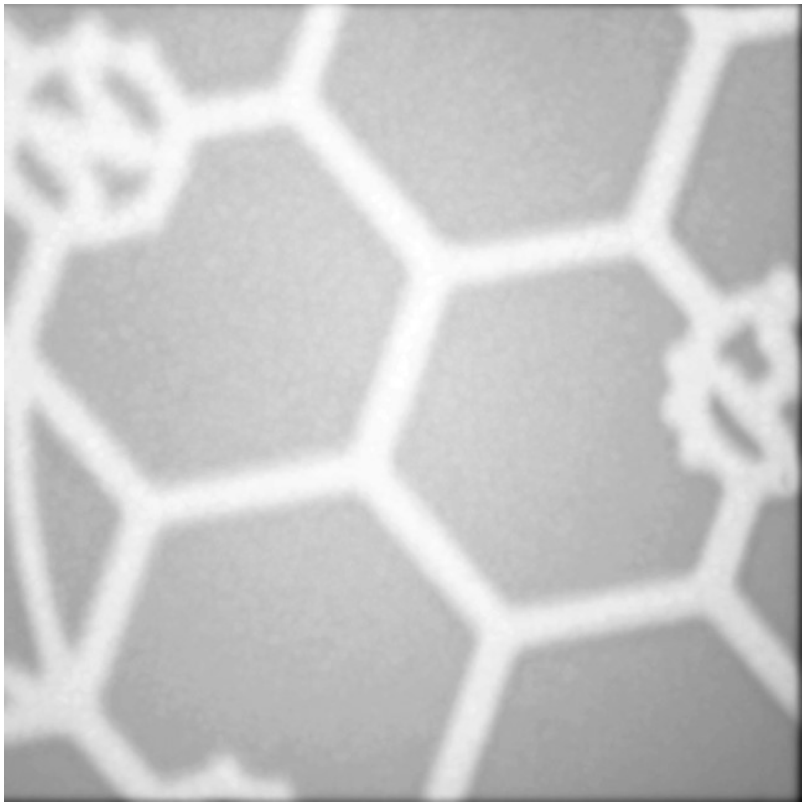

Figure 5.22: Widefield image of the sample.

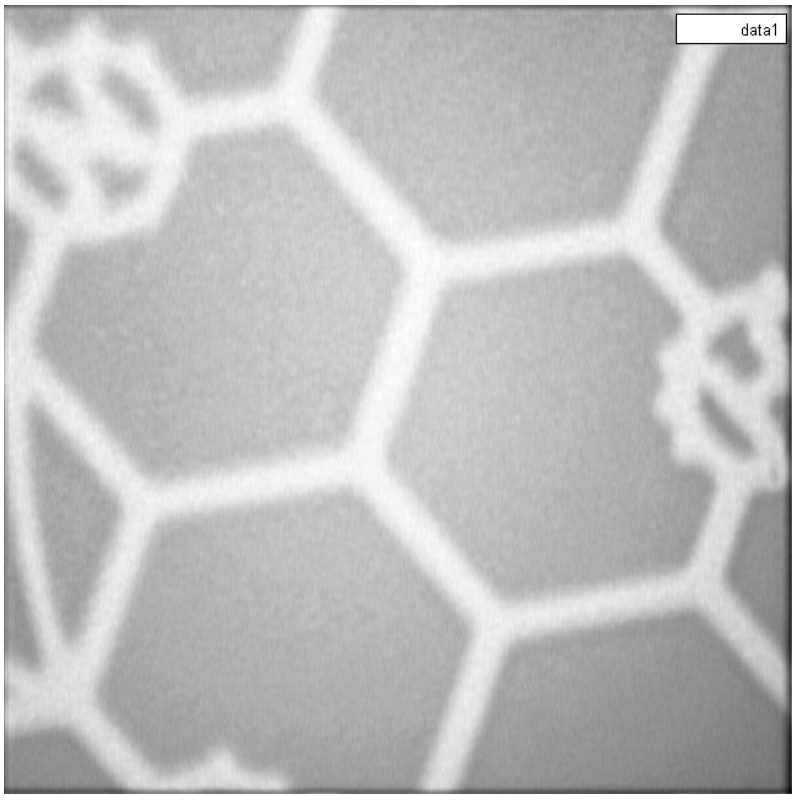


Figure 5.23: SI reconstructed image of the sample.

There is decrease in the optical blur. The edges of sample became less dispersed and more streamlined, sharp and defined indicating resolution was gained in the process. The intensity profiles of the reconstructed image was obtained and we observed higher peaks in SI reconstructed image. The high peak points were indicative of the gain of some higher order components which was not seen in the original widefield image conforming that resolution was gained.

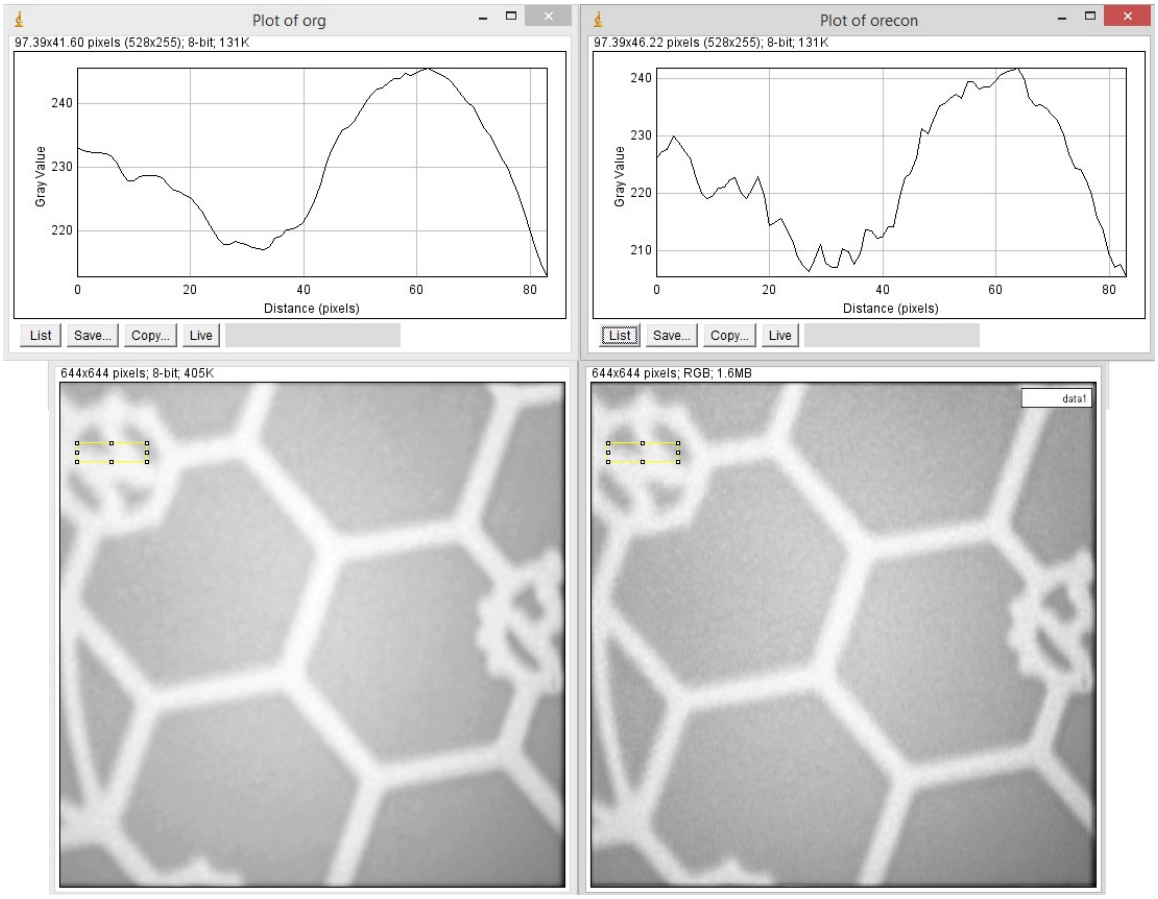


Figure 5.24: Intensity Profile; Left: Intensity Profile of the original widefield image; Right: Intensity Profile of the SI reconstructed image.

The SNR and PSNR values of the reconstructed image with original widefield image as reference was calculated as 0.0033 and 26.418 respectively.

Now the comparison between the experimental SI reconstructed image and the standard widefield image reconstructed through improvised simulation algorithm was conducted. The standard widefield image as shown in the Figure 5.22 was processed through our simulated reconstruction algorithm. This new reconstructed image is shown in the Figure 5.25.

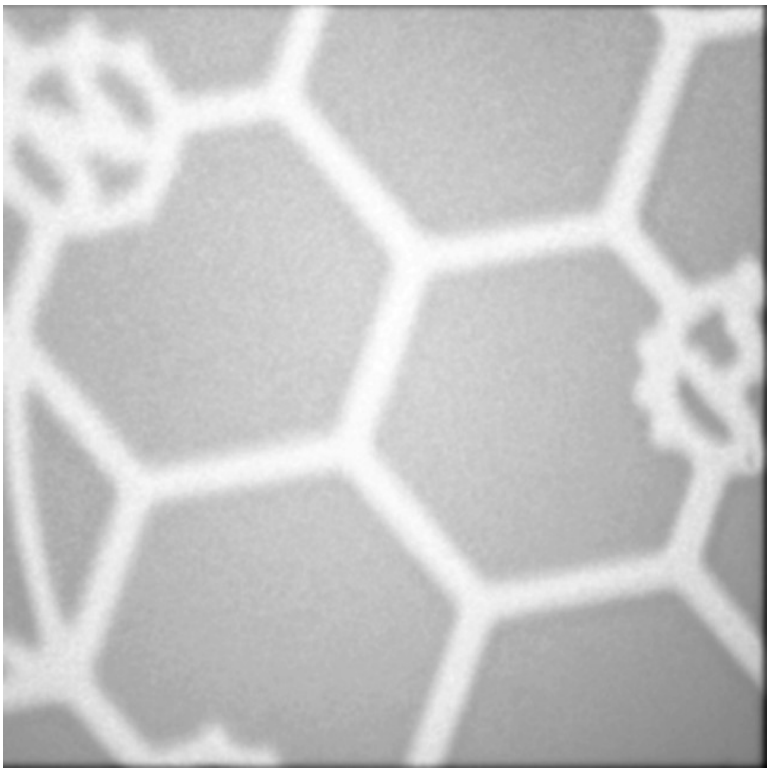

Figure 5.25: Reconstructed image of widefield image of fluorescence fiber sample reconstructed through the simulated reconstruction algorithm.

The second comparison was made between the SI reconstructed image given in Figure 5.22 and simulated reconstruction algorithm's reconstructed image given in Figure 5.25. Intensity profile comparison between standard widefield image and SI reconstructed image were analyzed again to help us confirm that actual Structured Illumination

Microscopy experiment resolved information in a sample the most. This analysis has been shown in Figure 5.26.

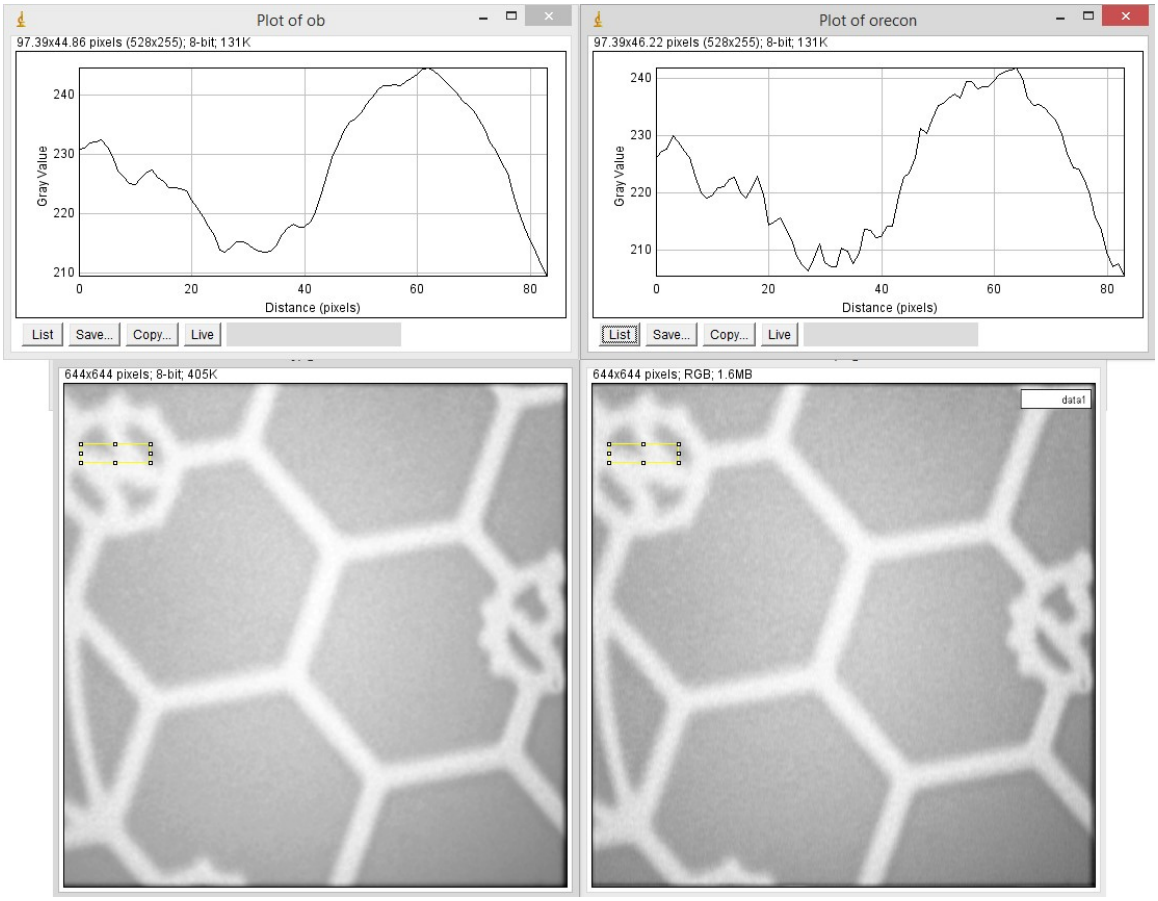


Figure 5.26: Intensity Profile; Left: Intensity Profile of the simulated reconstruction algorithm's reconstructed image; Right: Intensity Profile of the SI reconstructed image.

The image looked identical to the original widefield image and the SNR and PSNR values of this image were noted to be 0.0033 and 32.1906 respectively. The intensity profiles of the regions of the SI reconstructed image had higher peaks and thus much more resolved information than simulated reconstruction algorithm's reconstructed image.

The SNR and PSNR values are not reliable to compare the two reconstructed images because of errors and artifacts introduced during reconstruction such as scaling, noise due to filters, errors due to pattern mismatch in the SIM, etc. Intensity profiling and visual inspection outclasses SNR and PSNR and are the best way to compare experimental reconstructed images, known in the scientific community [4], [7], [18], and [20]. The use of SNR and PSNR as a metric is useful in comparison of software only test images evaluation but not suitable for SIM experimental images [2], [4], [7], and [8].

# Chapter 6

# Conclusion and Future Work

## 6.1 Conclusion

This thesis describes the role of structured illumination microscopy in attaining super-resolution for images acquired using a fluorescence microscope. However, the highlight of this project was to design and test a simulation of structured illumination microscopy on as well as extend and test the same for an actual structured illumination microscopy experiment. Our primary objective was to attain super-resolution in order to break down the physical limitation as posed by the diffraction limit theory. To do this we employed structured illumination microscopy or SIM. SIM has been extensively employed to study biological samples but the concept of using a simulation to do this process is a novel technique. To further the evidence in this direction we designed a program in MATLAB that simulates the process of SIM. This would form as a basis to create a superresolution algorithm. We tested this on a set of pre-defined images which were first blurred and then reconstructed. The quality and resolution of original and reconstructed images were compared. Superresolution was achieved during this process. We then extended our approach to a SIM experiment using a DMD with a fluorescence microscope and performing reconstruction. We also obtained widefield images of the samples using the experimental setup and reconstructed it with our simulation.

For the four test images, results showed a significant gain of resolution between the original and reconstructed images obtained from the simulation where the reconstructed images had a considerably high resolution compared to the original images. This was quantitatively evident by comparison of signal-noise ratio, peak signal to noise ratio and the peak signal to standard error of estimation ratio all which were higher for the reconstructed images. The pixel intensity plots showed a significantly higher number of intensity peaks for reconstructed images compared to the blurred ones.

Reconstructed image of the experiment samples as obtained using the DMD as SLM for structured illumination on the fluorescence microscope was also of higher resolution than original widefield images and when compared to the reconstructed image using simulation reconstruction algorithm of the same sample, again the experimental reconstructed image fared better.

Thus, we believe that SIM is a useful technique to improve resolution of images of microscopic samples. Our simulation process is efficient in reconstructing highly resolved images as well as our experimental setup of structured illumination microscopy.

## 6.2 Future Work

This research highlights the utility of structured illumination microscopy in super-resolution of microscopic samples. Despite what has been observed through the results of this study, there is a scope of future research that should be noted. First of all, the DMD that was incorporated with the microscope for experimental data collection for the purpose of this study was physically placed in front of the aperture of the microscope at a distance equal to the focal length of the DMD without any efficient focusing technique. Thus only a small fraction of the light coming from the DMD was utilized by the microscope. This arrangement resulted in intensity losses that in turn have affected the quality of images to much extent. Also because of the same reason, DMD pixel to charged-coupled device (CCD) camera pixel matching could not be carried out precisely for image acquisition. This resulted in a slight mismatch in the pixel matrix of the illumination pattern from the CCD. To overcome these issues, the most important future implication from this study is that instead of LED, laser can be used to increase the accuracy of the illumination pattern or proper focusing methods while using stock LEDs can be explored. This would also allow us to incorporate the DMD within the optical system to avoid any intensity losses and obtain best possible images. Additionally, this would also allow us to have even better precise pixel matching of CCD pixels and DMD pixels which would aid in more precise image reconstruction.

Secondly, the image acquisition process was done manually and thus there was no scope of increasing frame rates. This limited any ability to automatize the system. In lieu

of this, our system was not compatible for the purpose of performing live imaging by means of videography. To overcome this, high speed CCD can be used and then automatized the image processing system, which can then allow us to increase the frame rates for image acquisition that can permit us to perform live imaging. Last of all, it is worth noting that our system has only been tested for two-dimensional images. To perform three-dimensional optical sectioning a new algorithm can be set up that can perform fringe frequency variation which would allow us to stack images to obtain three-dimensional images.

# BIBLIOGRAPHY


[1] Abbe, E. (1873). "Beitrage zur Theorie des Mikroskops und der mikroskopischen Wahrmehmung". Archiv für Mikroskopische Anatomie 9: 413–420. doi:10.1007/BF02956173.

[2] Allen, J. R., Ross, S. T., & Davidson, M. W. (2014). Structured illumination microscopy for superresolution. ChemPhysChem, 15(4), 566-576.

[3] Neice, A. (2010). "Methods and Limitations of Subwavelength Imaging". Advances in Imaging and Electron Physics. Advances in Imaging and Electron Physics 163: 117. doi:10.1016/S1076-5670(10)63003-0. ISBN 978-0-12-3813145.

[4] Heintzmann, R. & Gustafsson, M. G. L. Nature Photon. 3, 362–364 (2009)

[5] T. Stathaki, Image Fusion: Algorithms and Applications, Academic Press, London, 2011.

[6] S. Farsiu, D. Robinson, M. Elad, P. Milanfar, “Fast and robust multi-frame superresolution,” IEEE Trans. Image Processing, vol. 13, pp. 1327–1344, 2004.

[7] M. Gustaffson, “Surpassing the lateral resolution limit by a factor of two using structured illumination microscopy,” Journal of Microscopy, vol. 198, pp. 82-87, 2000.

[8] S. C. Park, M. K. Park, M. G. Kang, “Super-resolution image reconstruction: a technical overview,” Signal Processing Magazine, IEEE, vol. 20, pp. 21-36, May 2003.

[9] Lira, I. (2006). Resolution revisited. Metrologia, 43(3), L14.

[10] Rayleigh, L. (1879). XXXI. Investigations in optics, with special reference to the spectroscope. The London, Edinburgh, and Dublin Philosophical Magazine and Journal of Science, 8(49), 261-274.

[11] C. M. Sparrow, 1916, ApJ, 44, 76

[12] Michael W. Davidson. "Resolution." ZEISS Microscopy Online Campus. Carl Zeiss Microscopy, LLC, United States, n.d. Web. 20 July 2014. <http://www.microscopyu.com/articles/formulas/formulasresolution.html

[13] Gray, Noah. "Knowing the Limit." Nature. Nature Publishing Group, 1 Oct. 2009. Web. 18 July 2014. <doi:10.1038/ncb1940>

[14] Rottenfusser, Rudi, Erin E. Wilson, and Michael W. Davidson. "Education in Microscopy and Digital Imaging." ZEISS Microscopy Online Campus. Carl Zeiss Microscopy, LLC, United States, n.d. Web. 20 July 2014. <http://zeiss-campus.magnet.fsu.edu/articles/basics/resolution.html

[15] J. W. Goodman, Introduction to Fourier Optics. 3, illustrated ed. 2005, New York: Roberts and Company Publishers.

[16] Roland Priemer (1991). Introductory Signal Processing. World Scientific. p. 1. ISBN 9971509199

[17] S. Alliney, S. A. Ruzinsky, “An algorithm for the minimization of mixed l1 and l2 norms with application to Bayesian estimation,” Signal Processing, IEEE Transactions on, vol. 42, pp. 618-627, 1994.

[18] N. Hagan, L. Gao, T. S. Tkaczyk, “Quantitative sectioning and noise analysis for structured illumination microscopy,” Optics Express, vol. 20, pp. 403-413, 2012.

[19] Wiener, Norbert (1949). Extrapolation, Interpolation, and Smoothing of Stationary Time Series. New York: Wiley. ISBN 0-262-73005-7.

[20] L. P. Yaroslavsky, H. J. Caulfield, “Deconvolution of multiple images of the same object,” Appl. Opt., vol. 33, pp. 2157-2162, 1994.

[21] Albert Van Helden, Sven Dupré, Rob Van Gent, Huib Zuidervaart, The Origins of the Telescope, pages 32-36

[22] Gould, Stephen Jay (2000). "Chapter 2: The Sharp-Eyed Lynx, Outfoxed by Nature". The Lying Stones of Marrakech: Penultimate Reflections in Natural History. New York, N.Y: Harmony. ISBN 0-224-05044-3.

[23] Wootton, David (2006). Bad medicine: doctors doing harm since Hippocrates. Oxford [Oxfordshire]: Oxford University Press. ISBN 0-19-280355-7.

[24] Goeggel, D. (2007). The History of Stereo Microscopy–Part II.

[25] Amsel, Sheri. “Anatomy Activities.” Microscope Labeling Activity. Exploring Nature Educational Resource. © 2005 - 2014. July 17, 2014. http://exploringnature.org/db/detail.php?dbID=45&detID=3043

[26] Humes, A. G., & Gooding, R. U. (1964). A method for studying the external anatomy of copepods. Crustaceana, 6(3), 238-240.

[27] Harding, J. P. (1939). A simple instrument for dissecting minute organisms. Journal of the Royal Microscopical Society, 59(1), 19-25.

[28] Wright, A. (1907). Principles of microscopy: being a handbook to the microscope. The Macmillan Company.

[29] Bausch, E. (1901). Manipulation of the Microscope. Publication department, Bausch & Lomb optical Company.

[30] Coltharp, C., & Xiao, J. (2012). Superresolution microscopy for microbiology.Cellular microbiology, 14(12), 1808-1818.

[31] Betzig, E., Patterson, G. H., Sougrat, R., Lindwasser, O. W., Olenych, S., Bonifacino, J. S., & Hess, H. F. (2006). Imaging intracellular fluorescent proteins at nanometer resolution. Science, 313(5793), 1642-1645.

[32] M. J. Rust, M. Bates, and X. W. Zhuang, "Sub-diffraction-limit imaging by stochastic optical reconstruction microscopy (STORM)," Nat. Methods 3, 793-795 (2006).

[33] R. Henriques, C. Griffiths, E. H. Rego, and M. M. Mhlanga, "PALM and STORM: Unlocking Live-Cell Super-Resolution," Biopolymers 95, 322-331 (2011).

[34] Hell, S. W., & Wichmann, J. (1994). Breaking the diffraction resolution limit by stimulated emission: stimulated-emission-depletion fluorescence microscopy. Optics letters, 19(11), 780-782.

[35] Klar, T. A., Jakobs, S., Dyba, M., Egner, A., & Hell, S. W. (2000). Fluorescence microscopy with diffraction resolution barrier broken by stimulated emission. Proceedings of the National Academy of Sciences, 97(15), 8206-8210.

[36] Wildanger, D., Medda, R., Kastrup, L., & Hell, S. W. (2009). A compact STED microscope providing 3D nanoscale resolution. Journal of microscopy, 236(1), 35-43.

[37] B. Harke, J. Keller, C. K. Ullal, V. Westphal, A. Schoenle, and S. W. Hell, "Resolution scaling in STED microscopy," Opt. Express 16, 4154-4162 (2008).

[38] Neil, M. A. A., Juskaitis, R., & Wilson, T. (1997). Method of obtaining optical sectioning by using structured light in a conventional microscope. Optics letters, 22(24), 1905-1907.

[39] Gustafsson, M. G. (2005). Nonlinear structured-illumination microscopy: wide-field fluorescence imaging with theoretically unlimited resolution. Proceedings of the National Academy of Sciences of the United States of America, 102(37), 13081-13086.

[40] Chang, B. J., Chou, L. J., Chang, Y. C., & Chiang, S. Y. (2009). Isotropic image in structured illumination microscopy patterned with a spatial light modulator. Optics express, 17(17), 14710-14721.

[41] Shao, L., Kner, P., Rego, E. H., & Gustafsson, M. G. (2011). Super-resolution 3D microscopy of live whole cells using structured illumination. Nature methods, 8(12), 1044-1046.

[42] Hornbeck, L J, (1997) Digital light processing for high-brightness, high-resolution applications. Proc. SPIE, 3013:27-41 [2] T. Vansiri, and C. Toumazou: Integrated high frequency low-noise current-mode optical transimpedance preamplifiers: theory and practice, IEEE J. of Solid-State Circuits, vol. 30(6), pp. 677-685, 1995.

[43] Sampsell, J. B. (1994). Digital micromirror device and its application to projection displays. Journal of Vacuum Science & Technology B, 12(6), 3242-3246.

[44] Dudley, D., Duncan, W. M., & Slaughter, J. (2003, January). Emerging digital micromirror device (DMD) applications. In Micromachining and Microfabrication (pp. 14-25). International Society for Optics and Photonics.

[45] Douglass, M. R. (1998, March). Lifetime estimates and unique failure mechanisms of the digital micromirror device (DMD). In Reliability Physics Symposium Proceedings, 1998. 36th Annual. 1998 IEEE International (pp. 9-16). IEEE.

[46] Yoder, L. A., Duncan, W. M., Koontz, E. M., So, J., Bartlett, T. A., Lee, B. L., & Rancuret, P. (2001, November). DLP technolgy: applications in optical networking. In International Symposium on Optical Science and Technology (pp. 54-61). International Society for Optics and Photonics.

[47] Dan, D., Lei, M., Yao, B., Wang, W., Winterhalder, M., Zumbusch, A., & Zhao, W. (2013). DMD-based LED-illumination Super-resolution and optical sectioning microscopy. Scientific reports, 3.

[48] Křížek, P., Raška, I., & Hagen, G. M. (2012). Flexible structured illumination microscope with a programmable illumination array. Optics express, 20(22), 24585-24599.

[49] S. A. Shroff, J. R. Fienup, D. R. Williams, "OTF compensation in structured illumination superresolution images," Proc. SPIE, vol. 7094, pp. 2-11, 2008.

[50] M. Gustafsson, "Extended resolution fluorescence microscopy," Current Opinion in Structural Biology, vol. 9, pp. 627-634, 1999.

[51] S. C. Park, M. K. Park, M. G. Kang, "Super-resolution image reconstruction: a technical overview," Signal Processing Magazine, IEEE, vol. 20, pp. 21-36, May 2003.

[52] T. Stathaki, Image Fusion: Algorithms and Applications, Academic Press, London, 2011.

[53] L. P. Yaroslavsky, H. J. Caulfield, "Deconvolution of multiple images of the same object," Appl. Opt., vol. 33, pp. 2157-2162, 1994.

[54] Middlebrooks, M. L., Pierce, S. K., & Bell, S. S. (2011). Foraging behavior under starvation conditions is altered via photosynthesis by the marine gastropod, Elysia clarki. PloS one, 6(7), e22162.

[55] Gilpin, R. W., Young, F. E. & Chatterjee, A. N., 1973. Characterization of a Stable L-form of Bacillus subtilis 168. Journal of Bacteriology, 113(1), pp. 486-499. & Frederick National Laboratory for Cancer Research

[56] Anatomical methods for C. elegans research. 2005. Altun, Z. F. and Hall, D. H. In WormAtlas. http://www.wormatlas.org/ver1/anatmeth/anatmeth.htm

[57] Howard, Louisa. "SEM Images." Various Images - SEM. Dartmouth Electron Microscope Facility, n.d. Web. 24 July 2014. http://remf.dartmouth.edu/Botanical_TEM/

[58] "Nikon MicroscopyU - The Source for Microscopy Education." Nikon MicroscopyU. Nikon, Inc., n.d. Web. 25 July 2014. <http://www.microscopyu.com/museum/e600pol.html>.

[59] Schaefer, L. H., Schuster, D., & Schaffer, J. (2004). Structured illumination microscopy: artefact analysis and reduction utilizing a parameter optimization approach. *Journal of microscopy*, *216*(2), 165-174.

[60] Samson, E. C., & Blanca, C. M. (2007). Dynamic contrast enhancement in widefield microscopy using projector-generated illumination patterns. New Journal of Physics, 9(10), 363.

[61] Yu, J. Y., Holland, D. B., Blake, G. A., & Guo, C. L. (2013). The wide-field optical sectioning of microlens array and structured illumination-based plane-projection multiphoton microscopy. Optics express, 21(2), 2097-2109.

[63] Chowdhury, S., & Izatt, J. (2013). Structured illumination quantitative phase microscopy for enhanced resolution amplitude and phase imaging. Biomedical optics express, 4(10), 1795-1805.

[64] Huynh-Thu, Q.; Ghanbari, M. (2008). "Scope of validity of PSNR in image/video quality assessment". Electronics Letters 44 (13): 800. doi:10.1049/el:20080522